

DI Elisabeth Ziegler

Investigation of the rubber-brass adhesion

DISSERTATION

Zur Erlangung des akademischen Grades
eines Doktors der technischen Wissenschaften

erreicht an der

Technischen Universität Graz

Betreuer: Assoc.Prof. DI Dr. Gregor Trimmel
Institut für Chemische Technologie von Materialien
Technische Universität Graz

2012

EIDESSTATTLICHE ERKLÄRUNG

Ich erkläre an Eides statt, dass ich die vorliegende Arbeit selbstständig verfasst, andere als die angegebenen Quellen/Hilfsmittel nicht benutzt, und die den benutzten Quellen wörtlich und inhaltlich entnommene Stellen als solche kenntlich gemacht habe.

Graz, am

.....

(Unterschrift)

STATUTORY DECLARATION

I declare that I have authored this thesis independently, that I have not used other than the declared sources / resources, and that I have explicitly marked all material which has been quoted either literally or by content from the used sources.

.....

date

.....

(signature)

No one knows what he can do till he tries.

(Publilius Syrus)

ABSTRACT

The aim of this thesis was the investigation of the adhesion between rubber and brass-plated steel wires. This adhesion determines the mechanical strength of many rubber products such as radial tires, handrails or hydraulic hoses.

This thesis can be divided into three major parts: the first part dealt with the examination of brass-plated wires, which had, according to their manufacturer, the same specifications (diameter, brass plating thickness, brass composition). The analysis of these wires showed differences, which could explain the different behavior of these wires during the vulcanization.

The adhesion interface between rubber and brass is difficult to analyze. Therefore, in the second part, different methods to investigate the adhesion layer were tested and compared to each other. The first one is the squalene method, which uses a low-molecular weight model substance for natural rubber to investigate the sulfidation reaction. The second one is the filter paper method, where a filter paper is inserted in between the rubber and the wire during the vulcanization. After the vulcanization this filter paper allows to separate the rubber from the wire. Due to the use of rubber compounds, almost real conditions can be studied, however, the interlayer inhibits the formation of the actual adhesion. The third method is a chemical degradation of the rubber by an olefin metathesis and allows the study of an actual adhesion layer. These methods were compared to each other to evaluate advantages and limitations.

The last part dealt with the investigation of the influence of various components, which are typically employed in rubber compounds (e.g. stearic acid, cobalt adhesion promoter or antioxidant agent). This was accomplished by varying the amounts of the used chemicals and consequently, the effect of these changes on the physical properties of the compounds as well as on the adhesion properties and the adhesion layer between rubber and brass were monitored.

KURZFASSUNG

Das Ziel dieser Arbeit war die Untersuchung der Haftung zwischen Gummi und Messing-beschichteten Stahldrähten. Nur durch diese Haftung kann in vielen Gummiprodukten, wie z.B.: Radialreifen, Handläufen oder auch Hydraulikschläuchen, eine ausreichende mechanische Stärke erzielt werden.

Im Großen und Ganzen kann diese Arbeit in drei Teile unterteilt werden: Im ersten Teil wurden Messing-beschichtete Stahldrähte untersucht, welche laut Hersteller dieselben Spezifikationen (Drahtdurchmesser, Messingschichtdicke, Messingzusammensetzung) aufwiesen. Allerdings zeigte die Analyse dieser Drähte einige Unterschiede, mit denen das unterschiedliche Verhalten der Drähte während der Vulkanisation erklärt werden konnte.

Im Normalfall ist die Untersuchung der Gummi-Messing Haftschrift eine äußerst schwierige Aufgabe, weshalb sich der zweite Teil dieser Arbeit mit der Untersuchung und dem Vergleich unterschiedlicher Methoden beschäftigt, welche es erlauben die Haftschrift zu analysieren. Die erste Methode war der Squalen Versuch, bei der Squalen als niedermolekulare Modellsubstanz für Naturkautschuk verwendet wird um die Sulfidierungsreaktion der Messingschicht zu beobachten. Die zweite Variante ist die Filterpapier Methode, bei der ein Filterpapier zwischen Kautschuk und Draht eingebracht und mitvulkanisiert wird. Nach der Vulkanisation kann man mit Hilfe des Filterpapiers den Gummi vom Draht lösen, wobei die Verwendung einer Kautschukmischung die Untersuchung bei annähernd realen Bedingungen ermöglicht. Allerdings behindert das Filterpapier die Ausbildung der tatsächlichen Haftung, weshalb auch diese Methode nur ein Modellversuch ist. Die dritte Methode ist ein chemischer Abbau des Gummis durch eine Olefin-Metathese, wodurch die Untersuchung einer realen Haftschrift möglich ist. Anschließend wurden diese drei Methoden untereinander verglichen, um ihre Möglichkeiten, aber auch ihre Grenzen aufzuzeigen.

Im letzten Teil wurde der Einfluss unterschiedlicher Chemikalien, welche typischerweise in Kautschukmischungen verwendet werden (z.B.: Stearinsäure, Kobalt-Haftvermittler, Alterungsschutzmittel), untersucht. Dazu wurde die Menge der eingesetzten Bestandteile variiert und sowohl die physikalischen Eigenschaften der Gummimischung, als auch die Haftwerte und die Grenzschicht zwischen Gummi und Messing analysiert.

ACKNOWLEDGEMENTS

I want to thank particularly my supervisor Gregor Trimmel for his support and guidance during the work for my PhD thesis, which has been very helpful. Further, I would like to thank Franz Stelzer for the opportunity to carry out this PhD thesis at the Institute for Chemistry and Technology of Materials (ICTM) and additionally, I want to express my gratitude to Martin Payer and Wolfgang Kern for the financial support of the Polymer Competence Centre Leoben GmbH (PCCL). The research work of this doctoral thesis was performed within the COMET-project „*Interfacial engineering towards improved adhesion between polymers and inorganic substrates*“ (project-no.: 4.02) at the Polymer Competence Center Leoben GmbH (PCCL, Austria) within the framework of the COMET-program of the Federal Ministry for Transport, Innovation and Technology and Federal Ministry of Economy, Family and Youth with contributions by Graz University of Technology (Institute for Chemistry and Technology of Materials) and Semperit Technische Produkte GmbH. The PCCL is funded by the Austrian Government and the State Governments of Styria and Upper Austria.

Further, I am very grateful to all the people of the ICTM for the good collaboration and especially to the people of my working group. Special thanks go to Verena Kaltenhauser for her support concerning all kinds of different questions.

Many of the activities related to this work would not have been possible without collaborations. Therefore, I would like to thank Johannes Macher and Dieter Gruber (PCCL) for their assistance in performing the focus variation microscopy and for the roughness calculations. Additional thanks go to Franz-Andreas Mautner and Brigitte Bitschnau (Institute for Physical and Theoretical Chemistry) for performing the X-ray diffraction measurements, to Peter Pölt (Institute for Electron Microscopy) for the SEM-EDX analysis and to Boril Chernev (Institute for Electron Microscopy) for the Raman characterization. I also want to thank Varta Micro Innovation GmbH (VMI) for their support in performing the SEM-EDX measurements.

Finally, I want to thank all my friends and last but not least, I wish to express my gratitude to my family, my sister Renate, my brother Martin and my parents Andrea and Werner for their ongoing support. This would not have been possible without you.

TABLE OF CONTENTS

1	INTRODUCTION	1
2	BASICS - THEORY	3
2.1	Rubber-brass adhesion in general	3
2.2	Mechanism of rubber-brass adhesion interlayer build-up	6
2.3	Influence of compound ingredients	10
2.4	Adhesion promoter	12
2.4.1	Compound additives	12
2.4.1.1	Cobalt salt	12
2.4.1.2	Resin	14
2.4.1.3	Alternative adhesion promoter	17
2.4.2	Surface pretreatment	17
2.5	Adhesion testing	20
2.6	How to investigate the adhesion interface	22
3	AIM OF THIS THESIS	25
4	RESULTS AND DISCUSSION	27
4.1	Comparison of different wires	27
4.1.1	Sulfidation of Sp ₂ , Sp ₃ and Sp ₆ in squalene experiments	31
4.1.2	Conclusion	33
4.2	Sulfidation reaction in squalene experiments	35
4.2.1	Comparison Appearance – Composition	35
4.2.2	Comparison of optical microscopy images and SEM-EDX results	39
4.2.3	Correlation structures, elemental composition	42
4.2.4	Conclusion	44
4.3	Influence of stearic acid on rubber-brass adhesion	46

4.3.1.1	Introduction.....	46
4.3.1.2	Results and Discussion.....	47
4.3.1.3	Conclusion	58
4.3.1.4	Further results	58
4.4	Comparison of different analytical methods	63
4.4.1	Introduction	63
4.4.2	Results and Discussion	64
4.4.3	Conclusion.....	72
4.5	Influence of different compound components on rubber-brass adhesion	74
4.5.1	Cobalt stearate.....	74
4.5.1.1	Conclusion	90
4.5.2	Antioxidant agent	92
4.5.2.1	Conclusion	103
5	SUMMARY AND OUTLOOK.....	104
6	EXPERIMENTAL.....	111
6.1	Chemicals	111
6.2	Equipment and Methods	112
6.2.1	Optical microscopy	112
6.2.2	Focus variation microscopy	112
6.2.3	Roughness calculation	112
6.2.4	Scanning electron microscopy coupled with Energy dispersive X-ray spectroscopy (SEM-EDX).....	113
6.2.5	Raman	113
6.2.6	X-ray diffraction (XRD)	113
6.2.7	Vulcanization.....	114
6.2.8	Pull-out testing.....	115
6.2.9	Rubber properties testing.....	115
6.3	Squalene experiments.....	116

6.4	Filter paper experiments.....	118
6.5	Olefin metathesis experiments.....	120
6.5.1	Olefin metathesis degradation method 1	120
6.5.2	Olefin metathesis degradation method 2	121
7	APPENDIX	122
7.1	List of Abbreviations.....	122
7.2	List of Tables.....	124
7.3	List of Figures	126
7.4	Literature.....	130
7.5	Publications	135
7.6	Curriculum Vitae	138

1 INTRODUCTION

Rubber-to-metal bonding is an important topic in rubber industry, because many rubber products, such as radial tires, hydraulic hoses and handrails need metal wires and cords for reinforcement. A typical passenger tire contains about 1 kg of steel and commercial vehicle tires 3 – 7 kg, depending on size.¹ Therefore, failure of the adhesion between the steel cords and the rubber consequently results in a damage of the tire itself. The same applies to hydraulic hoses and handrails.

Every year, about 260 million car tires² and about 12 million truck and bus tires³ are sold in Europe. The demand on tires is even increasing over the years (see Figure 1). In 2011 sales for Bridgestone have been 31 billion US-Dollars and 28 billion US-Dollars for Michelin.⁴ This clearly shows that the production of tires is an important manufacturing branch.

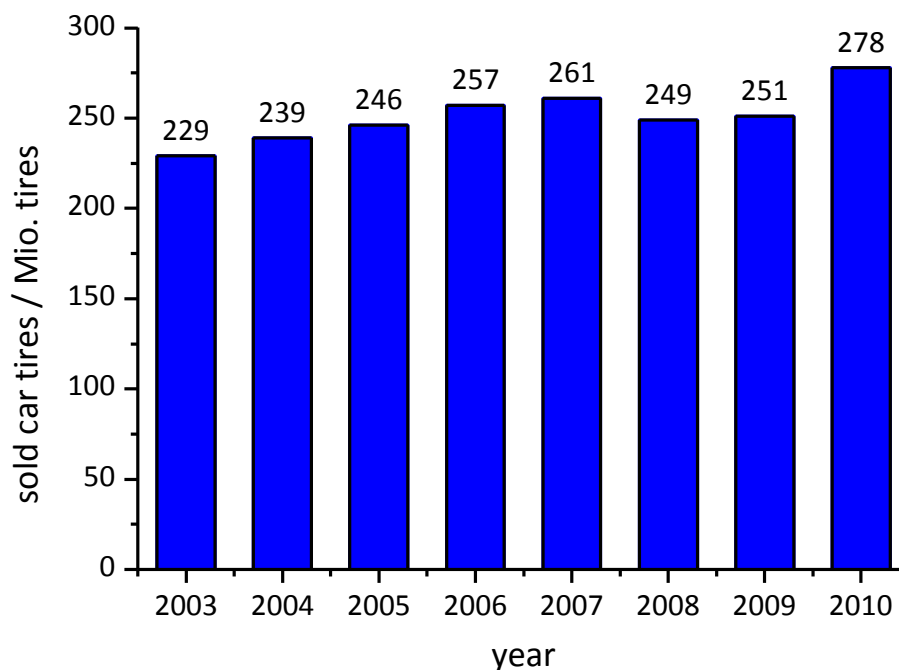


FIGURE 1. CAR TIRE SALES IN EUROPE BETWEEN 2003 AND 2010

For a convincing performance, a good adhesion and also adhesion retention between the reinforcing metal and the rubber is essential. The adhesion mechanism has been studied for years and many aspects concerning the adhesion mechanism are already known. But still, there are many open questions, so that most companies work with empirical knowledge. As a consequence, small changes in the rubber compound or the wire system can lead to a totally different adhesion behavior.

As far as it is known today, adhesion is achieved through a mechanically interlocking of the rubber with an adhesion interlayer,^{5,6} whereas a covalent bond is considered to be only a minor factor.⁷ One of the major challenges concerning the study of the rubber-to-metal adhesion is how to characterize the adhesion interlayer, since it is located in between the rubber and the metal. During the years, many different approaches were developed to overcome this problem. All of them have their advantages and on the other hand also certain drawbacks.

For this reason, individual studies can completely change the general knowledge and therefore, the study of rubber-to-metal adhesion is still a very interesting topic, including many challenges.

2 BASICS - THEORY

2.1 RUBBER-BRASS ADHESION IN GENERAL

Rubber-metal bonding is an important topic in rubber industry, since steel wires and cords are extensively used as reinforcement for many rubber products, such as radial tires, hydraulic hoses and handrails. For a convincing performance a good adhesion between the reinforcing metal and the rubber is essential. However, steel does not directly bond to rubber.⁸ For some applications zinc-coated steel cords are used⁹, but most times, a thin brass layer is applied to get appropriate adhesion performance, although, there are also studies to investigate alternative alloys. For example, Jeon et al.¹⁰ published a study on the performance of a ternary-alloy-coated steel cord with 2 wt% of cobalt. Van Ooij and Kleinhesselink¹¹ compared CuZn to CuZnNi (12 % Ni) and CuNi (65/35) and Giridhar and van Ooij¹²⁻¹⁴ investigated the adhesion properties of a copper-free alloy system based on NiZn/ZnCo. Nevertheless, brass is still the most used adhesive layer. Further, it has the advantage that brass can act as drawing agent during the wire production process.¹⁵

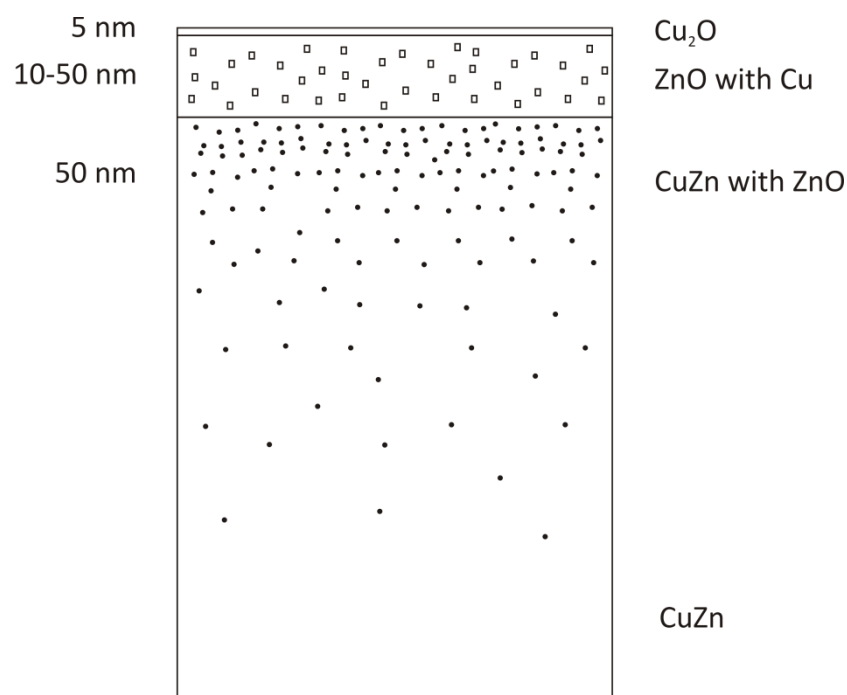


FIGURE 2. SCHEMATIC IMAGE OF BRASS-COATED STEEL WIRE SURFACE

Normally, the surface of brass consists of a complex layer system of different oxides (see Figure 2).¹⁶ On the very top, there is a Cu_2O layer, which is very thin (approximately 1 nm) and can therefore be neglected. In between this layer and the brass bulk is a layer of ZnO with copper inclusions as a result of a surface oxidation mechanism of zinc.

During scorch (time till 5 % conversion)¹⁷, at an early stage of vulcanization, copper and zinc ions as well as free electrons diffuse to the metal surface, where they react with active sulfur-containing molecules, generated in the rubber compound. Initially, some ZnS is formed, but is rapidly overgrown by a rough non-stoichiometric Cu_xS ($x \rightarrow 1.8$) layer (see Figure 3).¹⁶ This process is called sulfidation. At the beginning, this sulfidation is very slow and the diffusion of the copper ions through the ZnS layer is slow-going, as ions migrate by interstitial diffusion and the migration is hindered because of the different ion radii of zinc and copper ions. As the copper ions migrate into the copper sulfide layer, the diffusion rate is much higher, due to the non-stoichiometry of the Cu_xS .¹ Through this process the Cu_xS layer thickens until all copper inclusions of the ZnO layer are used up. Then the process will slow down. Therefore the amount of copper inclusions in the ZnO is of crucial importance for a good bond formation.^{1,18}

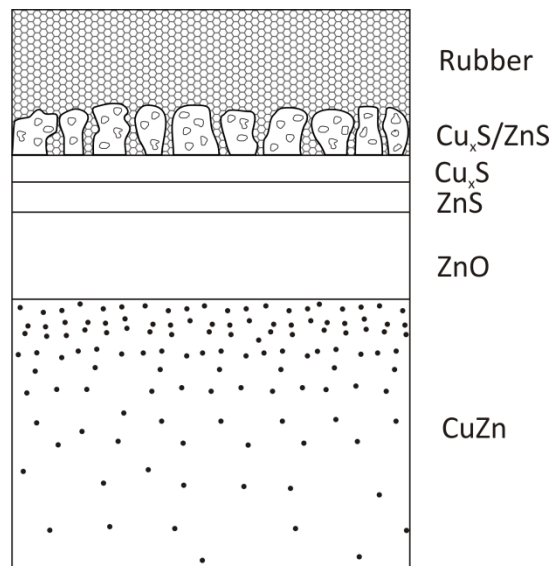


FIGURE 3. SCHEMATIC IMAGE OF THE BRASS-RUBBER INTERFACE AFTER VULCANIZATION

Up to the present, it is not absolutely clarified how the adhesion is achieved. Most likely it is through a mechanically interlocking of the rubber in the rough non-stoichiometric Cu_xS layer.¹⁶ In some papers, a covalent bonding is proposed^{7,19}, but as van Ooij illustrated¹⁶, there is strong evidence that it is a pure mechanical binding process or at least, that the covalent adhesion is a minor factor. For example, a minimum critical thickness of the Cu_xS layer is needed to ensure good adhesion.²⁰ But, for a covalent bonding, a copper sulfide monolayer should be enough.¹⁶

However, for a good adhesion performance, there are certain prerequisites concerning the brass-alloy on the one hand and the rubber compound composition on the other hand.

For example, the composition of the brass-alloy is of extreme importance.²¹ Only with a copper content between 60 and 70 % satisfactory adhesion is accomplished. If the copper content is low, copper ion diffusion is low as well and almost no copper sulfide is formed. At high copper amounts, the Cu_xS layer grows too fast and the adhesion layer gets brittle and breaks.⁵ The best initial adhesion is achieved with a copper content of 67 – 72 %^{1,22}, but better adhesion retention after humidity aging is gained at lower copper content. Furthermore, there is an optimum plating thickness, which is between 0.2 and 0.3 μm and also organic residues from the lubricant bath (mostly organic phosphates) could have an influence on the adhesion.¹ Additionally, the ZnO layer has a mediating effect on the sulfidation reaction and therefore, the ZnO layer thickness is of critical importance.¹⁶

As far as the rubber compound composition is concerned, van Ooij²³ pointed out that especially a high sulfur/accelerator ratio (> 4 per hundred rubber (phr)) and high unsaturation of the rubber are important for good adhesion. Further, the right choice of the additives, such as the accelerator type, and their amounts (e.g. of stearic acid and ZnO) can have an effect on the bond formation.^{16,23} Almost every compound ingredient has an influence on the overall adhesion performance and therefore, there are still many open questions concerning the adhesion mechanism.

2.2 MECHANISM OF RUBBER-BRASS ADHESION INTERLAYER BUILD-UP

Sulfenamide accelerators have proved to be the most suitable for a good adhesion of rubber-to-brass.²⁴ Therefore, the model of the adhesion layer build-up, postulated a few years ago by van Ooij, uses cyclohexylbenzothiazole sulfenamide (CBS) as accelerator, but any other sulfenamide accelerator would act in a similar way, only at different rates.²³

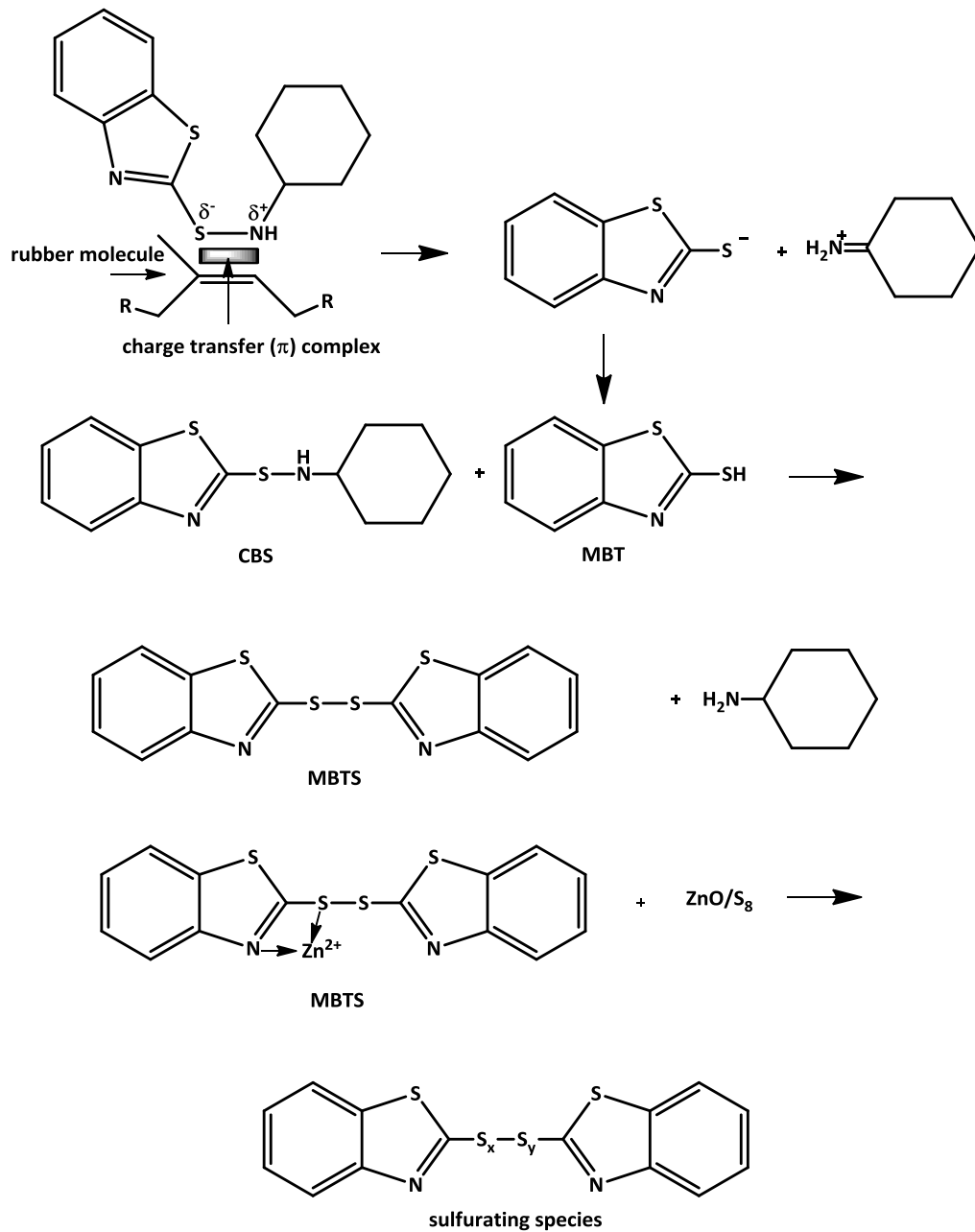


FIGURE 4. STAGE 1, FORMATION OF ACTIVE INTERMEDIATE FROM THE ACCELERATOR

He divided the process into five stages, which cover the curing period until the beginning of the cross-linking. In the first stage (see Figure 4) the active intermediate is formed. Important for this stage is the presence of double bonds in the rubber. The high electron density of the π -orbital polarizes the S-N bond of the sulfenamide accelerator and accelerates the cleaving of the bond. The negative charge is preferentially located at the sulfenamide moiety due to the large size of the sulfur atom and the possibility of charge delocalization by resonance. Various experiments yielded evidence for this interaction.^{8,16} The scission of the sulfenamide accelerator leads to the formation of 2-mercaptobenzothiazole (MBT), which reacts with another sulfenamide to create 2,2'-dithiobenzothiazole (MBTS). Through a complexation with zinc ions the active accelerator intermediate is created.

The second stage (Figure 5) involves a partial dissolution of the surface oxides by stearic acid and absorption of MBT or MBTS on the surface.

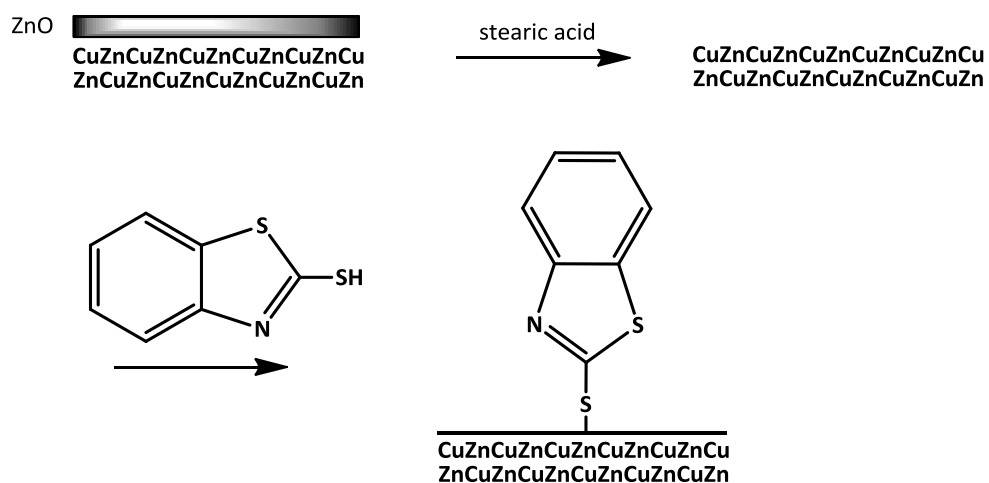


FIGURE 5. STAGE 2, ABSORPTION OF THE ACCELERATOR FRAGMENTS ON THE BRASS SURFACE

In the third stage (Figure 6), the S_8 -rings are opened by the metal-sulfur bonds and so the insertion of sulfur is possible. This reaction can be aided by rubber-soluble zinc, which forms a chelate complex with the sulfur and nitrogen atoms of the MBT. In compounds including cobalt salt, metallic cobalt precipitates on the brass surface, where it also forms such metal-sulfur bonds. The same applies to zinc, but there the sulfide growth rate is much lower.

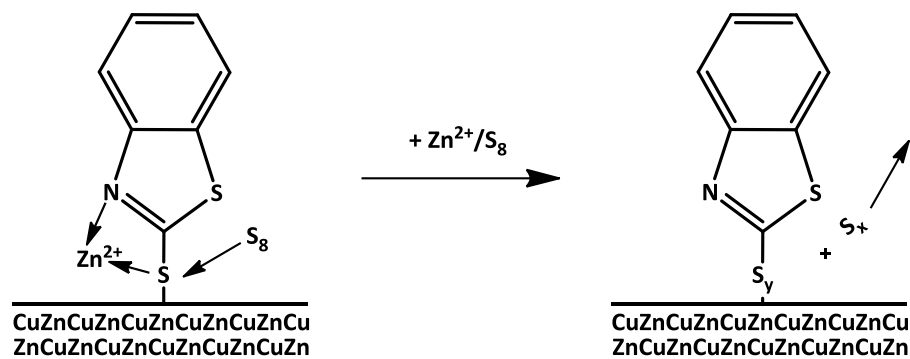


FIGURE 6. STAGE 3, SULFUR INSERTION

At higher temperatures, stage four takes place (Figure 7). The absorbed metal-sulfur-accelerator complexes are decomposed to form metal sulfides and $\text{S}_{y-1}\text{-X}$, an active radical for rubber crosslinking, where X is an accelerator fragment. $\text{S}_{y-1}\text{-X}$ can now either react with a rubber molecule or it can absorb once more at the metal surface to react with copper, which has diffused to the metal surface. By this mechanism, a Cu_xS layer is built-up until the entire fresh accelerator or MBT is consumed.

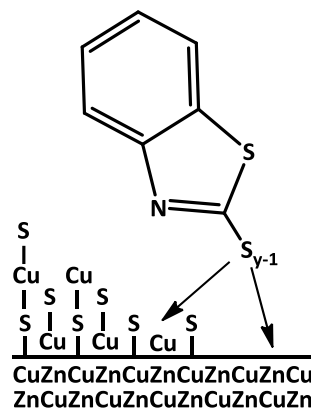


FIGURE 7. STAGE 4, COMPLEX DECOMPOSITION AND SULFIDE LAYER GROWTH

The last step (stage five, Figure 8) involves crosslinking of the rubber, and by this reaction, the formation of a tight rubber network interlocked with the rough Cu_xS layer. An important aspect of this mechanism is that the concentration of the active crosslinking species close to the surface is much higher than in the rubber bulk, which

leads to a higher crosslinking density of the rubber adjacent to the metal surface. Additionally, a covalent Cu-S-rubber bond is discussed in literature, however, it is thought to be of minor importance.⁷

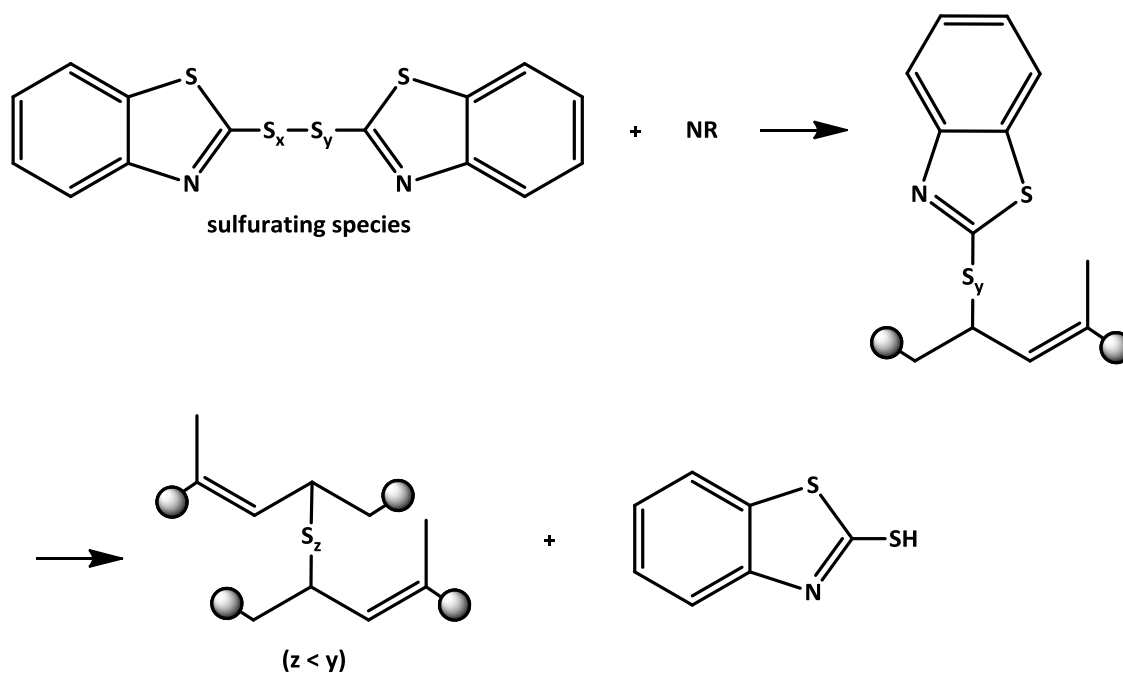


FIGURE 8. STAGE 5, RUBBER CROSS-LINKING

2.3 INFLUENCE OF COMPOUND INGREDIENTS

Mostly all rubber compound ingredients, such as sulfur, accelerator, carbon black etc., have an influence on the adhesion performance of rubber to brass. For example, a correlation between the thickness of the bonding layer and the sulfur content in the compound could be observed.⁵ Since a certain adhesion layer thickness is necessary for good bonding, a sulfur level of at least 3 phr or, still better, 4 phr is necessary.²⁵ On the other hand, with very high sulfur loadings the binding layer becomes very thick and as a result gets brittle and easily breaks.⁵ Furthermore, it was noticed that the sulfur to accelerator ratio is of extreme importance. High sulfur levels and high levels of accelerator applied together normally result in poor adhesion.²⁶ For a good adhesion performance a sulfur to accelerator ratio of greater than 4 is necessary.¹⁶

Another factor, which has an influence on the adhesion, is the type of accelerator used. It has been stated, that delayed-action accelerators, such as sulfenamides, are necessary. Ultra accelerators (very fast and short scorch times), for example tetramethylthiuram disulfide (TMTD), give rather poor results. Hamed and Donatelli²⁴ concluded that this is due to an excessive sulfidation of the brass in the presence of TMTD. The result is a porous and mechanically weak copper sulfide layer, which easily detaches from the metal surface. As far as the sulfenamide accelerators are concerned, N-dicyclohexylbenzothiazole 2-sulfenamide (DCBS) performs better than many other sulfenamides.¹⁶ However, it was reported that 2-morpholinothiobenzothiazole (MBS) gives superior results after steam aging.²⁵

A high degree of unsaturation in the rubber is another important factor for a good adhesion performance. In the absence of double bonds, accelerator decomposition is suppressed.²⁷ As was shown by van Ooij, the decomposition of the accelerator is a major prerequisite for a good sulfidation reaction.²³ As a consequence, in the absence of double bonds, the formation of the copper sulfide layer is slowed down.²⁷

Zinc oxide is used in rubber compounds as an activator and therefore has on the one hand, an influence on the rubber properties¹⁷ and on the other hand, it can also affect the adhesion performance. According to the reaction mechanism of van Ooij concerning the rubber-brass adhesion interlayer build-up, zinc oxide is needed to create the active sulfurating species (see Figure 4).²³ In different studies, it was observed that good bonding can be achieved with high zinc oxide content and small particles.⁵ For example, an excess of zinc oxide in the compound is known to help

maintain the adhesive strength after aging.²⁸ Furthermore, the ratio of zinc oxide to stearic acid should be high.¹⁶

Filler, such as carbon black or silica, were also found to influence the bonding behavior. Similar to the double bonds, carbon black has an influence on the accelerator decomposition rate and as a consequence on the sulfide layer formation.²⁷ With increasing amount of carbon black in the compound, a higher amount of sulfur is detected in the adhesion interface.²⁹ Additionally, carbon black has a positive effect on the pull-out strength. This was explained by two factors: first, carbon black is a reinforcing filler and therefore, the physical properties of the rubber improve with increasing carbon black content. Second, carbon black is able to entrap residual amine components (from the accelerator), which may absorb at the rubber-metal interface and in consequence, support stress-induced corrosion crack.

Silica is also frequently used as filler in rubber compounds. Apart from its effect on the physical properties of the rubber (modulus and tensile strength decrease, elongation at break increases), it also influences the adhesion performance. With increasing silica content of the compound both, the pull-out force and the rubber coverage, increase as well.^{30,31} As far as the interface is concerned, silica in the rubber compound decreases the total amount of sulfur and increases the oxygen and zinc levels. It seems as if silica has a mediating effect on the adhesion interface, resulting in a thinner copper sulfide layer.²⁹ As a consequence, an increased stability of the bonding layer with increasing silica loading was observed.³¹

2.4 ADHESION PROMOTER

2.4.1 COMPOUND ADDITIVES

2.4.1.1 COBALT SALT

Cobalt salts are very popular adhesion promoter for bonding rubber to brass-plated steel cords and wires. They affect the initial adhesion strength as well as the durability of the adhesion.¹ There is a great many of different cobalt salts, which are applied, such as cobalt stearate, cobalt naphthenate, cobalt neodecanoate or cobalt boroacylate. The traditional cobalt disoaps, such as cobalt stearate, contain two molecules of acid per cobalt atom (Figure 9A), whereas the second generation cobalt adhesion promoters (e. g. cobalt boroacylate, Figure 9B) have higher cobalt content.¹ As a consequence, less cobalt boroacylate is needed to apply the same amount of cobalt as in the cobalt stearate.

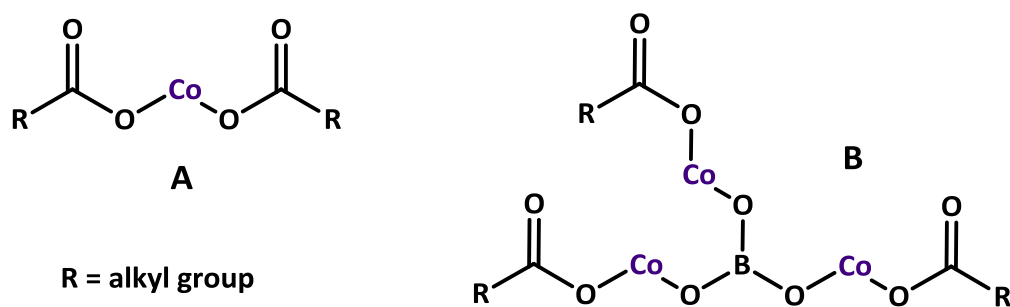


FIGURE 9. STRUCTURES OF COBALT ADHESION PROMOTERS A: COBALT DISOAP, B: COBALT BOROACYLATE

Chandra et al.³² postulated that the effect of the cobalt salt on the adhesion energy can be attributed to three different factors:

- the change of rubber properties;
- the modification of the adhesion interlayer;
- the chemical stability of the promoter.

Concerning the first point, it was observed that cobalt salt in the rubber compound reduces not only the viscosity^{33,34}, but also the curing time.^{20,27,33,35,36} Further, the crosslink density is increased.^{27,33,34,37} As a consequence, hardness and tensile strength increase as well, while elongation-at-break decreases.³³ However, the thermal stability of the rubber network is adversely affected by the cobalt^{16,36} which in consequence leads to the degradation of the rubber (e. g. by chain scission of the sulfur crosslinks).³³

The modification of the adhesion interlayer with addition of cobalt salt was observed in many studies. All of them agree on the fact, that cobalt ions are incorporated into the adhesion interface where they change the relative diffusion rates of copper and zinc ions.^{1,16} Chandra et al.²⁰ and Fulton et al.³⁸ both report that cobalt is incorporated into the ZnO layer as Co^{3+} early in the vulcanization process, before the onset of sulfidation. Impurity cations in a higher oxidation state, such as Co^{3+} , reduce the diffusion rate of Zn^{2+} ions. As a consequence, ZnS formation at the surface is diminished and copper sulfide formation enhanced. Kim and van Ooij⁷ studied squalene treated brass panels by time-of-flight secondary ion mass spectrometry (TOF-SIMS) and detected cobalt in the entire adhesion layer. Close to the surface, cobalt exists mostly in its organic form and in deeper layers as cobalt sulfides. Jeon³³ investigated the influence of the loading amount of cobalt on the adhesion. He found that low levels of cobalt increases the adhesion performance but at higher loading amounts a decline of pull-out force was observed, especially at long aging times in humid conditions. With increasing amounts of cobalt, copper migration increases and in consequence, causes defects in the brass layer. This results in activated zinc, which is easily oxidized. Hotaka et al.¹⁹ report of an alternative mechanism which explains the enhanced performance of cobalt containing compounds. They suggest that there are two kind of copper sulfides in the adhesion layer: Cu_2S , which is responsible for adhesion and CuS , which does not bond. For compounds containing cobalt, the sulfide layer consists mainly out of Cu_2S , for compounds without, it is mostly CuS . Hotaka et al. postulated that cobalt may activate the reaction of CuS to Cu_2S .

During the aging, the adhesion interface continues to react and the sulfide layer and the zinc oxide layer increase in thickness. Consequently, the adhesion layer becomes brittle and tends to crack more easily. By the addition of cobalt this reaction is clearly slowed down.³⁵ Furthermore, it was observed that in the presence of cobalt less dendritic structures are built up during aging. Due to their crystalline character, they

are more brittle and therefore crack easily. Actually, in the presence of cobalt crystallinity is lower.³⁸

In most cases, cobalt salts are used as adhesion promoter. However, it is the cobalt ion which is responsible for the adhesion promotion and not the salt itself.³⁴ But the anion is also of importance, for example the usage of cobalt boroacylate results in better adhesion than cobalt stearate. Cobalt stearate sometimes gives slightly increased adhesion but just as often the result is poorer than with no cobalt salt at all.³² Studies including cobalt boroacylate as well as cobalt stearate have shown the superiority of the boroacylate. Cobalt boroacylate improved the adhesion properties^{20,32}, crystallinity and the aging resistance of the adhesion layer (less dezincification).³⁸ One reason for these differences may be the chemical stability of the promoter. The bond between cobalt and the stearate anion is a very weak one, hence they dissociate very fast. Furthermore, the stearate ion itself is corrosive and tends to dissolve some of the zinc oxide layer, whereas the boroacylate anion helps to prevent corrosion.³⁴ Further, the stearate has an accelerator activating effect and as a consequence sulfur is increasingly used for crosslinking, resulting in incomplete sulfidation of the brass surface.³² Boroacylate salt on the other hand, has a higher activity, which results in higher cobalt incorporation.³⁸

2.4.1.2 RESIN

Additionally, resin systems are also typically employed as additives for adhesion promotion. Normally, a combination of a methylene donor, such as hexamethoxymethylmelamine (HMMM) or hexamethylene tetramine, and a methylene acceptor, such as resorcinol, is applied.³⁹ The methylene donor reacts together with the methylene acceptor to create a highly cross-linked polymeric network as is depicted in Figure 10.⁴⁰ Traditionally, hexamethylene tetramine was used as methylene donor, alternatively, it was replaced by HMMM on a silica carrier. Further, resorcinol can be exchanged for resorcinol/formaldehyde (RF resin) condensation products to reduce the fuming.¹

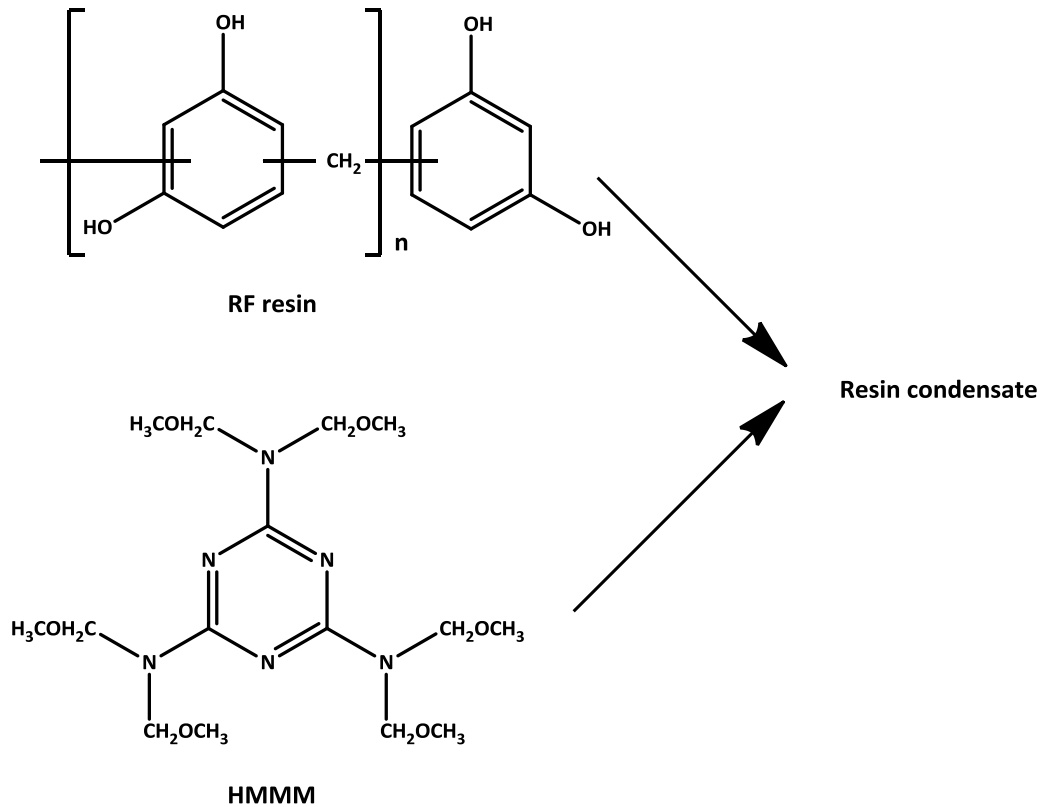


FIGURE 10. CROSS-LINKING OF RF RESIN AND HMMM

Lately, one-component resins were developed, which dispense with the usage of resorcinol at all. These one-component resins are more or less dimers of HMMM, bridged by either a methylene ether or a methylene group. The triazine ring is not fully substituted with methoxymethyl groups (see Figure 11), leaving some residual amine-type hydrogen atoms, which allow a self-condensing of the resin.⁴¹

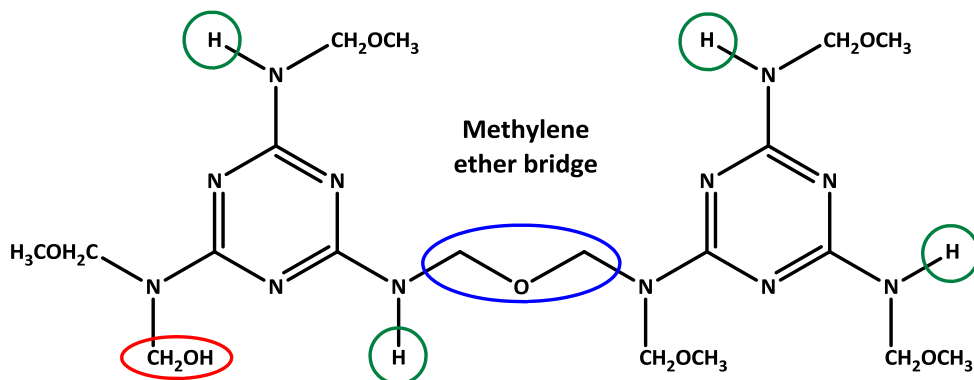


FIGURE 11. ONE-COMPONENT MELAMINE RESIN

The addition of resin systems to a rubber compound not only affects the adhesion performance but also the rubber properties. Normally, the cure rate is decreased, but this effect can be reduced by the addition of cobalt salts.^{35,39} Furthermore, resins increase the hardness³⁹ and the maximum torque.³⁵ The positive effect of resin systems on the adhesion performance was shown in several studies.^{35,39,41-43} Especially, adhesion after various aging treatments was improved. Furthermore, one-component resins normally improve the adhesion performance to a greater extent than two-component resins whereby the best results were obtained with the additional usage of cobalt salts.^{39,41,42} Actually, it has been shown that cobalt salts and resin systems work together in a synergistically way.^{35,39,41,42}

The effects of resin systems on the adhesion performance between rubber and brass-coated steel cords and wires can be traced back to several factors:

- Polar resins, such as RF resins, are insoluble in rubber and migrate to the brass surface, where they build a protecting layer against moisture attack.³⁵
- It was shown that resin systems remove cobalt from a squalene solution. Since cobalt is a well-known oxidation catalyst, this might help to prevent degradation of the rubber during aging.³⁵
- Hotaka et al.⁴³ showed that HMMM is capable of trapping residual amine components, which may easily penetrate into the rubber-metal interface and in consequence support stress-induced corrosion crack.
- In several studies, Patil and van Ooij^{39,41,42} showed that resin systems help to control the structure of the adhesion interface, resulting in a mostly amorphous Cu_xS layer, which also have a greater tendency to stay amorphous during aging. Such an amorphous Cu_xS layer is more stable than a crystalline one and does not break as easily. Therefore, the binding layer built in resin containing compounds is much more corrosion-resistant.

Further, it was postulated that the improved performance of one-component resins compared to the two-component resins are due to free hydrogen atoms, generated during the resin cross-linking. They can diffuse into the bonding layer and might alter the crystal structure in a beneficial way, which results in an adhesion interface that stays amorphous for a longer period.⁴¹

2.4.1.3 ALTERNATIVE ADHESION PROMOTER

Further substances, which were explored as adhesion promoter, are for example zinc borate^{34,44}, chlorotriazine^{34,45} and tetrachlorobenzoquinone^{34,45}. The addition of zinc borate to a rubber compound had almost no effect on the cure rate for low zinc borate loading (< 1 phr) but decreased the cure rate for higher loading amounts. Furthermore, the changes of the mechanical properties were very slight until 1 phr. For higher zinc borate amounts the physical properties of the rubber declined. Incorporation of zinc borate into the rubber compound further lead to a decrease of the adhesion properties for unaged compounds but improves the adhesion for long-time humidity aging. The optimum loading amount was found to be 1 phr. Jeon concluded that low levels of zinc borate depresses the copper migration, leading to a moderate copper sulfide and zinc oxide formation. At high zinc borate loadings, excessive amounts of copper sulfide and zinc oxide are grown, resulting in a poor adhesion performance.⁴⁴

Addition of chlorotriazine reduced the cure rate but had little effect on the physical properties of the cross-linked rubber.³⁴ It was shown that chlorotriazine accelerates the sulfidation reaction of brass⁴⁵ and the conversion of zinc oxide to zinc sulfide.³⁴ At high chlorotriazine loadings (> 2 phr) a negative effect on the adhesion performance was observed.³⁴

Similar to chlorotriazine, tetrachlorobenzoquinone reduced the cure rate but had almost no effect on the physical properties of the compound.³⁴ Again an acceleration of sulfidation^{34,45} could be observed which was explained by an increased copper diffusion. As a result, the interfacial copper sulfide layer had a higher surface area. Loading amounts above 0.5 phr resulted in excessive copper sulfide diffusion and zinc oxide formation and as a consequence, in poor adhesion.³⁴

2.4.2 SURFACE PRETREATMENT

Jayaseelan and van Ooij⁴⁶ explored an alternative adhesion system, where they coated metal substrates (e.g. steel, zinc, brass) with a combination of bis-(trimethoxysilylpropyl)amine and bis-(triethoxysilylpropyl)tetrasulfide (at a ratio of 1 to 3) prior to their exposure to the rubber compound. With this system, the authors were able to gain good adhesion not only to brass but also to steel and zinc. Furthermore, they were able to improve the adhesion of cobalt-free compounds and compounds with low sulfur levels. Both thermal aging (70 °C) and humidity aging (70 °C at 70 %

relative humidity) mostly resulted in cohesive failure which is typical for a good adhesion between rubber and the metal substrate. Aging in a NaCl-solution resulted in an adhesive failure for the brass substrate but did not affect the bonding between rubber and steel, even though an excessive corrosion of the steel substrate and a degradation of the rubber could be observed.

The bis-(triethoxysilylpropyl)tetrasulfide is a silane which is typically employed in rubber compounds in combination with silica to enable a better distribution of the filler. This silane is very hydrophobic and as a consequence, insoluble in water. Therefore, the hydrolysis (necessary to build a dry film on the metal substrates) is a very slow process. The amino silane on the other hand, is able to create a dry film, even at room temperature. By combining the two silanes, a dry silane film can be achieved.

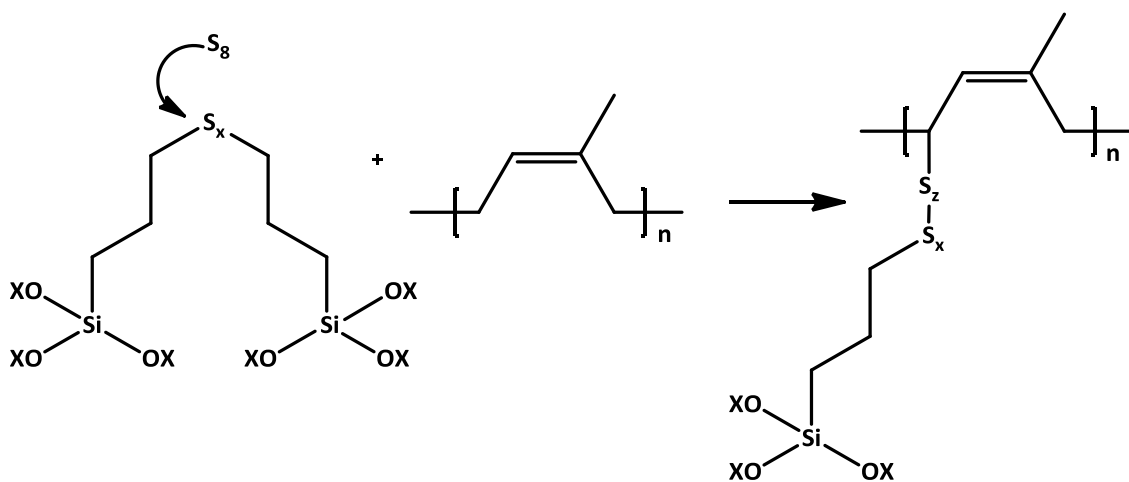


FIGURE 12. SCHEME OF SILANE-RUBBER CROSS-LINKING

Bonding to the rubber is achieved through the tetrasulfide silane. The authors stated that during the vulcanization free sulfur can be integrated into the polysulfide chain of the silane. As a consequence, the reactivity of the silane with the rubber is increased and a reaction between the two molecules is possible (see Figure 12). Through this process a covalent bonding between rubber and silane is achieved and consequently, also a bonding to the metal substrate. Furthermore, the silane layer and the rubber network penetrate into each other, resulting in a further improvement of the adhesion performance.

Furthermore, there are several other approaches for surface pretreatment, such as coating metal substrates (steel, brass or zinc) with plasma-polymerized acetylene, butadiene or thiophene³⁴ or activation of the surface with HCl, NaOH or emery cloth (P 500)⁶.

2.5 ADHESION TESTING

Strength of adhesion between rubber and brass can be determined by various testing settings such as shear testing for planar metal samples or TCAT (tire cord adhesion test) for cords and wires. In the shear testing a brass-rubber-brass sandwich is fixed in a sample cavity between two stress arms which move in opposite direction.⁶ In the TCAT testing two wires are embedded into a rubber block and after the vulcanization the opposite cord ends are pulled at a constant rate until one of the cords is pulled out (seen Figure 13). Through this procedure, pull-out force and rubber coverage can be determined.^{24,32,35} In this testing, it is essential to maintain all parameters as similar as possible, because, as Maesele and Debruyne²² pointed out, the measured values can be influenced by various factors, such as the stress exerted on the sample during the test, the size of the slit where the wire or cord is pulled out and so on.

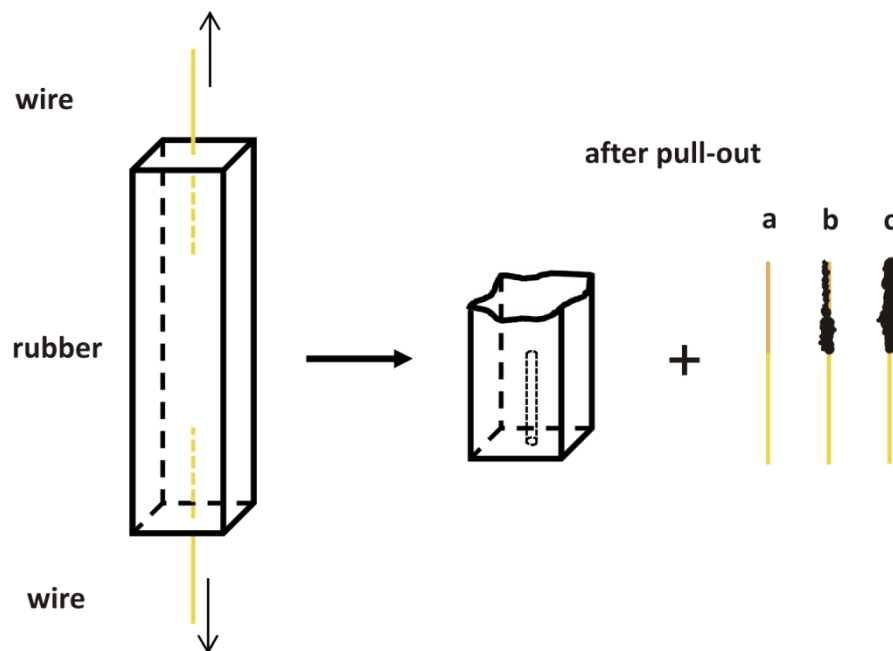


FIGURE 13. TCAT PULL-OUT TESTING AND DIFFERENT FAILURE MODES OF THE PULLED WIRES (A: ADHESIVE FAILURE, B: PARTLY ADHESIVE, PARTLY COHESIVE FAILURE, C: COHESIVE FAILURE OF THE RUBBER)

As mentioned before, not only the pull-out force, but also the rubber coverage is typically determined in adhesion testing. Depending on the rubber coverage,

conclusions can be drawn concerning the type of failure in the rubber-wire composite. According to van Ooij²⁶, there are several modes of failure possible:

- cohesive failure of the rubber,
- adhesive failure at the interface between the rubber and the sulfide layer,
- cohesive failure of the sulfide layer,
- adhesive failure at the interface between the sulfide and the zinc oxide layer,
- adhesive failure at the zinc oxide – metal interface.

Therefore, if the wire is fully covered with rubber, the failure mode is a cohesive fracture in the rubber. The other extreme is no rubber coverage at all: here the locus of failure is somewhere in the adhesive layer. However, very often, a mixed failure mode can be found and the pulled-out wire is partly covered with rubber.

In this thesis, adhesion was tested similar to ASTM D 1871. A schematic image of the used T-test specimen can be seen in Figure 14. The adhesion performance was evaluated by pulling out the wires at a constant rate (= 100 mm/min) applying a preload of 50 N. Rubber coverage was rated from 0 to 3 (0 = 0 %, 1 = 1-49 %, 2 = 50-99 %, 3 = 100 % rubber coverage).

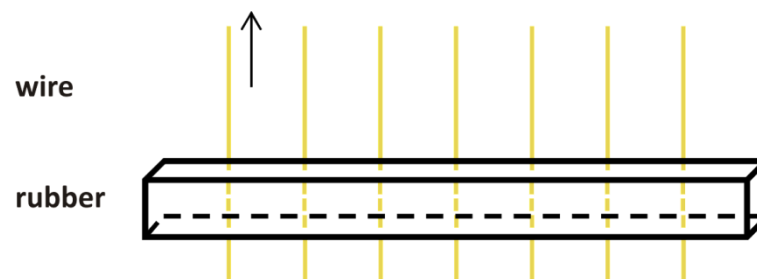


FIGURE 14. T-TEST SAMPLE FOR PULL-OUT TESTING

2.6 HOW TO INVESTIGATE THE ADHESION INTERFACE

One of the greatest challenges for the investigation of rubber-to-brass adhesion is the characterization of the adhesion interface. The adhesion layer is located in between the wire and the rubber phase, therefore, a sample preparation is necessary to obtain a “free” interface. As far as the characterization is concerned, there are several possibilities: one is to expose the adhesive interface, which allows the use of a broad spectrum of different characterization methods such as scanning electron microscopy (SEM)^{26,35,47,48}, Auger electron microscopy (AES)^{49–52}, X-ray photoelectron spectroscopy (XPS)^{8,11,29,53–55}, grazing-incidence X-ray diffraction (GIXRD)⁴¹ and so on. SEM allows an optical characterization of the adhesion layer surface and, in combination with energy-dispersive X-ray spectroscopy (EDX), also an elemental characterization. AES and XPS are very surface sensitive techniques and are therefore often coupled with a sputter etching process to examine the composition over the entire width of the adhesion layer. XPS further allows the determination of the chemical state and the binding energy of the elements. GIXRD uses very low angles of incidence ($\theta = 0.1^\circ$) to determine the crystal structure of thin surface layers (300-400 nm).⁴¹

Alternatively, cross-sections can be analyzed by transmission electron microscopy (TEM).^{5,6,28,56–58} Examination by TEM has the advantage that the shape and the thickness of the adhesion layer can be directly observed but on the other hand, only small areas can be studied. Furthermore, samples for TEM characterization need to be thin enough for the incident electrons to pass through (thinner than 100 nm), which implies a lot of sample preparation. There are several possibilities, however, nowadays mostly focused ion beam (FIB) milling technique is used to prepare ultrathin cross-sections of rubber-brass composites.^{38,58}

Over the years, several methods, which allow the study of the adhesive interface, were developed. The simplest method is to only analyze areas, where the adhesion failed and consequently parts of the surface are available for characterization.⁵⁸ Another method, which has been used for years, is the so-called squalene method.^{11,24,27,42,47,54} This is a model system, where squalene is used as a low molecular weight analog to natural rubber or polyisoprene, which allows the study of the sulfidation reaction. Normally, a mixture of squalene (instead of natural rubber or polyisoprene) and all essential vulcanization components is prepared and the wires or cords are immersed into this mixture at elevated temperatures. After a certain vulcanization period the substrates are removed from the mixture and cleaned with an organic solvent. This

method has the advantage that squalene is a liquid (even in a slightly cross-linked state) and can therefore be easily removed after the vulcanization reaction. However, this method also has some disadvantages such as an uneven dispersion of the cure ingredients and further, it is only a model system and there are major differences in the way of curing compared to natural rubber vulcanization.³⁷ Also, it is not possible to study the influence of aging on the sulfidized interface.⁵⁹

Another approach is the brass-to-glass method^{31,57,59,60}, which allows the study of the rubber-brass interface without removing the rubber from the brass. A thin film of Cu and Zn is vapor coated or sputtered on the glass substrate and afterwards transformed into a relatively homogenous brass layer with a thickness of 60 to 150 nm. This substrate is sandwiched between two uncured rubber pads and subsequently vulcanized. After the vulcanization reaction, the rubber brass composite can be easily removed from the glass substrate, due to the low adhesion between glass and brass. Starting at the brass side, the adhesion layer can now be easily characterized. Since the removal of the glass substrate often resulted in cracks of the brass layer a refined system with a polycarbonate film as substrate was developed.^{57,59} The polycarbonate film is further coated by a bromobutyl compound, which acts as vapor barrier. Further, it was found that a brass layer thickness of 60 to 150 nm is not always sufficient and therefore, the brass layer thickness was increased to 500 nm.^{57,59}

One of the oldest methods uses liquid nitrogen: the rubber of the test sample is frozen by liquid nitrogen and consequently removed with a hammer.^{8,43,49,61,62} The advantage of this method is that wires and cords from actual rubber products and also after different lifetimes and aging conditions can be investigated. However, the weak point where the separation occurs, is often between the brass and the sulfide layer and therefore, the exposed surface is not always the real interface.³⁷

Another method, which allows the study of wires from actual rubber products, is the solvent swelling method. Here the rubber-wire composite is soaked in *ortho*-dichlorobenzene for up to several days. Afterwards, the loosened rubber is either way immediately removed by wiping it off with a clean lens tissue³⁸ or the sample is first heated at 120 °C for several hours and then the rubber is wiped off^{41,42}. However, the possibility of a mechanical damage of the adhesion layer, due to the wiping process, cannot be ruled out.

A relatively new technique to model the adhesion interface is the so-called filter paper method. Since its introduction a few years ago it has been widely used to study rubber-brass adhesion.^{19,63–66} This method uses a real rubber compound, but an interlayer, such as a filter paper, is inserted in between the rubber and the wires before the vulcanization. This filter paper allows the active sulfidating species (required to build-up the sulfide layers responsible for adhesion) to get through. Further, it should retain certain components of the rubber mixture (in particular polymeric constituents and carbon black) and therefore helps to remove the rubber after the curing reaction. A clean interface can be obtained by simply delaminating the rubber phase after the vulcanization process.¹⁹ However, the question rises whether samples obtained by this method reflect the real situation.

3 AIM OF THIS THESIS

The topic of this thesis is the investigation of the rubber-to-brass adhesion. The focus is set on the investigation of various factors (e.g. the compound composition) which might have an influence on the adhesion performance. In the future, this information can help to understand the adhesion mechanism of rubber-to-brass and as a result, may help to overcome some of the problems in reinforced rubber products.

Basically, this work can be divided into three major parts:

- The investigation of wires, which had similar dimensions and a very similar composition, but showed very different adhesion behavior.
- The investigation and comparison of different analytical methods which allow the study of the sulfidation reaction or the adhesion interface.
- The investigation of the influence of various rubber compound ingredients such as stearic acid, cobalt stearate and antioxidant agents.

In the first part, several wires which have the same design (diameter, brass-plating thickness, brass composition) will be examined by optical microscopy, focus variation microscopy, scanning electron microscopy coupled with energy-dispersive X-ray spectroscopy (SEM-EDX) and X-ray diffraction (XRD) to analyze the effect of the wire composition on the adhesion performance. Furthermore, the wires will be used in a squalene experiment to investigate differences in the sulfidation reaction. Afterwards, one wire sample will be chosen to be used for further experiments.

The second part of this work deals with the development of an appropriate sample preparation method. For this reason, two different methods described in literature (squalene method, filter paper method) will be tested, as well as one, developed in-house (metathesis method), and subsequently, compared to each other. The squalene method is a model system where a low-molecular weight analogue to natural rubber (squalene) is used. The filter paper method uses a real rubber compound but has a filter paper inserted in between the rubber and the wire, which helps to separate these two components after the vulcanization reaction. The metathesis method uses a catalytic system to chemically degrade the cross-linked rubber and thereby enables to remove the rubber without a mechanical impact on the adhesion interface.

In the last part, the influence of the rubber compound composition on the adhesion performance will be studied. This will be done by analyzing the effects of individual compound ingredients (stearic acid, cobalt stearate and antioxidant agents), on the adhesion properties (pull-out force, rubber coverage, adhesion interface), on the one hand, and on the rubber properties, on the other hand. A main part will be the investigation of the adhesion interface which will be obtained by squalene, filter paper or metathesis experiments.

4 RESULTS AND DISCUSSION

4.1 COMPARISON OF DIFFERENT WIRES

For the adhesion of brass-plated wires to rubber compounds not only the composition of the rubber mixture has an influence on the adhesion performance but also the wires themselves. Different wires may vary in terms of brass plating thickness, brass composition, ZnO layer thickness, lubricant residues, surface roughness etc.¹ In this chapter, three different wires (**Sp2**, **Sp3**, **Sp6**) were analyzed by different characterization methods, such as optical microscopy, focus variation microscopy, scanning electron microscopy coupled with energy dispersive X-ray spectroscopy (SEM-EDX) (15 keV) and X-ray diffraction (XRD). Optical characterization methods (optical microscopy, focus variation microscopy, SEM) were used to get an impression of the surface roughness and EDX and XRD were applied to determine the chemical composition of the wires. Furthermore, the XRD characterization allows the determination of the brass alloy phases (e.g. α -brass, β -brass). Although, all of these wires are supposed to have, according to their manufacturer, the same specifications (diameter, brass-plating thickness, brass composition 67.5 wt% Cu), they showed different behavior in terms of adhesion properties. For example, rubber-brass composites with **Sp2** always yielded better adhesion than **Sp3** and **Sp6**. **Sp6** sometimes resulted in good and sometimes in bad adhesion whereas composites with **Sp3** always gave the worst results. Therefore, the aim of this study was to detect the reason for these differences. In a further step, the reaction of the wires during the sulfidation process was investigated by squalene experiments.

Optical microscopy, focus variation microscopy and SEM images of the wires are shown in Figure 15. For the focus variation microscopy images an area of 145 x 110 μm was measured and further, the images were stretched 4fold in z-direction for a better visualization of the surface structures. On all samples drawing lines from the wire production process can be seen, which in consequence, lead to an irregular brass plating thickness. In the case of **Sp2**, the surface seems to be slightly rougher than for the other two wires. Apart from this difference, the wire samples look almost the same.

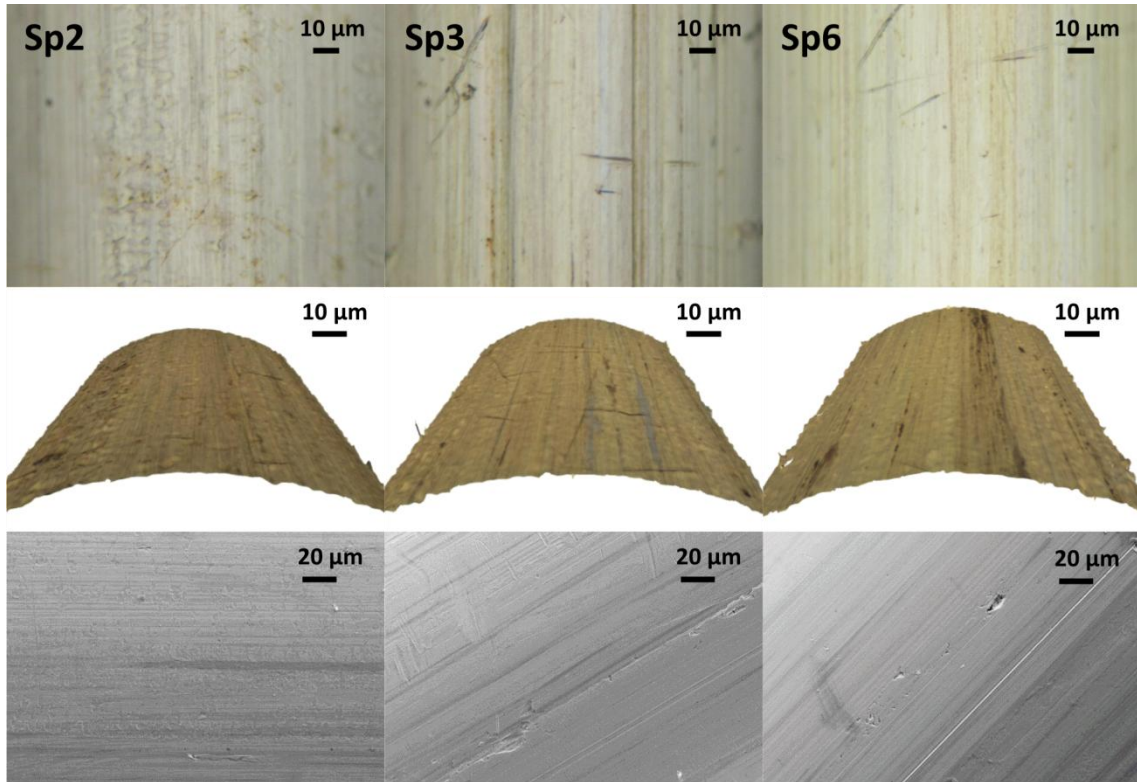


FIGURE 15. OPTICAL MICROSCOPY IMAGES (TOP), FOCUS VARIATION MICROSCOPY IMAGES (MIDDLE) AND SCANNING ELECTRON MICROSCOPY IMAGES (BOTTOM) OF THE DIFFERENT WIRE SAMPLES (SEM IMAGES RECORDED BY PETER PÖLT)

Therefore, the brass composition was analyzed by EDX and XRD. EDX results are shown in Table 1. The detected Cu levels are definitely lower than expected (67.5 wt% Cu). This discrepancy stems from the fact, that the surface is not flat and therefore, the calculated concentrations are rather roughly approximated values than accurate results. However, the wires all have the same diameter and therefore, values can be evaluated in comparison to each other to analyze a general trend. **Sp6** has the highest Cu content and **Sp3** the lowest. **Sp2** is in between, but closer to the Cu content measured for **Sp3**.

TABLE 1. EDX RESULTS FOR SP2, SP3 AND SP6

	Weight %		
	Sp2	Sp3	Sp6
Cu	62 ± 0	60 ± 1	66 ± 1
Zn	38 ± 0	40 ± 1	34 ± 1

XRD pattern and results are shown in Figure 16 and Table 2. For the measurement of the XRD patterns several wires were put next to each other and then placed into the XRD chamber in a way that the X-ray beam is parallel to the wire. This method allows analyzing the wires despite their curved surface and further the obtained result is an average of several pieces of the same wire. Nevertheless, the calculated concentrations should not be considered as accurate results, but values can be evaluated in comparison to each other.

In the XRD pattern (Figure 16) not only α -brass can be detected (42° , 49°) but also Fe from the steel core (45° , 65°). In the case of **Sp6**, an additional reflection around 63° can be seen. This reflection can be attributed to β -brass (43° , 63°), in which the second reflection at 43° is overlapped by the α -brass reflection. Normally, the occurrence of β -brass on wires for rubber reinforcement is undesirable, since β -brass is rather brittle and easily detaches from the wire surface. Such unstable parts would enhance the possibility of failure in the metal interface. Furthermore, in the case of **Sp6**, two separated α -brass reflections can be detected and for **Sp3** a shoulder also indicates a second α -brass phase. With the help of the lattice parameters of these reflections (determined by a Rietveld calculation) the composition of the α -brass phases can be calculated, as can be seen in Table 2. On all wires a Cu rich and a Cu depleted phase can be detected but to a different extent. For **Sp2** the brass composition is almost uniform, whereas for **Sp3** and **Sp6** two distinct phases can be determined. On the basis of these results, an average brass composition was calculated. Here the Cu content is definitely higher than for the results obtained by the EDX measurements but the same trend can be observed: **Sp6** has the highest Cu content, **Sp2** is in the middle and the Cu content of **Sp3** is slightly lower than for **Sp2**. Comparison of these results with the expected value (67.5 wt% Cu) shows the best correlation with the result for **Sp2**. Therefore, **Sp2** not only has the most uniform brass composition but the experimental determined composition is also closest to the wanted one.

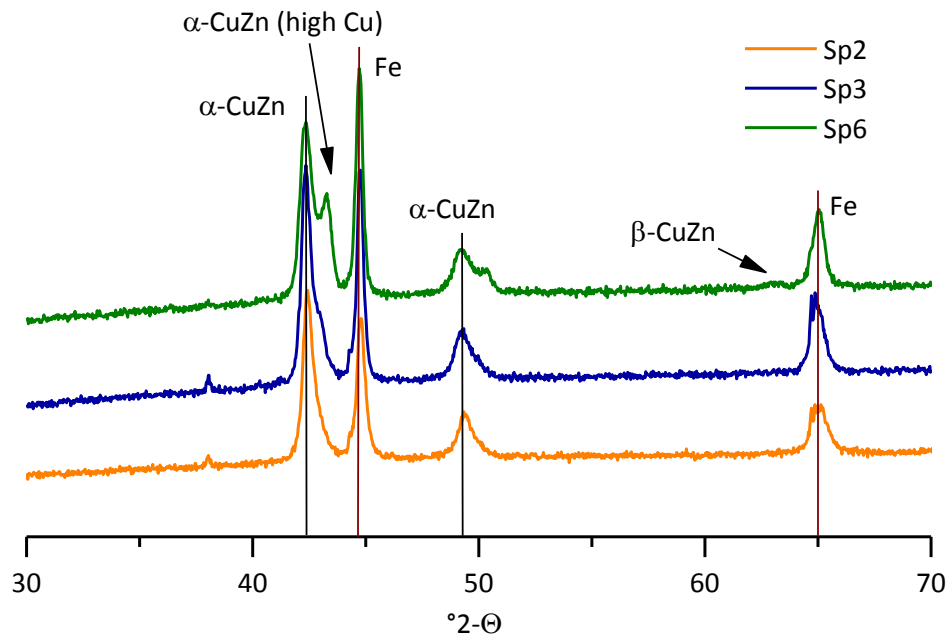


FIGURE 16. X-RAY DIFFRACTION PATTERN OF SP2, SP3 AND SP6

As mentioned before, not only brass is detected by XRD but also Fe from the steel core. With the help of a Rietveld calculation the ratio of the Fe to CuZn signal can be used to estimate the brass layer thickness. Due to the fact that the measured wires all have the same geometry, it is possible to compare the calculated values. As can be seen in Table 2, the brass layer for **Sp2** and **Sp3** are of the same dimension, but for **Sp6** the steel wire is plated by a thicker brass layer.

TABLE 2. X-RAY DIFFRACTION RESULTS FOR SP2, SP3 AND SP6

		wt% Cu ^{a)}	ratio CuZn/Fe (layer thickness)	average Cu content / wt%
Sp2	low Cu	65 ± 0 (97 ± 1)	0.69	66 ± 1
	high Cu	90 ± 2 (3 ± 1)		
Sp3	low Cu	59 ± 1 (57 ± 6)	0.69	65 ± 1
	high Cu	72 ± 4 (43 ± 6)		
Sp6	low Cu	64 ± 1 (70 ± 2)	0.72	72 ± 0
	high Cu	91 ± 1 (30 ± 2)		

^{a)} Data in parentheses give the percentage of the high and the low copper phase in the brass phase

4.1.1 SULFIDATION OF SP2, SP3 AND SP6 IN SQUALENE EXPERIMENTS

To study how the differences of the wires affect the sulfidation reaction, squalene experiments (compound formulation in Table 3, 90 min reaction time, see also chapter 4.2) were performed for all three wires.

TABLE 3. COMPOUND FORMULATION E

	phr
Squalene	100
Naphthenic oil	6
ZnO	7
Sulfur	6.25
DCBS	0.7
Cobalt stearate	1
Stearic acid	2

Results for the wires after the squalene experiment are shown in Figure 17. The upper part of the image shows the optical microscopy results, the middle part the focus variation microscopy images and the lower one, the SEM results. It is clearly visible, that the three wires react in different ways. In the optical microscopy image, **Sp2** has a yellow color with dark areas (mostly spots and some lamellar areas as well), **Sp3** and **Sp6** are greenish with dark spots. The same features can be seen in the focus variation microscopy images. In the SEM images, evenly distributed spot-shaped structures can be found on the surface of **Sp2**. The same applies to **Sp3**, but here, the structures seem to be smaller. **Sp6** shows a totally different picture. Spot-shaped structures can be found as well, but they are not as evenly distributed and further, these structures are bigger but also fewer.

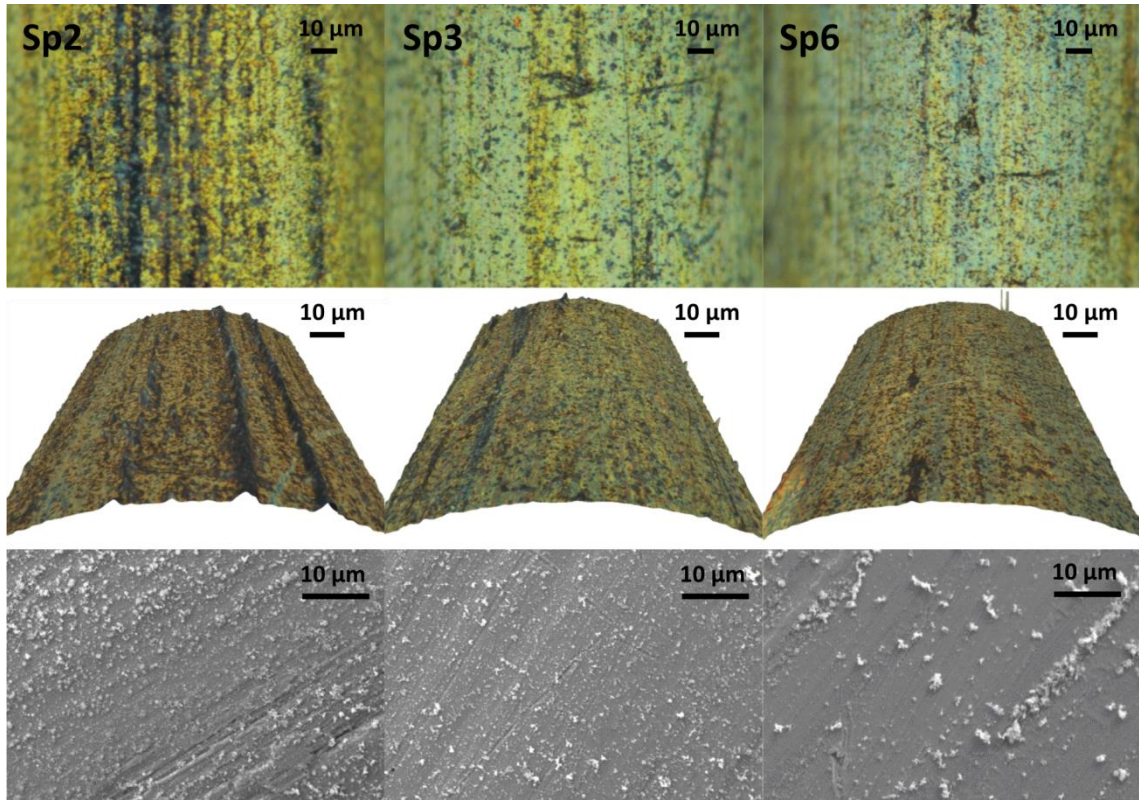


FIGURE 17. OPTICAL MICROSCOPY IMAGES (TOP), FOCUS VARIATION MICROSCOPY IMAGES (MIDDLE, 145X110 μM) AND SEM IMAGES (BOTTOM) OF SP2, SP3 AND SP6 AFTER THE SQUALENE EXPERIMENT

To analyze the effect of these optical differences on the sulfidation of the wires, the specimens were additionally analyzed by EDX (Table 4). The elements were normalized proportional to Cu, which was used as internal standard and set to a value of 100. Fe cannot be used as internal standard since it varies depending on the brass layer thickness and Zn cannot be used neither because it may change during the sulfidation reaction. On the one hand, parts of the ZnO layer of the wire surface might get dissolved by the stearic acid from the compound and on the other hand, some ZnO from the compound can be deposited on the wire surface. During the sulfidation reaction, some of the Cu is converted into Cu_xS , but this reaction has no impact on the total Cu amount. Therefore, Cu was used as internal standard.

TABLE 4. EDX RESULTS FOR SP2, SP3 AND SP6 AFTER THE SQUALENE EXPERIMENT

	Atom %			
	Cu	Zn	O	S
Sp2	100 ± 0	65 ± 2	27 ± 6	24 ± 2
Sp3	100 ± 0	66 ± 2	14 ± 2	21 ± 10
Sp6	100 ± 0	59 ± 2	25 ± 1	20 ± 5

The degree of reaction was determined by comparing the S levels of the wire surfaces. For **Sp2** the highest S level was detected, **Sp3** and **Sp6** have almost the same S level, which is clearly lower than the one measured for **Sp2**.

4.1.2 CONCLUSION

Three wires (**Sp2**, **Sp3**, **Sp6**), which had the same specifications, but behaved differently in terms of adhesion, were analyzed to determine the reason for this effect. Analysis of the untreated wires showed differences regarding the surface texture, the brass composition (two brass phases, Cu content) and the brass layer thickness. Also during squalene experiments the three wire types behaved differently. **Sp2**, which is known to yield good adhesion, had the highest sulfidation level after the squalene experiments. A possible explanation is that due to the rough wire surface, the sulfidation process starts more easily and further in a uniform way. Additionally there is only one brass phase, with an optimum Cu content.

Sp3 gives bad adhesion and the squalene experiments resulted in a lower sulfidation than for **Sp2**. **Sp3** has a very smooth surface and the Cu content is lower than for **Sp2**. Most probably the smooth surface hinders the sulfidation.

Sp6 has two distinct α -brass phases and an additional β -brass phase. This could be the explanation for the non-uniform distribution of the surface structures found in the squalene experiments. As a consequence, some parts of the wire have a higher sulfidation level than others and therefore, adhesion is sometimes good and sometimes bad.

This indicates that both, the brass layer composition and the surface roughness, are important parameters for the adhesion of rubber to brass. The composition should be

mostly uniform (and only α -brass) and further, a certain degree of surface roughness is necessary to ensure a good sulfidation.

Based on these results, **Sp2** was used for further studies (chapter 4.2). After this wire was finished a new wire sample (**Sp7**), which has the same good properties (similar results for the brass composition and the surface roughness) as **Sp2**, was used for all subsequent studies (chapter 4.3, chapter 4.4, chapter 4.5).

4.2 SULFIDATION REACTION IN SQUALENE EXPERIMENTS

In this chapter, specimens prepared by the squalene method were used to determine the relationship between the optical appearance, like color and structures, of the sulfidated wires and their composition. This was done by comparing optical microscopy and SEM-EDX results. Further, the correlation between the elements on a sulfidated wire was studied with the help of elemental maps.

Squalene experiments were performed as a model system to simulate the adhesion layer creation during the vulcanization reaction. For these experiments, a mixture of squalene (instead of natural rubber or polyisoprene) and all essential vulcanization components (e.g. zinc oxide, stearic acid, sulfur, accelerator, etc.) was prepared and the wires immersed into this mixture at 160 °C. To guarantee a uniform distribution, stirring of the mixture is necessary; however, to minimize flow effects it was paid attention to retain a turbulent stirring. After the reaction, the sulfidated wires were washed with toluene to remove all adhering components. Subsequently, the created adhesion layer was characterized by various methods.

4.2.1 COMPARISON APPEARANCE – COMPOSITION

Compound E (see Table 5) was used for a squalene experiment, in which treated wires were removed from the mixture every 2 minutes. This procedure allows studying the change of the optical appearance during the sulfidation reaction. Optical microscopy images of these specimens are shown in Figure 18.

TABLE 5. COMPOUND FORMULATION TO STUDY THE REALTIONSHIP OF OPTICAL APPEARANCE AND COMPOSITION

	A	B	C	D	E
	phr				
Squalene	100	100	100	100	100
Naphthenic oil	6	6	6	6	6
ZnO	7	7	7	7	7
Sulfur	6.25	6.25	6.25	6.25	6.25
DCBS	0.7	0.7	0.7	0.7	0.7
Cobalt stearate	1	1	1	1	1
Stearic acid	-	0.5	1	1.5	2

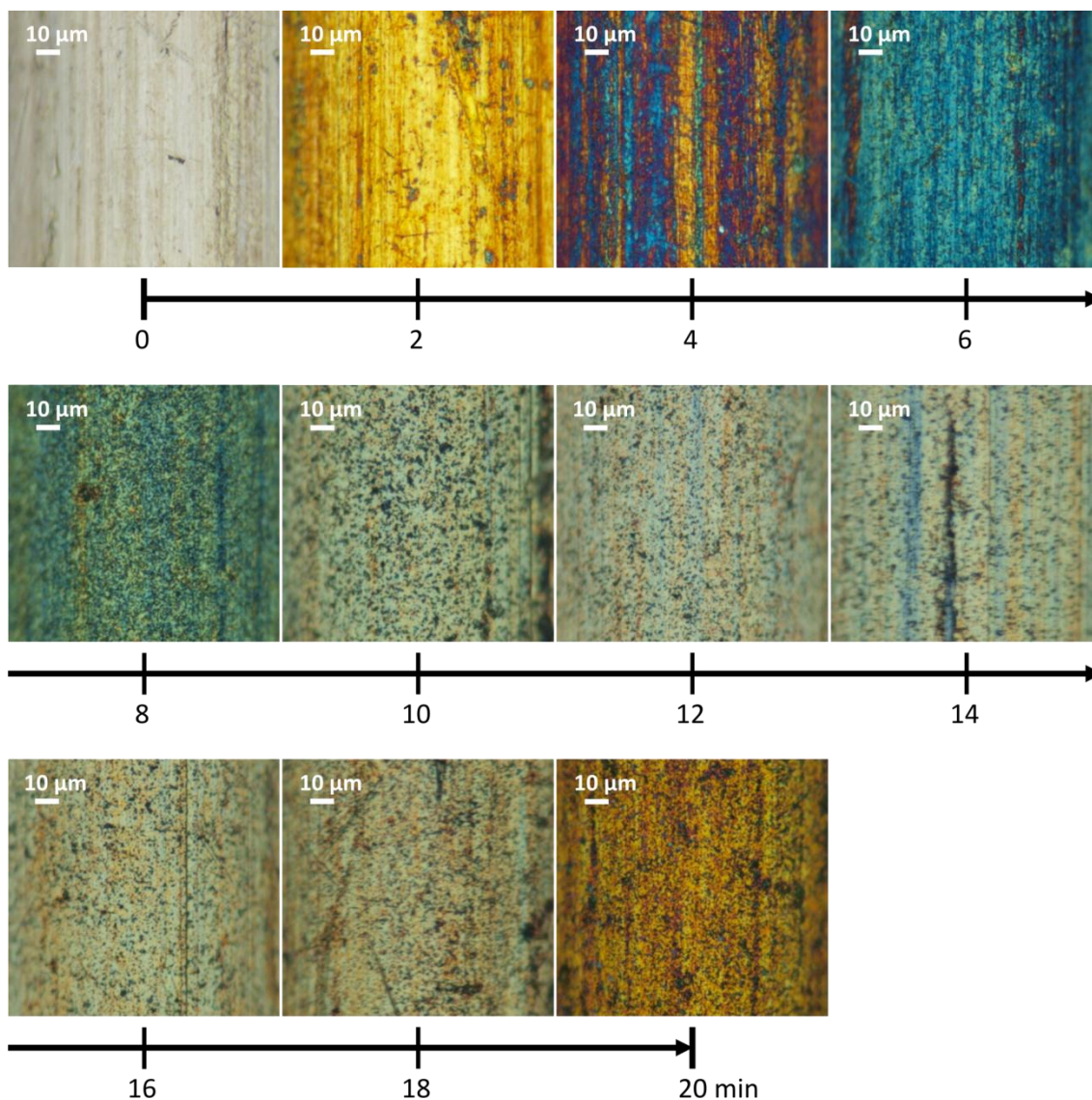


FIGURE 18. WIRES OBTAINED AFTER DIFFERENT REACTION TIMES IN A SQUALENE MIXTURE (COMPOUND E)

It is clearly visible, that the variation of the reaction time leads to different surface colors and structures. The untreated brass-plated wire has a pale color and is dominated by drawing lines from the wire production process. After 2 minutes of reaction time the color changes to a strong yellow, but the drawing lines can still be seen. After another 2 minutes (4 minutes reaction time) the surface color is now a mixture of orange, red and blue and after 6 minutes the wire has a completely blue color. With continuing reaction time, the color changes further from blue to green, to pale yellow and after 20 minutes reaction time to orange. But not only has the color changed during the reaction, the surface structures change as well. As mentioned

before, the untreated wire mainly consists of drawing lines, which can still be seen after short reaction times. After 8 minutes, additional spot-like structures can be found on all specimens, whereas the drawing lines almost vanish with increasing reaction time.

These structures can be seen especially well in the focus variation microscopy images (Figure 19). For the untreated wire, the most dominant surface structures are the drawing lines. After 20 minutes in the squalene mixture of compound **E** almost no drawing lines can be seen any more and the surface seems to be definitely rougher. Comparison of the real color and the color coded focus variation microscopy images shows that the dark spots seen in the optical microscopy images are actually peaks.

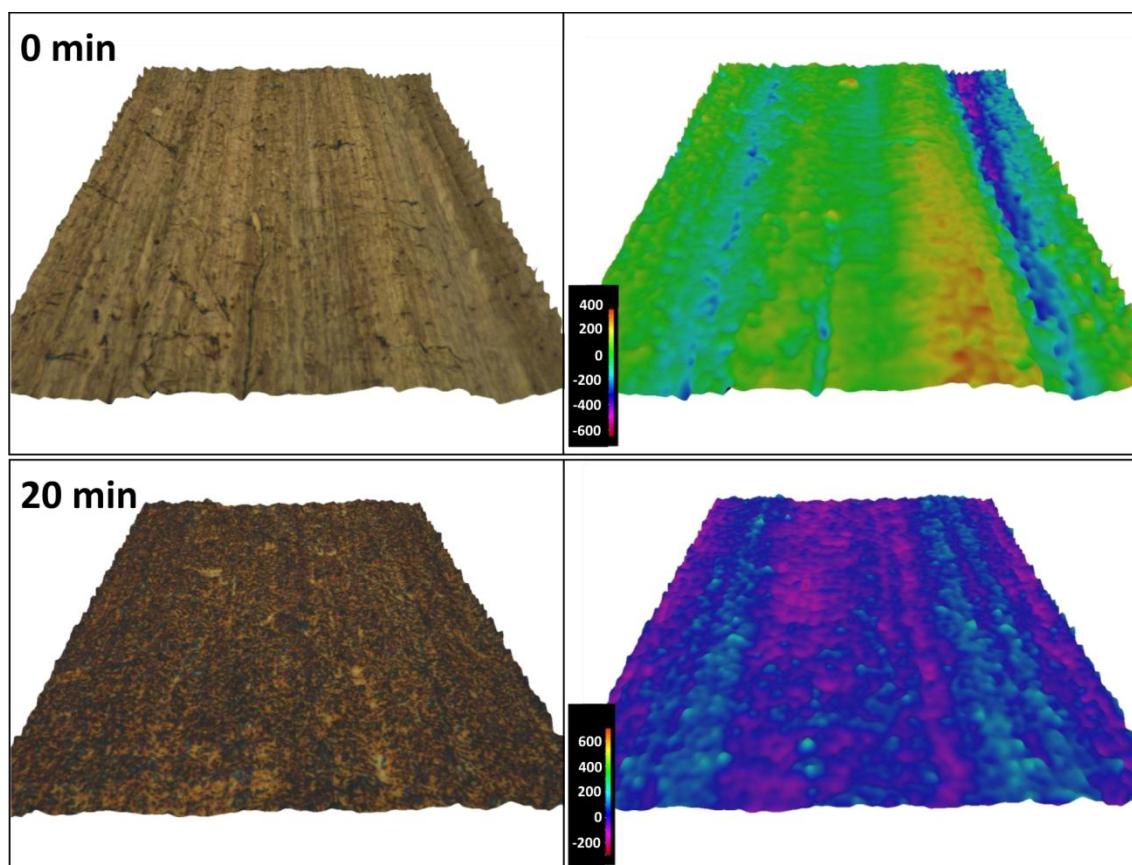


FIGURE 19. PLANARIZED FOCUS VARIATION MICROSCOPY IMAGES IN REAL COLOR (LEFT) AND COLOR CODED (RIGHT) OF THE UNTREATED WIRE (TOP) AND THE WIRE AFTER 20 MINUTES IN THE SQUALENE MIXTURE OF COMPOUND E (BOTTOM)

The same different surface colors of wires obtained in squalene experiments are not only caused by the variation of the reaction time but also by different compound compositions (see Figure 20). Wires were treated in squalene mixtures with different stearic acid levels (A-E, Table 5) to analyze the effect of the compound composition on the optical appearance. Furthermore, these wires were analyzed by EDX to compare the evolution of the element levels to the change of the surface colors (Figure 20). Zinc and iron levels are almost the same for all specimens. The iron level is not as constant as the zinc level, which can be explained by a non-uniformity of the brass plating. The oxygen level rises a little, but the changes are within the measuring inaccuracy. The biggest differences between the individual samples are the carbon and the sulfur levels. Both elements clearly increase, if the color changes from blue to green, yellow and finally orange. This leads to the conclusion that the surface color of the squalene treated wires is mainly a function of the sulfidation level. Therefore, the surface color can be used as a tool to get a first impression of the sulfidation level achieved during the experiment.

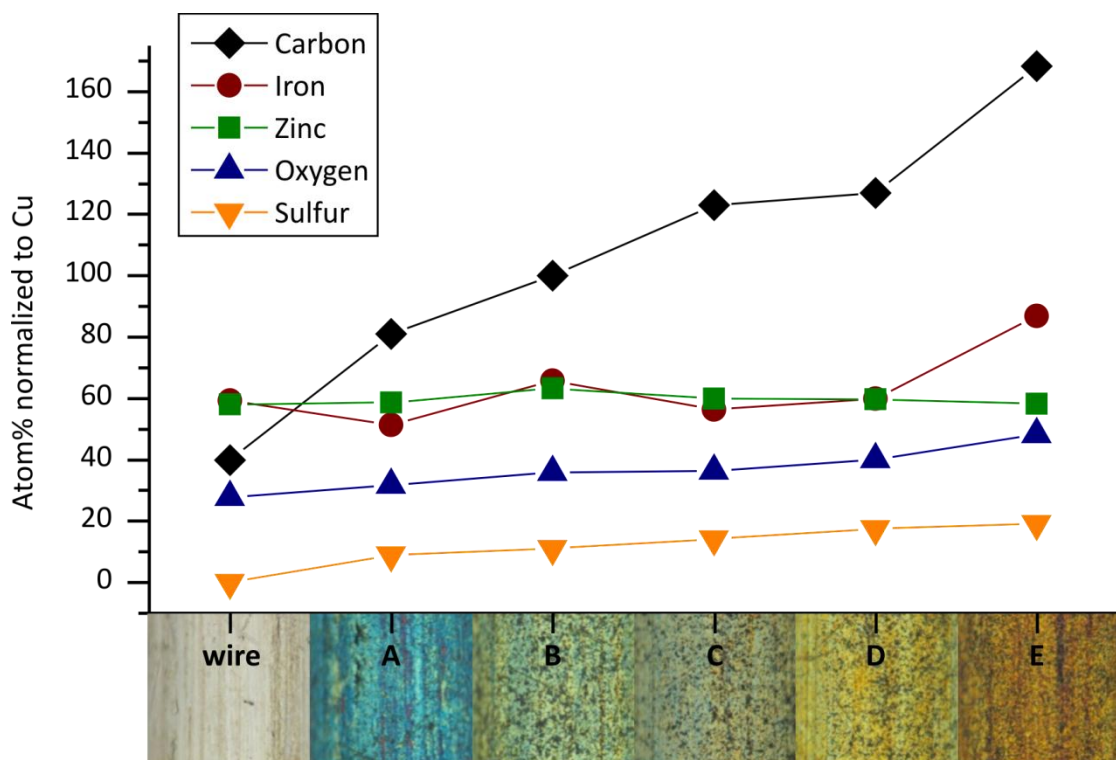


FIGURE 20. EDX ANALYSIS OF SQUALENE SPECIMENS FROM DIFFERENT COMPOUNDS (A-E)

4.2.2 COMPARISON OF OPTICAL MICROSCOPY IMAGES AND SEM-EDX

RESULTS

Three different squalene mixtures (see Table 6), one without ZnO (**F**), one without cobalt stearate (**G**) and one containing both ZnO and cobalt stearate (**E**) were prepared and the treated wires analyzed with optical microscopy and SEM-EDX. The structures and colors, which were observed in the optical microscopy, were compared to structures found in the SEM analysis and their elemental composition, which was determined by EDX. Compounds **F**, **G** and **E** were used because they result in very different sulfidation layers (e.g. different colors, structures, composition, etc.).

TABLE 6. COMPOUND FORMULATION TO COMPARE OPTICAL MICROSCOPY IMAGES AND SEM-EDX RESULTS

	F	G	E
	phr		
Squalene	100	100	100
Naphthenic oil	6	6	6
ZnO	-	7	7
Sulfur	6.25	6.25	6.25
DCBS	0.7	0.7	0.7
Cobalt stearate	1	-	1
Stearic acid	2	2	2

Optical microscopy images, SEM images and EDX results of wires treated in compounds **F**, **G** and **E** are shown in Figure 21, Figure 22 and Figure 23. Reaction time for these experiments was set to 90 minutes. Optical microscopy and SEM images are of the same magnification, so that structures found can be easily compared.

Results obtained for compound **F** (without ZnO) are shown in Figure 21. In the optical microscopy image, the surface mostly consists of lamellar arranged orange and blue areas. In the SEM image, drawing lines from the wire production process can be seen very well and further, some particles can be found on the surface. Two areas were chosen to be compared to the average composition. Area 1 is a part of the surface, where almost no surface structures can be found. The orange area in the optical microscopy has a similar appearance. The composition of this area is almost the same as the average composition of the image. The second region (2) analyzed by EDX, is one of the lamellar areas found in the SEM image. Again a similar area was marked in

the optical microscopy image. Comparison of the EDX results shows a definitely higher iron level for this area, which leads to the conclusion that this is a drawing line. There is almost no brass and therefore the iron level is considerably higher than in the average composition.

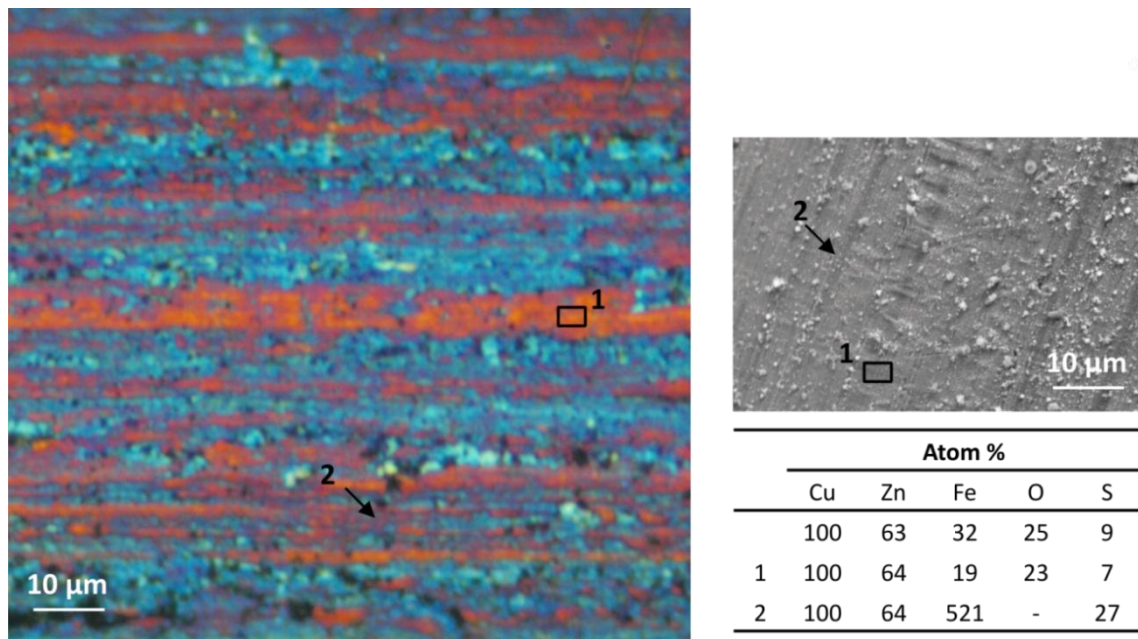


FIGURE 21. OPTICAL MICROSCOPY IMAGE (LEFT), SEM IMAGE (RIGHT, TOP) AND EDX RESULTS (RIGHT, BOTTOM) OF THE WIRE OBTAINED IN A SQUALENE EXPERIMENT WITHOUT ZNO (COMPOUND F) (SEM IMAGE RECORDED BY PETER PÖLT)

Results for compound **G** (without cobalt stearate) can be seen in Figure 22. The optical microscopy shows a pale green surface with a few dark spots. The most dominant features in the SEM image are the drawing lines, but a few spot-shaped structures can be seen as well. Two surface areas were chosen to be compared to the average composition. The first area (1) is one of the spot-shaped structures on the wire surface. A similar structure can be found in the dark spots found in the optical microscopy image. EDX analysis of this structure reveals very high zinc and oxygen levels as well as a high iron level. Therefore, it can be concluded that in this case, this structure is a ZnO particle, immobilized on a drawing line. Area 2 is a part of the surface, where almost no surface structures can be found. A similar area, green, without any dark spots, can be found in the optical microscopy image as well. The copper and zinc levels of this area are the same as for the average composition of the image, whereas the oxygen

and the sulfur level are a little bit lower. This leads to the conclusion that the sulfidation is higher in highly structured areas and lower in areas without surface structures.

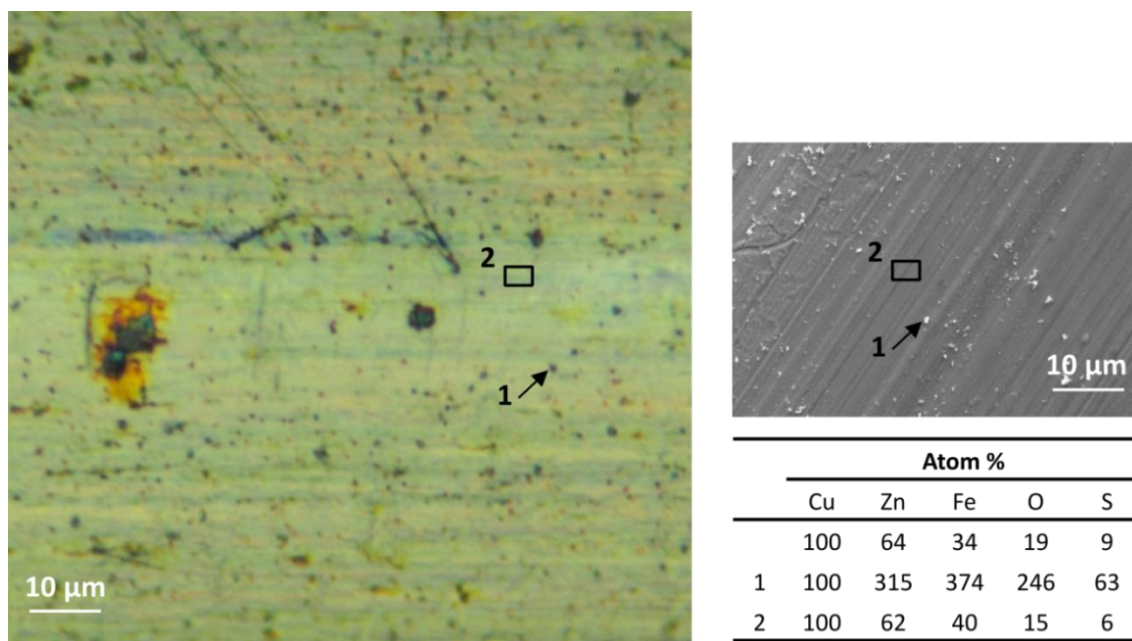


FIGURE 22. OPTICAL MICROSCOPY IMAGE (LEFT), SEM IMAGE (RIGHT, TOP) AND EDX RESULTS (RIGHT, BOTTOM) OF THE WIRE OBTAINED IN A SQUALENE EXPERIMENT WITHOUT COBALT STEARATE (COMPOUND G) (SEM IMAGE RECORDED BY PETER PÖLT)

Results obtained for compound **E** (containing both ZnO and cobalt stearate) are shown in Figure 23. In the optical microscopy image the specimen has a yellow color with a lot of dark spots on the surface. In the SEM image almost no drawing lines can be seen but instead many, partly accumulated structures can be found. These structures preferentially exist in lines, along the length of the wire. Two surface areas were chosen to be compared to the average composition. Area 1 is a part of the surface, where accumulated surface structures can be found. The dark area marked in the optical microscopy image has a similar appearance. EDX analysis of this region shows a very high sulfur level, whereas the zinc and iron levels are lower than in the average composition. This leads to the conclusion that these accumulated structures mostly consist of Cu_xS . The second analyzed area (2) is a region where almost no surface structures can be found. A similar region is the pale yellow area marked in the optical microscopy image. The copper and zinc levels of this area are almost the same as for

the average composition of the image, whereas the oxygen and the sulfur level are a little bit lower. Therefore the analysis of this specimen leads to the same conclusion as before, that highly structured surface areas have a high sulfidation level, whereas in areas without surface structures sulfidation is low.

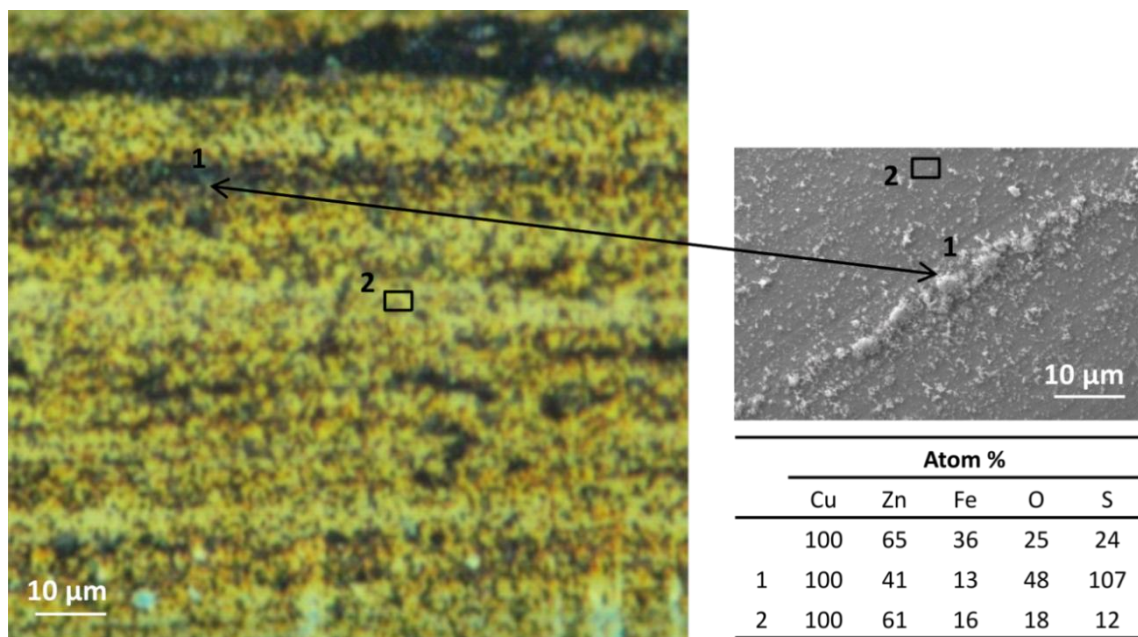


FIGURE 23. OPTICAL MICROSCOPY IMAGE (LEFT), SEM IMAGE (RIGHT, TOP) AND EDX RESULTS (RIGHT, BOTTOM) OF A WIRE OBTAINED IN A SQUALENE EXPERIMENT CONTAINING BOTH, ZNO AND COBALT STEARATE (COMPOUND E) (SEM IMAGE RECORDED BY PETER PÖLT)

4.2.3 CORRELATION STRUCTURES, ELEMENTAL COMPOSITION

A brass-coated wire was treated in a squalene mixture containing all essential vulcanization components (compound E, see Table 3; reaction conditions: 90 min, 160 °C) and consequently analyzed. Elemental maps of the surface were recorded by SEM-EDX and then used to investigate the correlation between the individual elements on a sulfidated wire.

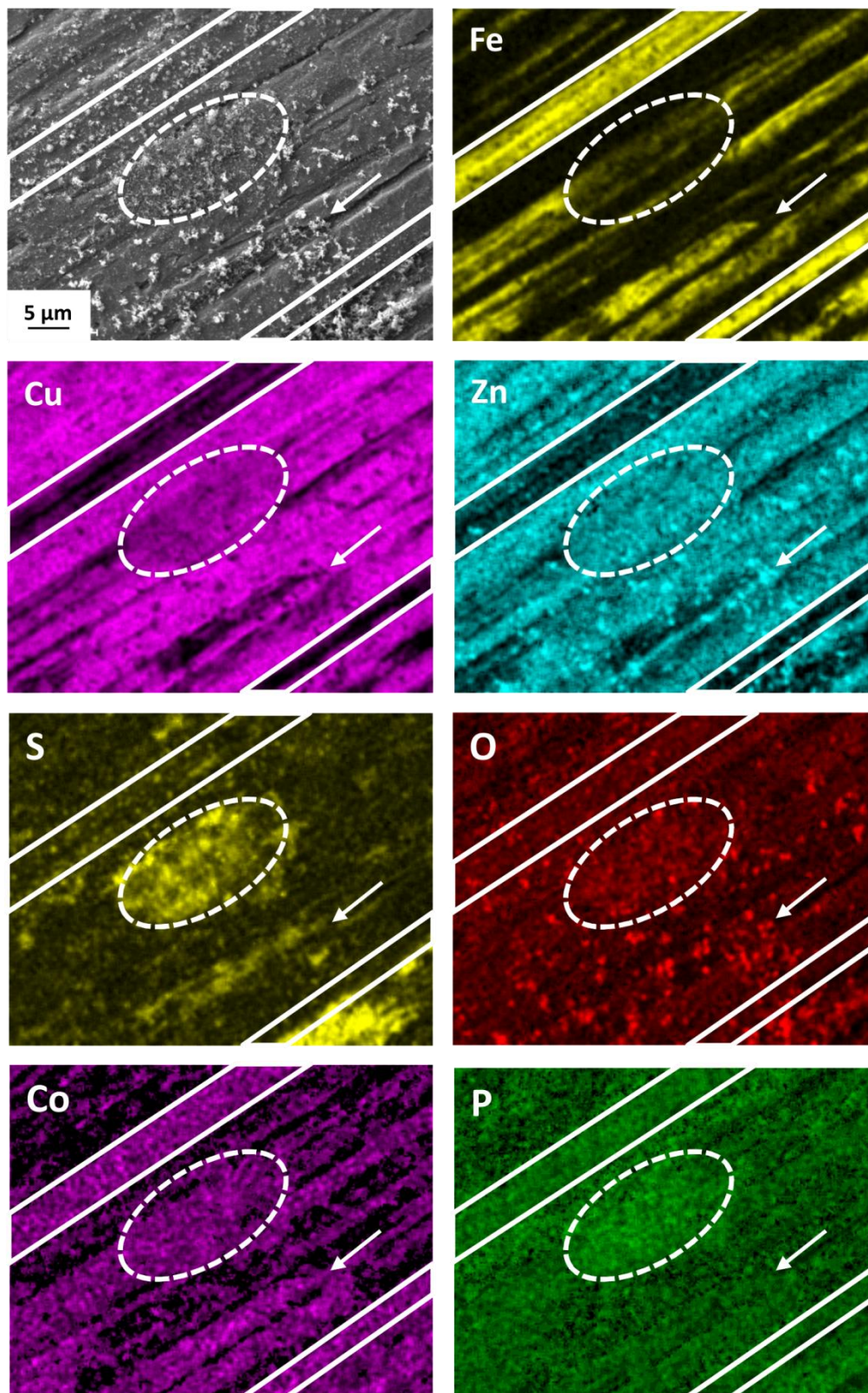


FIGURE 24. ELEMENTAL MAPS OF A SULFIDATED WIRE FROM COMPOUND E (IMAGES RECORDED BY PETER PÖLT)

Elemental maps of the squalene treated wire are shown in Figure 24. In these maps brighter colors correspond to higher concentrations of the respective element. Copper, zinc, iron sulfur, oxygen, cobalt and phosphor were measured. As can be seen in the maps, each element shows a different distribution on the wire surface. For a closer study two kinds of regions were analyzed in detail. The first area is marked in the maps with a solid line. Here the iron level is very high, whereas the copper and the zinc levels are rather low; this region is clearly a drawing line. Sulfur and oxygen levels are neither especially high nor low but cobalt seems to be attached to the drawing lines. Phosphor, which stems from the wire production process, seems to be a little bit higher in the drawing lines than in the surrounding area.

The second region, marked with a dashed line, is an area with accumulated surface structures. In this area the sulfur level is clearly increased and copper and cobalt as well. Zinc, oxygen and phosphor are partly increased. Therefore, it can be concluded that these structures are a complex accumulation of sulfides with some zinc oxide particles in between.

Results obtained by these elemental maps confirm the findings from the previous chapter, that sulfidation is higher for textured areas. A further look on the maps shows that some of the surface structures show high oxygen and zinc levels (marked with an arrow); these structures are most probably ZnO particles. This leads to the conclusion that the structures found on the surface are a mixture of complex sulfides (especially Cu_xS) and ZnO.

4.2.4 CONCLUSION

The comparison of the appearance (color, structure) of sulfidated wires with EDX results showed a correlation between the sulfur levels and the surface color. Therefore, it is possible to use the surface color to get a first impression of the sulfidation levels achieved during the experiments. However, if there are major modifications in the compound, the color scale has to be renewed.

Closer studies of the specimens revealed, that areas without many surface structures have a lower sulfidation level than highly textured areas. The analysis of the lines observed in the SEM images (and sometimes also in the optical microscopy images) showed high iron and low copper and zinc levels, which confirms the assumption that these structures are drawing lines from the wire production process. Further, it was

revealed that the accumulated dark spots mostly consist of Cu_xS . But not all of the particle-shaped structures are due to sulfides, in some cases, they are ZnO particles immobilized on the sulfidated surface.

4.3 INFLUENCE OF STEARIC ACID ON RUBBER-BRASS ADHESION

Parts of this chapter are already published in:

Investigation of the influence of stearic acid on rubber-brass adhesion – Ziegler, E.; Macher, J.; Gruber, D.; Pölt, P.; Kern, W.; Lummerstorfer, T.; Feldgitscher, C.; Holzner, A.; Trimmel, G.; *Rubber Chemistry and Technology*, **2012**, *85*, 264-276

4.3.1.1 INTRODUCTION

The purpose of this investigation is to determine the effect of the stearic acid concentration on the rubber adhesion. Stearic acid is normally added to rubber compounds to work in combination with ZnO as activator.^{67,68} Stearic acid reacts with ZnO to create soluble zinc stearate. A zinc-accelerator complex is built-up and stearic acid or amines work as ligands. This complex reacts with S₈-rings of the sulfur in the compound to create a polysulfide complex, which is responsible for sulfur transfer.⁶⁹ By this process, the effectiveness of the accelerator is enhanced. For this reason stearic acid loading affects not only the rubber properties but also the adhesion of rubber to brass-coated steel.

The effect of stearic acid on the adhesion was investigated by Jeon et al.,⁶⁰ who studied the effect of stearic acid contents in the range of 0 to 10 phr. The best adhesion values were achieved with a mixture containing 3 phr stearic acid for unaged compounds. Furthermore, he concluded that very high stearic acid loading deteriorates the adhesion properties.⁶⁰ Therefore, the present study investigates the influence of small variations in the stearic acid content in a range (0-2 phr), which is typically employed in rubber compounds.

In this study a simplified squalene mixture was used to analyze the adhesion interlayer created during the vulcanization reaction. But this approach cannot be used to investigate all aspects that concern actual adhesion. For this reason, a rubber compound, which is in analogy to the squalene mixture, was used to determine rubber properties and adhesion values depending on the stearic acid loading. The characterization of the adhesion layer was done by optical microscopy, focus variation microscopy and scanning electron microscopy coupled with energy dispersive X-ray analysis (SEM-EDX).

4.3.1.2 RESULTS AND DISCUSSION

The squalene method was used to analyze the influence of stearic acid on the adhesion layer created during the vulcanization reaction. Brass-plated wires were immersed into a mixture of squalene and all essential curing components for 20 minutes at 160 °C. After the reaction, the wires were washed with toluene and the newly built-up layer on the wire surface can be characterized without further pretreatment. This method has the advantage that the adhesion interface on the wire surface can be characterized without further pretreatment.

Squalene experiments were performed according to Hamed et al.⁴⁵ Formulations are given in Table 7. All mixtures contained squalene, naphthenic oil, zinc oxide, sulfur, DCBS and varying amounts of cobalt stearate and stearic acid. Co stearate has the function to act as an adhesion promoter. In samples **H_S** no Co stearate was used to obtain samples which are totally free from stearic acid.

TABLE 7. COMPOUND FORMULATIONS TO STUDY THE EFFECT OF STEARIC ACID ON RUBBER-BRASS ADHESION

	H / H _S	A / A _S	B / B _S	C / C _S	D / D _S	E / E _S
	phr					
NR / Squalene ^{a)}	100	100	100	100	100	100
Naphthenic oil	6	6	6	6	6	6
ZnO	7	7	7	7	7	7
Sulfur	6.25	6.25	6.25	6.25	6.25	6.25
DCBS	0.7	0.7	0.7	0.7	0.7	0.7
Cobalt stearate	-	1	1	1	1	1
Stearic acid	-	-	0.5	1	1.5	2

^{a)} Rubber compounds abbreviated H, A-E, squalene mixtures abbreviated H_S, A_S-E_S

Specimens for pull-out testing were prepared similar to ASTM D 1871. Compound formulations are identical to the formulations used in the squalene experiments, which are given in Table 7. A second testing series with carbon black (see Table 8) was also produced to get a better comparability with real rubber compounds. In compounds **H** and **O** no Co stearate was used to obtain samples which are totally free from stearic acid.

TABLE 8. NATURAL RUBBER COMPOUND FORMULATIONS TO STUDY THE EFFECT OF STEARIC ACID ON RUBBER-BRASS ADHESION

	O	P	Q	R	S	T
	phr					
Natural rubber	100	100	100	100	100	100
N 550 Carbon black	50	50	50	50	50	50
Naphthenic oil	6	6	6	6	6	6
ZnO	7	7	7	7	7	7
Sulfur	6.25	6.25	6.25	6.25	6.25	6.25
DCBS	0.7	0.7	0.7	0.7	0.7	0.7
Cobalt stearate	-	1	1	1	1	1
Stearic acid	-	-	0.5	1	1.5	2

Cure rate data (scorch time t_{05} , optimum curing time t_{90} , minimum torque ML , maximum torque MH) of the rubber compounds were obtained according to DIN 53529/3 (Table 9). Without carbon black, no distinct influence of stearic acid on the cure characteristics can be observed. However, with the addition of 50 phr carbon black, the optimum curing time slightly decreases. Additionally, the natural rubber specimens (H, A-E, O-T) were thermally aged for 4 h at 150 °C (data marked with prime symbol (')). These conditions should lead to an accelerated aging and thus should give information about the long term stability of the specimens.

TABLE 9. CURE CHARACTERISTICS (SCORCH TIME T05, OPTIMUM CURING TIME T90, MINIMUM TORQUE ML, MAXIMUM TORQUE MH) OF RUBBER COMPOUNDS WITH DIFFERENT AMOUNTS OF STEARIC ACID DETERMINED FROM THE RHEOMETER CURVES

	t_{05} , min	t_{90} , min	ML , dNm	MH , dNm
H	2.0	12.5	0.29	5.65
A	2.0	13.3	0.38	6.49
B	1.7	11.2	0.44	5.90
C	1.6	11.3	0.48	5.23
D	2.0	13.6	0.38	5.70
E	2.3	13.1	0.33	6.78
O	1.1	15.0	0.92	12.70
P	1.1	10.2	0.93	14.79
Q	1.3	9.8	0.74	17.23
R	1.2	8.9	0.95	16.08
S	1.3	9.1	0.94	17.21
T	1.4	9.8	0.82	16.24

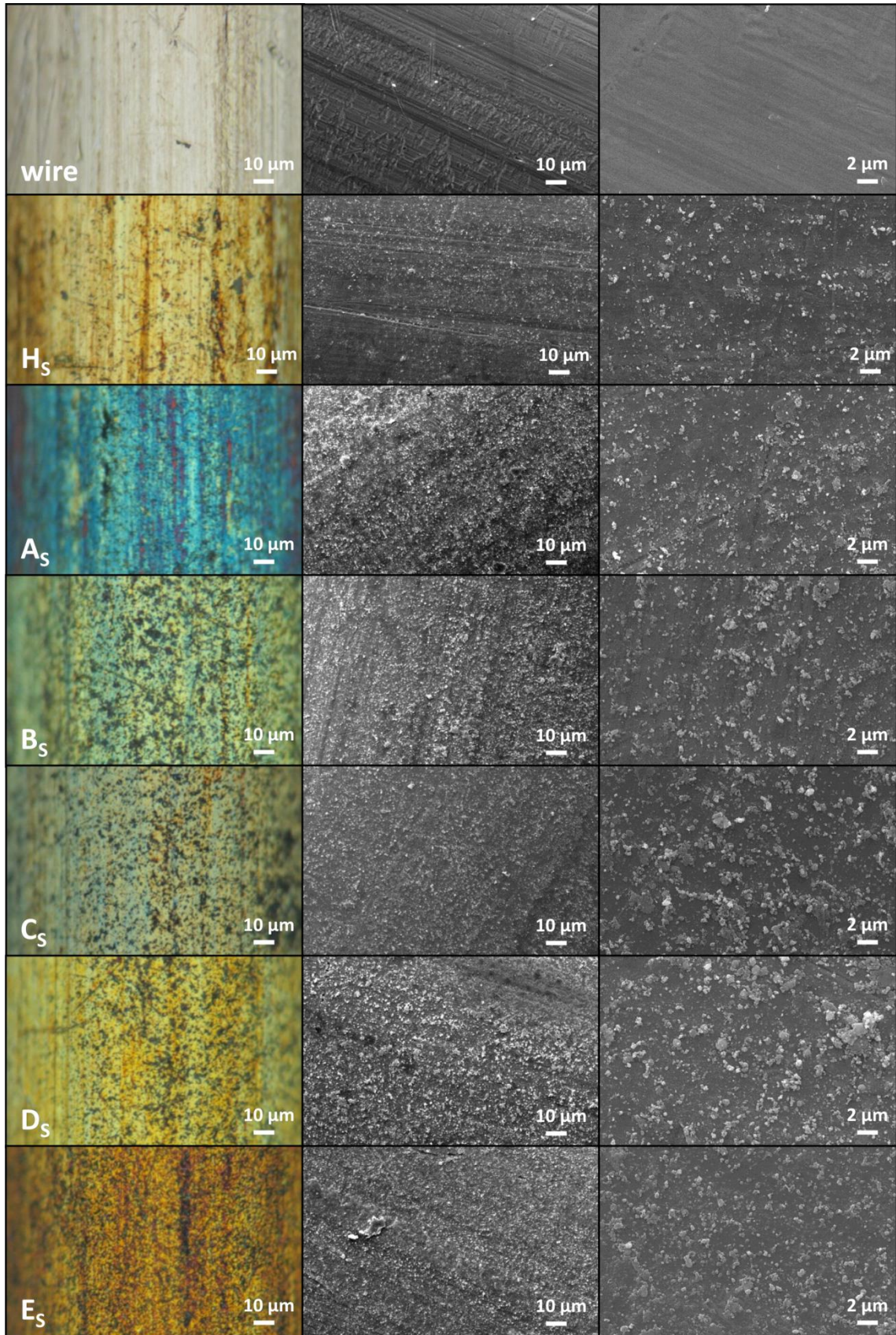


FIGURE 25. OPTICAL MICROSCOPY IMAGES (LEFT) AND SEM IMAGES (MIDDLE AND RIGHT) OF UNTREATED WIRE AND SAMPLES H_s, A_s-E_s

The samples, obtained by the squalene experiments were analyzed by optical microscopy and SEM-EDX (see Figure 25). The images show the wire surface after reaction in squalene mixtures with increasing amount of stearic acid. As can be seen in the optical microscopy images, the surface appearance changes depending on the amount of stearic acid used. The untreated brass-plated wire is dominated by drawing lines from the wire production process which can be easily seen in the optical microscopy image as well as in the SEM images. Sample **H_S** (without cobalt stearate and stearic acid) has a yellowish color but sample **A_S** is bluish. If the amount of stearic acid is increased, the color changes from greenish, over yellow to orange. But not only an alteration of the surface colors can be observed but also the surface structures change. Moreover, the structures seen in the samples are different depending on the amount of stearic acid used. Samples with lower stearic acid content (**H_S**, **A_S**, **B_S**) show drawing lines from the wire as the most dominant structures, in samples with higher stearic acid content, dark spots can be seen. Sample **B_S** shows both, pronounced drawing lines and dark spots. In samples with medium amount of stearic acid (**B_S**), the observed dark spots are bigger but fewer than the ones observed in samples with high stearic acid loading (**E_S**). The change of color and structure suggests an increasing sulfidation of the wires with increasing stearic acid content in the squalene mixture.

The structures seen in the optical microscopy can also be observed in the SEM images. Drawing lines can be easily seen in the images of the brass-plated wire. Samples with no or low stearic acid content (**H_S**, **A_S**, **B_S**) still show drawing lines but also some spot-like structures, which increase with higher amounts of stearic acid. The diameters of the observed structures are the biggest for samples **B_S-D_S** and decrease again with higher stearic acid loading.

Based on the optical differences observed between the samples with various amount of stearic acid, it can be assumed, that the stearic acid content has a direct influence on the reaction of the brass with the compound. With no or low stearic acid content the reaction of the wire seems to be less since the drawing lines can still be seen. If the amount of stearic acid is increased a spot-like structure can be identified on the squalene samples. These spots are fewer but more pronounced on samples with medium stearic acid amount in the squalene mixture (**B_S**) than on wires which have been treated in squalene mixtures with higher stearic acid content (**E_S**).

The obtained data suggests two possible mechanisms at the brass surface which would explain how the stearic acid loading affects the sulfidation. Firstly, the zinc oxide layer

is partly dissolved by the stearic acid and therefore, the reaction of the brass is accelerated. The second explanation is that because of the higher stearic acid content, more active sulfurating accelerator complexes are created and thus the brass reaction is accelerated.

TABLE 10. EDX ANALYSIS OF THE SEM IMAGES IN FIGURE 25

	Atom %					
	Cu	Zn	Fe	O	S	C
wire	100 ± 0	58 ± 1	59 ± 3	28 ± 1	-	40 ± 2
H_s	100 ± 0	60 ± 1	60 ± 1	36 ± 0	2 ± 0	34 ± 2
A_s	100 ± 0	59 ± 1	51 ± 0	32 ± 2	9 ± 0	81 ± 3
B_s	100 ± 0	63 ± 2	66 ± 0	36 ± 1	11 ± 0	100 ± 5
C_s	100 ± 0	60 ± 0	56 ± 0	36 ± 1	14 ± 0	123 ± 7
D_s	100 ± 0	60 ± 0	60 ± 6	40 ± 2	18 ± 1	127 ± 4
E_s	100 ± 0	58 ± 0	80 ± 21	34 ± 7	18 ± 2	144 ± 4

To prove these assumptions, additional characterization was done by EDX analysis of the wires from the squalene experiments (**wire**, **H_s**, **A_s**-**E_s**, see Table 10). In most cases, the specimens consist of a steel substrate with two layers on it: a brass layer, which may contain some additional elements like oxygen, sulfur and phosphor, and a mainly carbonaceous layer on top. At the electron energy used for the analysis (20 keV) the penetration depth of the electrons is bigger than the thickness of these layers and in the x-ray spectra there is also the signal from the steel substrate present. Therefore, the analysis volume is not homogeneous, additionally the surface is not flat and therefore any calculated concentrations of elements are rather roughly approximated values than accurate results. Additional errors can result from the fact that some elements, like oxygen or sulfur, can be bound to two layers. For example, oxygen can be bound in the ZnO layer as well as in the carbonaceous layer. But values can be evaluated in comparison to each other to analyze a general trend.

According to the EDX analysis (see Table 10) the surface of the untreated wire consists mainly of Cu, Zn and O. Fe of the steel core is detected as well. Before characterization, the wire was washed with toluene to remove organic residues and subsequently dried. Nevertheless, a carbon signal was detected which probably stems either from residual lubricant or from a contamination caused by the handling during the SEM-EDX analysis. Wires from the squalene experiments have an additional S peak, because of

the sulfide layer created during the sulfidation reaction. With increasing amounts of stearic acid, increasing amounts of S are detected, thus confirming the observations made by the optical characterization of the wires from the squalene experiments: stearic acid accelerates the sulfidation reaction on the wire surface.

As far as Zn is concerned, it is almost the same for all samples. The variation of the oxygen signal is constant within the experimental inaccuracy. With increasing amount of stearic acid content, a growing amount of carbon was detected. We attribute this increase to immobilized organic residues caused by the better interlocking of the cross-linked squalene with the peak shaped surface structure. Sample E_5 (2 phr stearic acid) shows increased amounts of Fe. This is caused by a thinner brass layer (probably due to drawing lines) and therefore more steel is detected.

Further characterization was done by focus variation microscopy. The focus variation microscope is a powerful tool to analyze surface structures. It enables the recording of an entirely sharp 3D-representation of a surface structure despite the wire geometry and it provides a good visualization of surface structures as can be seen in Figure 26. Drawing lines as well as new peak-like structures can be seen very well. The comparison of the real color and the color coded focus variation microscopy images (Figure 26) shows that the dark spots seen in the optical microscopy images are actually peaks, which is in accordance with Buytaert.⁶⁵

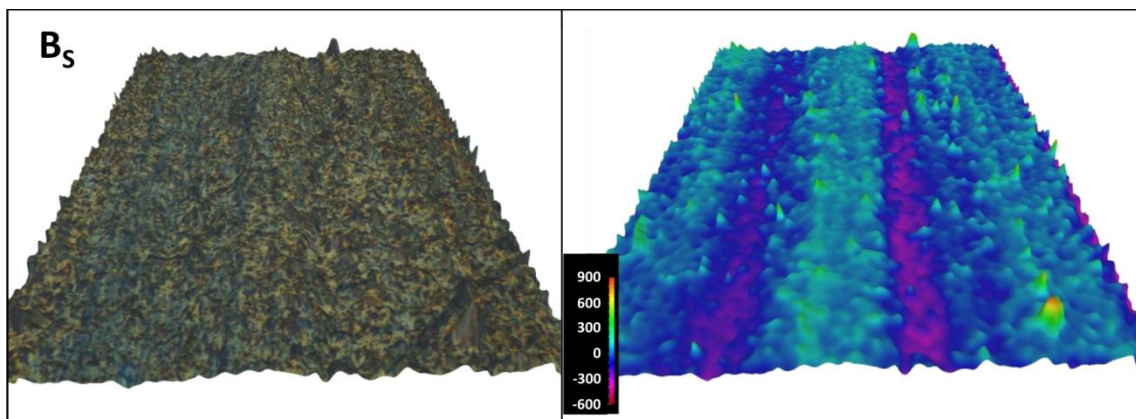


FIGURE 26. PLANARIZED FOCUS VARIATION MICROSCOPY IMAGE IN REAL COLOR (LEFT) AND COLOR CODED (RIGHT) OF A WIRE AFTER THE SQUALENE EXPERIMENT IN COMPOUND B_s

The focus variation data was further used to perform numerical calculations of the surface roughness. The mean surface roughness (S_a) represents a 2-dimensional measure of the texture comprising the surface. It is in analogy to the R_a parameter which represents the averaged roughness of a one-dimensional profile scan. S_a carries significantly more information about a given surface texture than the R_a parameter. Therefore, outliers have minor influence on the S_a values and its reproducibility is also better. However, it does not discriminate deep valleys from high peaks and it is not recommended to use S_a in case of height symmetry texture features. In this case, S_a may provide misleading signals. The R_a parameter is widely used in the field of mechanical engineering since decades.⁷⁰ The more powerful S_a parameter, which needs more sophisticated instrumentation for its determination, is about to be established in technical science as well. Overall, the S_a parameter is a good choice for detecting deviations in the texture characteristics.

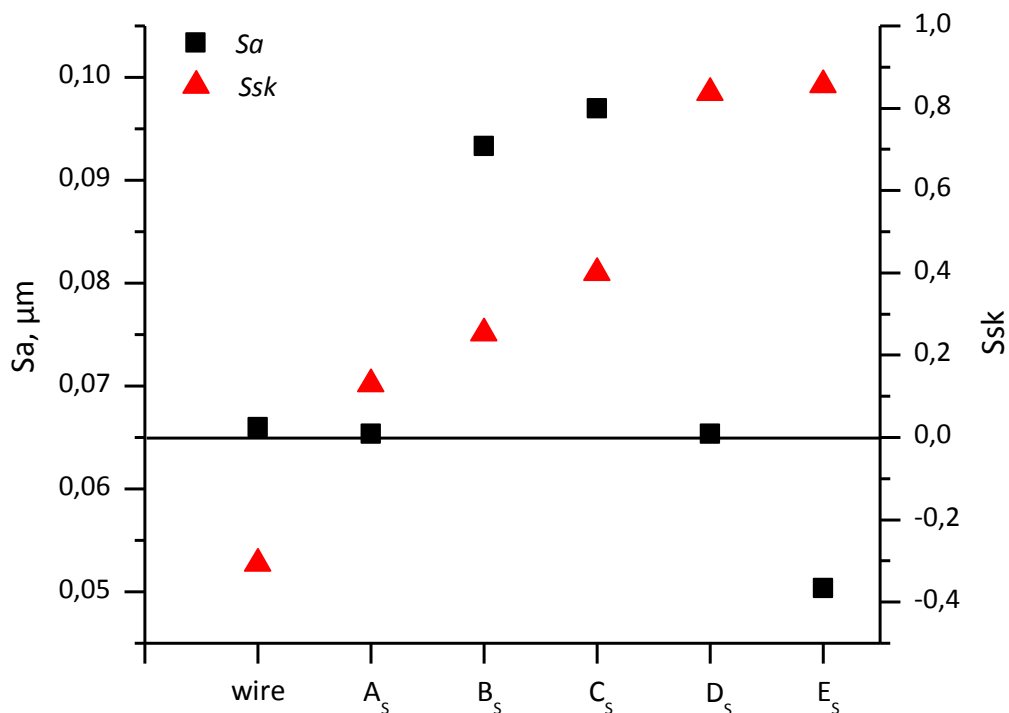


FIGURE 27. MEAN SURFACE ROUGHNESS (S_A) AND SKEWNESS (S_{SK}) OF THE UNTREATED SAMPLE AND THE SAMPLES AFTER THE SQUALENE EXPERIMENTS IN COMPOUNDS A_s - E_s

The calculated results are shown in Figure 27. For the untreated wire and samples A_s - E_s three similar samples were investigated each. As can be seen in the plot an overall

trend can be observed. The calculated Sa parameter (see Figure 27) is the highest for compound **B_s** and **C_s**. This can be explained by the results obtained through the optical characterization. The structures in the untreated wire and compound **A_s** are mainly dominated by drawing lines, while compound **D_s** and **E_s** lead to finely distributed peaks. In compounds **B_s** and **C_s** both type of structures, drawing lines and peaks, can be found. The existence of drawing lines and peaks at the same time leads to greater differences in the surface profile and therefore increases the surface roughness.

Another proof for these results is the analysis of the skewness (Ssk). Ssk is a parameter that relates the symmetry of the surface heights to the mean plane. The sign of Ssk shows the predominance of peaks ($Ssk > 0$) or valleys ($Ssk < 0$). If the value for Ssk is 0, the surface heights are symmetrically and normally distributed. Since Ssk involves the higher order powers of the surface heights a considerable amount of measurements is needed to provide statistically significant values. It also needs proper filtering to eliminate erroneous peaks and valleys.⁷¹ In Figure 27 Ssk values start from the negative for the untreated wire and turn to the positive for compounds with increasing amounts of stearic acid. Positive values show a tendency for peak-dominated surfaces, while negative values are indicative for valleys at the surface. For that reason, it can be concluded that for the untreated wire the drawing lines are the dominant structures. For **A_s**, **B_s** and **C_s**, the values are around zero or maybe slightly positive, which means that drawing lines as well as peaks are present as mentioned before. For wires treated in compound **D_s** and **E_s** the value is very high, which means a strong tendency to peak-dominated surface structures.

These roughness calculations explain clearly how the rough surface, which is necessary for mechanical interlocking, forms during the vulcanization process. Furthermore, it is an additional explanation for the fact that there is an optimal thickness of the sulfide layer. As can be seen in Figure 27, the roughness has a maximum and decreases again with stronger reaction of the brass.

However, not all aspects concerning the adhesion between rubber and brass can be investigated by squalene experiments as the created interface is only an artificial one. To correlate findings from the squalene experiments with actual values in rubber products two series of analog rubber compounds (containing natural rubber instead of squalene) were prepared. The first one had the same composition as the squalene mixtures (compounds **H**, **A-E**) and the second one additionally contained 50 phr carbon black (**O-T**) to get better comparability with real rubber compounds. Tensile strength,

elongation at break, tear strength (see Table 11) and pull-out forces (see Table 12) of these compounds were tested and compared to the results obtained from the squalene experiments. Thermally aged values for tear strength could not be obtained for compounds without carbon black, because the specimens were not mechanically stable enough after the aging treatment.

Carbon black in rubber compounds is used as reinforcing filler. Therefore, it is not surprising that compounds containing carbon black have higher values for tensile strength and tear strength.¹⁷ Values of unaged compounds are higher than aged ones (see Table 11). For compounds containing carbon black (unaged and aged), tensile strength slightly decreases with increasing amount of stearic acid. Compounds without carbon black show a contrary trend for the unaged specimens, the tensile strength increases with increasing amount of stearic acid.

TABLE 11. TENSILE STRENGTH, ELONGATION AT BREAK, AND TEAR STRENGTH OF RUBBER COMPOUNDS WITH DIFFERENT AMOUNTS OF STEARIC ACID

	Tensile strength, N/mm ²	Elongation at break, %	Tear strength, N		Tensile strength, N/mm ²	Elongation at break, %	Tear strength, N
H	3.6 ± 0.9	553 ± 69	8.3 ± 1.3	O	18.6 ± 0.2	418 ± 5	65.4 ± 8.1
A	8.1 ± 1.0	598 ± 22	15.5 ± 2.0	P	16.9 ± 0.7	390 ± 5	70.5 ± 12.0
B	9.8 ± 0.1	569 ± 9	16.3 ± 0.7	Q	15.5 ± 0.4	359 ± 5	89.3 ± 8.4
C	10.7 ± 2.1	582 ± 30	16.3 ± 1.6	R	15.9 ± 1.3	361 ± 25	57.6 ± 1.7
D	9.9 ± 1.3	597 ± 14	18.5 ± 3.9	S	15.0 ± 0.2	357 ± 9	63.4 ± 4.4
E	11.0 ± 0.8	568 ± 7	16 ± 1.3	T	14.6 ± 0.7	344 ± 8	67.2 ± 6.7
H'	3.9 ± 0.3	739 ± 176	-	O'	5.8 ± 0.3	308 ± 15	38.4 ± 2.5
A'	1.4 ± 0.2	450 ± 18	-	P'	5.2 ± 0.2	259 ± 2	38.4 ± 0.8
B'	1.1 ± 0.1	376 ± 32	-	Q'	4.5 ± 0.1	238 ± 5	37.6 ± 2.1
C'	1.0 ± 0.1	365 ± 6	-	R'	5.0 ± 0.1	242 ± 9	34.1 ± 0.7
D'	1.2 ± 0.2	409 ± 46	-	S'	4.9 ± 0.1	245 ± 8	35.3 ± 1.9
E'	0.9 ± 0.1	311 ± 15	-	T'	4.7 ± 0.1	247 ± 7	35.6 ± 1.7

Elongation at break for compounds without carbon black does not show a consistent trend with the loading amount of stearic acid. For compounds which contain carbon black, the elongation at break decreases with increasing content of stearic acid. This effect can be attributed to a higher crosslink density due to the activating effect of stearic acid.^{67,68} Values for tear strength are approximately of the same dimension

within a testing series (**H**, **A-E**; **O-T**; **O'-T'**) but do not show a consistent trend with stearic acid loading in any of the compound formulations.

Pull-out forces and rubber coverage are shown in Figure 28 and Table 12. No adhesion data could be obtained for thermally aged compounds without carbon black, because the specimens were not mechanically stable after the aging treatment. Compounds containing carbon black yielded higher values than unfilled compounds. In most cases level 3 coverage was observed, which means 100 % rubber coverage of the wire. Therefore, it can be concluded, that in these cases the adhesive strength exceeded the cohesive strength of the rubber and that the adhesion values obtained were only affected by the rubber properties. Filled unaged rubber compounds (**O-T**) have coverage levels between level 2 and 3 (level 2 = 50-99 %, level 3 = 100 % rubber coverage). This means that in cases with level 2 coverage, the adhesion partly fails. Therefore, these pull-out forces might be seen as real adhesion values. Aged filled compounds (**O'-T'**) have all coverage level 3. Thus it can be concluded, that it is mostly the rubber, which is the weak part whereas the adhesion interface does not break.

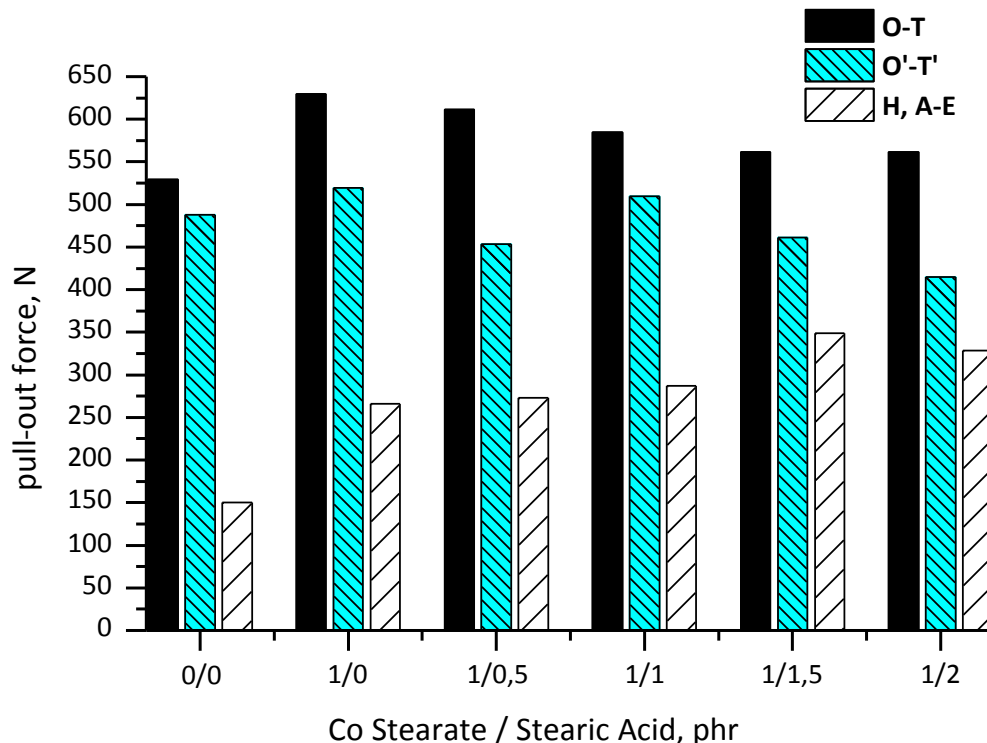


FIGURE 28. PULL-OUT FORCE OF RUBBER COMPOUNDS WITH DIFFERENT STEARIC ACID CONCENTRATIONS

TABLE 12. PULL-OUT FORCE AND RUBBER COVERAGE OF RUBBER COMPOUNDS WITH DIFFERENT AMOUNTS OF STEARIC ACID

	Pull-out force, N	Coverage		Pull-out force, N	Coverage		Pull-out force, N	Coverage
H	151 ± 35	3	O	530 ± 41	2	O'	488 ± 50	3
A	266 ± 31	3	P	630 ± 41	3	P'	520 ± 26	3
B	273 ± 15	3	Q	612 ± 50	2	Q'	454 ± 38	3
C	287 ± 16	3	R	584 ± 47	2	R'	509 ± 49	3
D	349 ± 29	3	S	561 ± 46	3	S'	461 ± 51	3
E	328 ± 16	3	T	562 ± 35	2	T'	415 ± 49	3

Compounds without Co salt (**H**, **O**, **O'**) showed lower values than comparable compounds with Co (**A**, **P**, **P'**). For compounds containing carbon black (aged and unaged), the highest values are obtained by compounds with low stearic acid contents (**P**, **P'**). These compounds contain a small amount of stearate due to the Co stearate, which has the function to act as an adhesion promoter.

In the case of the unfilled compounds highest pull-out forces were achieved with compound **D** (1.5 phr stearic acid). Coverage for all values was level 3. The comparison of the pull-out forces with tensile strength values show no correlation, but the comparison with tear growth data shows a similar trend. The tear strength values for unfilled compounds are quite low compared to the filled compounds. It seems as if tear growth is the weak point in these compounds. Therefore it is rather the rubber that fails than the adhesion layer, which is also shown by a rubber coverage level of 100 %.

Data obtained by pull-out testing suggests that very small amounts of stearic acid are good for the adhesion. Unfilled compounds have the best adhesion values for samples with 1.5 phr stearic acid, but coverage is 100 % and hence it is more likely that this results from the rubber properties of the sample. Unfortunately it is very likely that in most cases the adhesion values observed are due to the rubber properties, because the adhesive strengths exceed the cohesive strengths of the rubber compounds. Thus it is not possible to create a correlation between the data obtained through pull-out testing with the results from the squalene experiments.

4.3.1.3 CONCLUSION

In the squalene experiments, a great influence of stearic acid loading on the sulfidation reaction of brass-plated steel wires with rubber compounds could be observed. Increasing amounts of stearic acid accelerate the reaction of the rubber compounds with the brass-plated steel wires; this can be easily visualized by optical microscopy. The enhanced sulfidation with increasing amount of stearic acid can be attributed to two different effects: first, a partly dissolution of the ZnO layer on top of the brass surface, which leads to a faster reaction of the brass, and second, an activation effect. The higher concentration of formed zinc stearate leads to a higher concentration of the active zinc-accelerator complex and thus the sulfidation reaction is enhanced. However, this was not confirmed by the metathesis experiments. Here, variation of the stearic acid loading amount resulted in very small differences of the adhesion layer.

Investigation of roughness parameters showed an increasing amount of peaks and a vanishing of drawing lines with higher loading of stearic acid in squalene compounds. Furthermore, it was shown that there is an optimal amount of stearic acid (1.0 phr stearic acid) to achieve maximum surface roughness, which is important for good mechanical interlocking.

Variation of the stearic acid loading has a direct influence on the bonding interface but at the same time also a strong influence on the rubber properties. Therefore, a direct comparison of pull-out forces with rubber properties (tensile strength, elongation at break, tear strength) can help to separate these effects. Best pull-out forces were achieved with compounds with low stearic acid content. In most cases the rubber coverage was level 3, therefore, it was concluded that the measured adhesion values can be attributed to the rubber properties of these compounds, as can be seen by comparison with tensile strength and tear strength. Due to this fact it is not possible to directly correlate the results from the adhesion testing with the results obtained by the squalene experiments.

4.3.1.4 FURTHER RESULTS

In addition to the squalene experiments without carbon black, squalene experiments with 10 phr carbon black in the compound were performed to get a better comparability with actual rubber compounds (I₅-N₅, see Table 13). Furthermore, a real

adhesion interface obtained by the “metathesis method” was analyzed and the results compared to the ones from the squalene experiments.

The metathesis method uses a catalyst, which degrades the cured rubber by an olefin metathesis reaction, resulting in an exposed adhesion interface. Olefin metathesis reactions have been used for years to degrade all kinds of rubber chemically. For example it has been used to determine carbon black fillers in natural rubber⁷² or ethylene-propylene rubber in crosslink blends with 1,4-polybutadiene⁷³ as well as to study acrylonitrile/butadiene copolymers.⁷⁴ And there are many other examples.^{75–80} Lately olefin metathesis has been used as a tool to prepare techelic oligomers out of polyisoprene and natural rubber.^{81–83}

Here, the rubber of T-test specimens of the compounds without carbon black (see Table 7) was degraded by this method (metathesis degradation method 1) and the resulting samples labeled **H_M**, **A_M-E_M**.

TABLE 13. SQUALENE MIXTURE FORMULATIONS CONTAINING 10 PHR CARBON BLACK

	I_S	J_S	K_S	L_S	M_S	N_S
	phr					
Squalene	100	100	100	100	100	100
N 550 Carbon black	10	10	10	10	10	10
Naphthenic oil	6	6	6	6	6	6
ZnO	7	7	7	7	7	7
Sulfur	6.25	6.25	6.25	6.25	6.25	6.25
DCBS	0.7	0.7	0.7	0.7	0.7	0.7
Cobalt stearate	-	1	1	1	1	1
Stearic acid	-	-	0.5	1	1.5	2

The samples, obtained by the squalene and the metathesis experiments, were analyzed by optical microscopy and SEM-EDX (see Figure 29). Similar to the wires from the squalene experiments without carbon black (**H_S**, **A_S-E_S**), the surface color of the wires from the squalene experiments containing carbon black (**I_S-N_S**) changes depending on the stearic acid concentration of the squalene mixture. Sample **I_S** (no stearic acid, no cobalt stearate) has a yellow color, samples **J_S-L_S** (0-1 phr stearic acid) are orange-blue and the samples from the mixtures with the highest stearic acid concentration (**M_S-N_S**) are orange greenish. Compared to the specimens without carbon black (**H_S**, **A_S-E_S**), the changes in the color of specimens **I_S-N_S** are not as

pronounced. Therefore, it can be assumed that there are also fewer differences in the sulfidation level of these samples. Further drawing lines are very dominant in all samples (**I_S-N_S**), but dark spots are also seen on all samples of this series with exception of **K_S** (0.5 phr stearic acid). The dark spots in this series are more pronounced than in the series without carbon black. For this reason, these dark areas are most probably due to the carbon black, which is immobilized on the rough Cu_xS surface.

As far as the SEM images are concerned, sample **I_S** (no cobalt stearate, no stearic acid) looks totally different than the other specimens. In agreement with the optical microscopy images, drawing lines are the most dominant structures in **I_S**, whereas almost no spot-like structures can be detected. On the specimens **J_S-N_S** many bulky structures can be found, which correlate very well with the dark areas found in the optical microscopy.

For the metathesis samples (**H_M, A_M-E_M**), appearances of the individual samples in the optical microscopy are very similar to each other with the exception of sample **H_M** (no cobalt stearate, no stearic acid), which has a pale green color. The other samples are a mixture of green and yellow. This would suggest that the sulfidation level is also very similar for samples **A_M-E_M**. Further, it is evident, that all of the metathesis samples contain lamellar shaped dark areas. These are most probably due to an incomplete removal of the rubber compound. The optical appearance of the metathesis samples (**H_M, A_M-E_M**) in the SEM images differ from the ones obtained in the squalene experiments. The structures are not as clearly separated as in the squalene experiments and they seem to be a little bit more bulky. In agreement with the optical microscopy images, samples **A_M-E_M** look very similar to each other, but specimen **H_M** looks different. Here, the structures seem to be much finer.

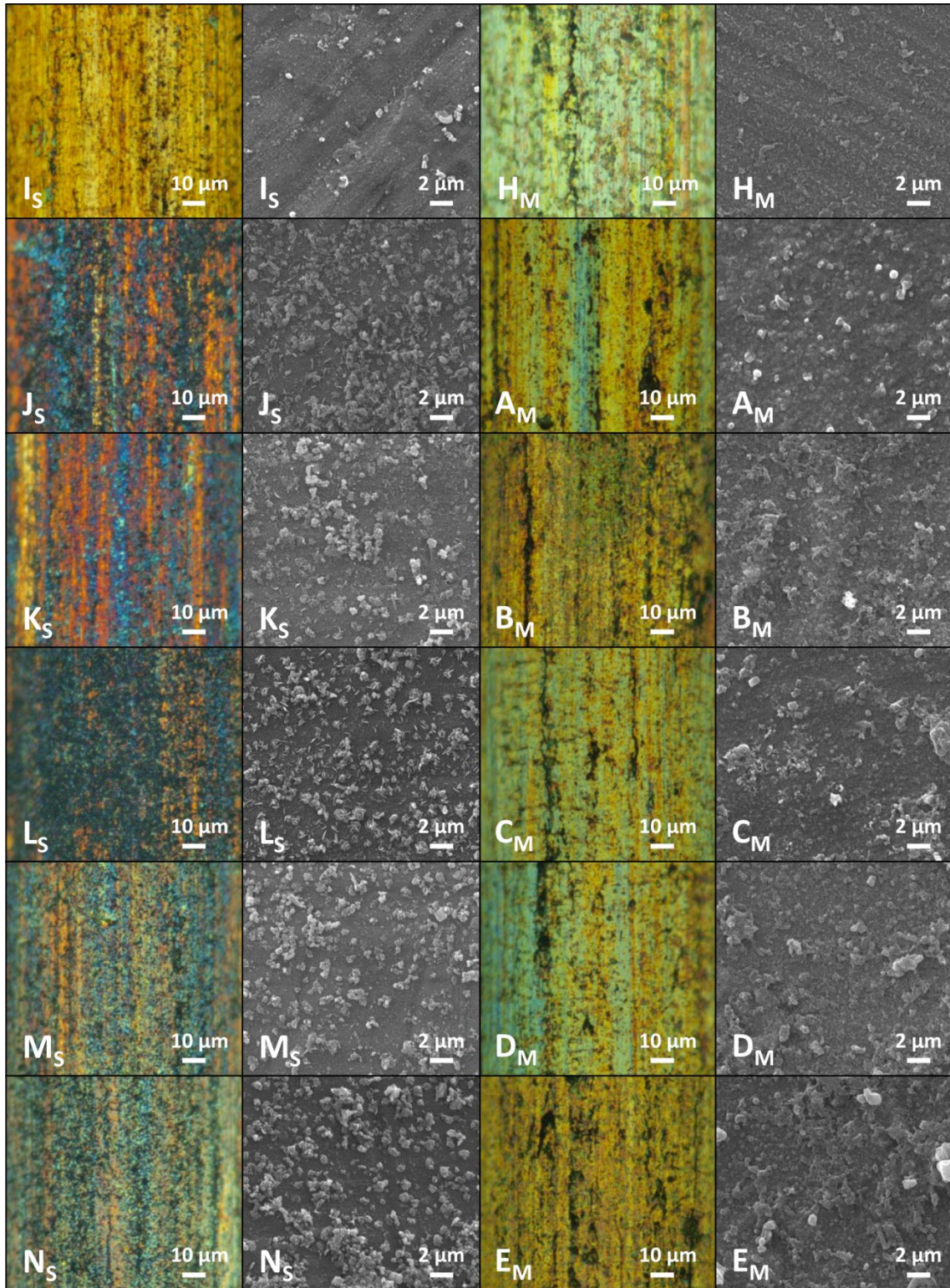


FIGURE 29. OPTICAL MICROSCOPY IMAGES AND SEM IMAGES OF SAMPLES FROM SQUALENE MIXTURES CONTAINING 10 PHR CARBON BLACK (LEFT) AND OF METATHESIS SAMPLES (RIGHT) TO STUDY THE INFLUENCE OF STEARIC ACID ON RUBBER-BRASS ADHESION

TABLE 14. EDX ANALYSIS OF THE SEM IMAGES IN FIGURE 29

	Atom %					
	Cu	Zn	Fe	O	S	C
I_S	100 ± 0	54 ± 2	73 ± 14	34 ± 3	5 ± 1	72 ± 15
J_S	100 ± 0	58 ± 0	56 ± 4	33 ± 0	8 ± 1	129 ± 13
K_S	100 ± 0	59 ± 1	57 ± 9	31 ± 1	7 ± 1	104 ± 5
L_S	100 ± 0	60 ± 2	71 ± 21	37 ± 5	10 ± 2	190 ± 70
M_S	100 ± 0	60 ± 1	54 ± 1	36 ± 4	11 ± 2	134 ± 3
N_S	100 ± 0	61 ± 1	62 ± 18	40 ± 8	14 ± 1	206 ± 76
H_M	100 ± 0	59 ± 2	38 ± 11	25 ± 4	3 ± 1	93 ± 11
A_M	100 ± 0	57 ± 1	73 ± 34	42 ± 5	7 ± 1	166 ± 24
B_M	100 ± 0	64 ± 4	43 ± 8	38 ± 7	8 ± 3	220 ± 89
C_M	100 ± 0	57 ± 4	71 ± 47	47 ± 13	7 ± 3	176 ± 64
D_M	100 ± 0	63 ± 4	40 ± 17	46 ± 8	8 ± 1	195 ± 38
E_M	100 ± 0	62 ± 2	45 ± 18	35 ± 2	8 ± 2	158 ± 22

For a further characterization, the samples were analyzed using EDX (see Table 14). The wires from squalene mixtures with carbon black (**I_S-N_S**) show increasing amounts of sulfur with increasing stearic acid concentrations, however, this increase is not as pronounced as for wires from squalene mixtures without carbon black (**H_S, A_S-E_S**, Table 10). This is in accordance with the observation made for the optical microscopy images: a change of color can be observed but the differences are smaller than for wires from squalene mixtures without carbon black. Further, considerably higher amounts of carbon are detected for the samples from squalene mixtures containing carbon black. Therefore, the dark areas observed on these samples are most probably due to immobilized carbon black in the rough non-stoichiometric copper sulfide layer.

For the wires obtained by the olefin metathesis degradation (**H_M, A_M-E_M**), the sulfur levels are almost the same with exception of the wire from compound **H_M** (no cobalt stearate, no stearic acid), where the sulfur levels is considerably lower.

Briefly summarized, for squalene mixtures containing carbon black (**I_S-N_S**) the same effects can be observed as in squalene mixtures without carbon black (**H_S, A_S-E_S**) but not as pronounced. However, totally different results are observed for the metathesis samples (**H_M, A_M-E_M**), where almost no influence of stearic acid could be observed.

Due to these observations, the squalene and the metathesis method are subjected to a closer examination (chapter 4.4 - Comparison of different analytical methods).

4.4 COMPARISON OF DIFFERENT ANALYTICAL METHODS

4.4.1 INTRODUCTION

In the previous chapter (4.3 - Influence of stearic acid on rubber-brass adhesion) it was shown, that there is no relation between results obtained by the squalene experiments and the measured pull-out forces. Therefore, the squalene experiments allow little prediction of the adhesion properties. Furthermore, very different results were obtained in the squalene and the metathesis experiments. In the squalene experiments, compound variations had a great influence on optical appearance and the composition of the adhesion layer. However, in the metathesis experiments this effect could not be observed.

Therefore, in this chapter these two methods, together with a third one (filter paper method), are closely investigated to show advantages and limitations of the three methods so that for further mechanistic studies they can be applied in the right way to gain new insight into the adhesion mechanism of rubber-to-brass. All of the presented methods allow the exposure of a clean interface (necessary for many characterization methods) without destroying the binding layer. Compared to the previous studies, the metathesis method is further extended to include carbon black filled rubber compounds to be closer to actual rubber compounds.

The third option, the so-called “filter paper method”, has been introduced a few years ago. Since then, it has been widely used to study rubber-brass adhesion.^{19,63–66} This method uses a real rubber compound, but a filter paper is inserted as an interlayer in between the rubber and the wires before the vulcanization. This filter paper allows the active sulfidating species (required to build-up the sulfide layers responsible for adhesion) to get through. But, it retains certain components of the rubber mixture (in particular polymeric constituents and carbon black) and therefore helps to remove the rubber after the curing reaction.¹⁹

For the experimental part brass-plated steel wires were treated by the three different methods, using analog compounds. In the case of the squalene experiments, simplified squalene mixtures were used, which contained all essential vulcanization components. However, squalene experiments with 50 phr carbon black were not performed, because carbon black increased the viscosity of the mixture a lot and, at 50 phr loading, a sufficient stirring could not be guaranteed. Analogous natural rubber

compounds were used to prepare T-test specimens (half of it with inserted filter paper, half without) to be analyzed with the help of the filter paper method and the metathesis degradation method 1. All experiments were carried out as similar as possible. The adhesion interface of the squalene treated wires (marked with a subscript S) as well as for sulfidated wires obtained by the filter paper (marked with a subscript F) and the olefin metathesis method (marked with a subscript M) was studied using optical microscopy, SEM-EDX and Raman spectroscopy.

4.4.2 RESULTS AND DISCUSSION

Compound formulations are shown in Table 15. All mixtures contained squalene or natural rubber, naphthenic oil, zinc oxide, stearic acid, sulfur, DCBS, cobalt stearate and varying amounts of carbon black. For the squalene experiments only compounds **E** and **N** were used, since the addition of 50 phr carbon black results in a very high viscosity, which inhibits the necessary stirring.

TABLE 15. COMPOUND FORMULATION TO STUDY THE INFLUENCE OF THE SAMPLE PREPARATION METHOD

	E ^a	N ^a	T
	phr		
Squalene / Natural rubber	100	100	100
Naphthenic oil	6	6	6
ZnO	7	7	7
Stearic acid	2	2	2
DCBS	0.7	0.7	0.7
Sulfur	6.25	6.25	6.25
Cobalt stearate	1	1	1
N550 Carbon black	0	10	50

^{a)} Labeled compounds were also used for squalene experiments

Optical microscopy images of the various samples are shown in Figure 30. Squalene samples from mixtures with different amount of carbon black are shown in the upper part (**E_S**, **N_S**). As can be seen in these images, the wire surfaces are different depending on the compound composition used. Sample **E_S** (no carbon black) has a bluish green color with dark spots and sample **N_S** (10 phr carbon black) is mostly bluish (containing

some orange areas) with many dark spots. This suggests different sulfidation levels depending on the carbon black concentration of the squalene mixture.

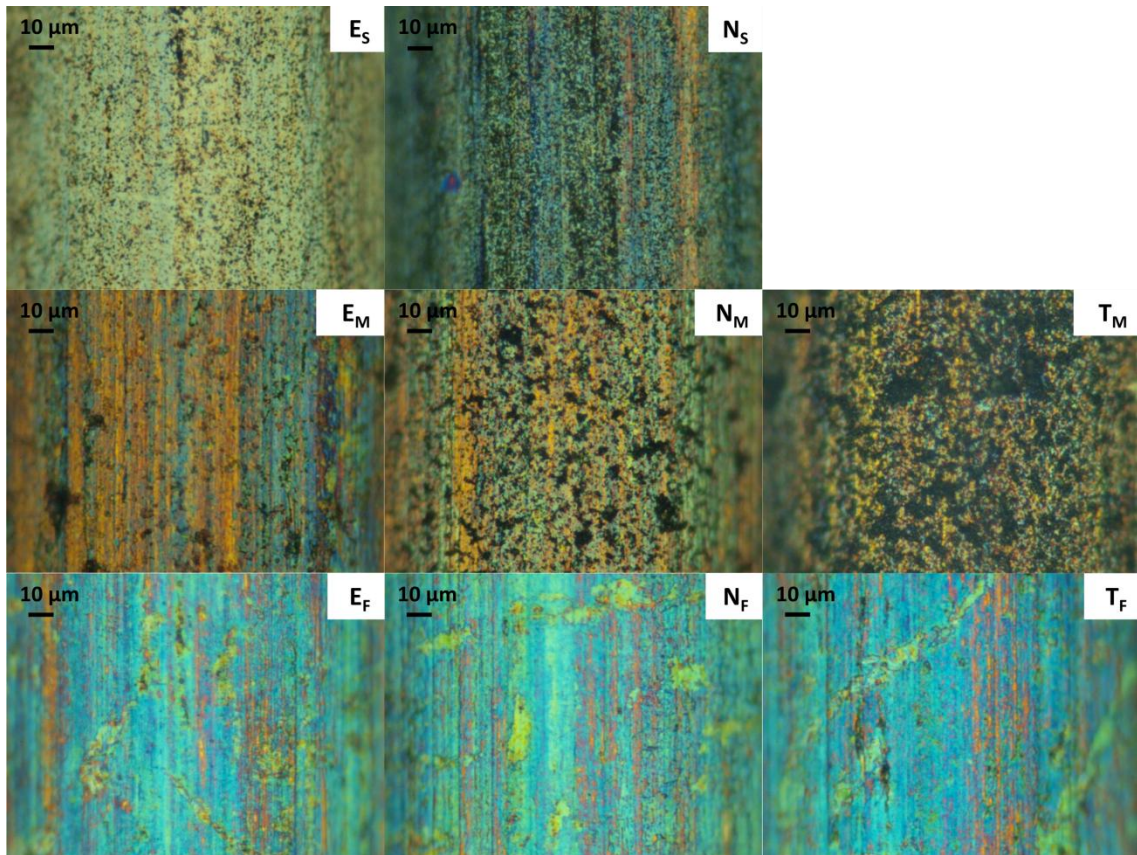


FIGURE 30. OPTICAL MICROSCOPY IMAGES OF THE VARIOUS SAMPLES (E_S : SQUALENE, 0 PHR CARBON BLACK; N_S : SQUALENE, 10 PHR CARBON BLACK; E_M : METATHESIS, 0 PHR CARBON BLACK; N_M : METATHESIS, 10 PHR CARBON BLACK; T_M : METATHESIS, 50 PHR CARBON BLACK; E_F : FILTER PAPER, 0 PHR CARBON BLACK; N_F : FILTER PAPER, 10 PHR CARBON BLACK; T_F : FILTER PAPER, 50 PHR CARBON BLACK)

Optical microscopy images of the metathesis samples are shown in the middle (E_M , N_M , T_M). Unlike the squalene samples, there is almost no difference between the specimens of the different mixtures. The specimens show a mostly greenish color with some lamellar orange areas. Although, there is no difference between the colors of the specimens with different amount of carbon black, it is obvious that for specimen N_M there are some black areas on the wire surface and an increasing amount of these dark areas on the sample T_M . The occurrence of these areas correlates very well with the

carbon black content, which also increases from E_M (no carbon black) over N_M (10 phr carbon black) to T_M (50 phr carbon black).

Optical microscopy images of the filter paper samples can be seen in the lower part of the image (E_F , N_F , T_F). Similar to the metathesis samples, there are almost no differences between the specimens from the various compounds visible. However, the optical appearances of the filter paper specimens are very different to the ones obtained by the metathesis experiments. The filter paper samples have a mostly bluish surface color. Unlike the metathesis samples, there is no effect of carbon black visible for the filter paper samples; no differences between the samples E_F , N_F and T_F can be observed.

To analyze if the observed differences between the squalene, the metathesis and the filter paper samples are only an optical phenomenon or if these differences are based on different surface structures, SEM was performed. SEM images of the squalene, the metathesis and the filter paper samples obtained from the compound without carbon black (compound **E**) are shown in Figure 31. Specimens from compound **E** were taken as an example, since the same effects can be seen in all compounds. Further, wires from compounds without carbon black are more suitable, because there are less carbon residues which might be interfering during the characterization. Similar to the results obtained by optical microscopy, different surface structures can be observed in the SEM images depending on the sample preparation technique used. On the squalene samples nodule-shaped structures can be found. On the surface of the metathesis samples, smaller and bigger structures can be seen. The bigger structures correlate with the dark areas found in the optical microscopy images, whereas the smaller structures may be due to the rough non-stoichiometric Cu_xS layer. On the filter paper specimens almost no surface structures can be observed or rather the structures are too small to be noticed. At higher magnification (Figure 31, right side) the differences between the squalene samples and the specimens cured in natural rubber are even more obvious. On the squalene specimens, the structures built-up are mostly scattered and seem to be dense, whereas for the metathesis and filter paper specimens, the surfaces seem to be very rough and covered with fine textured structures. But there are also differences between the structures on the filter paper specimen and the structures on the metathesis specimen: the filter paper specimen has a mostly uniform surface, which is rough with some crystalline areas (needle-

shaped) whereas the surface of the metathesis specimen is also rough, but there are only few scattered needle-shaped structures.

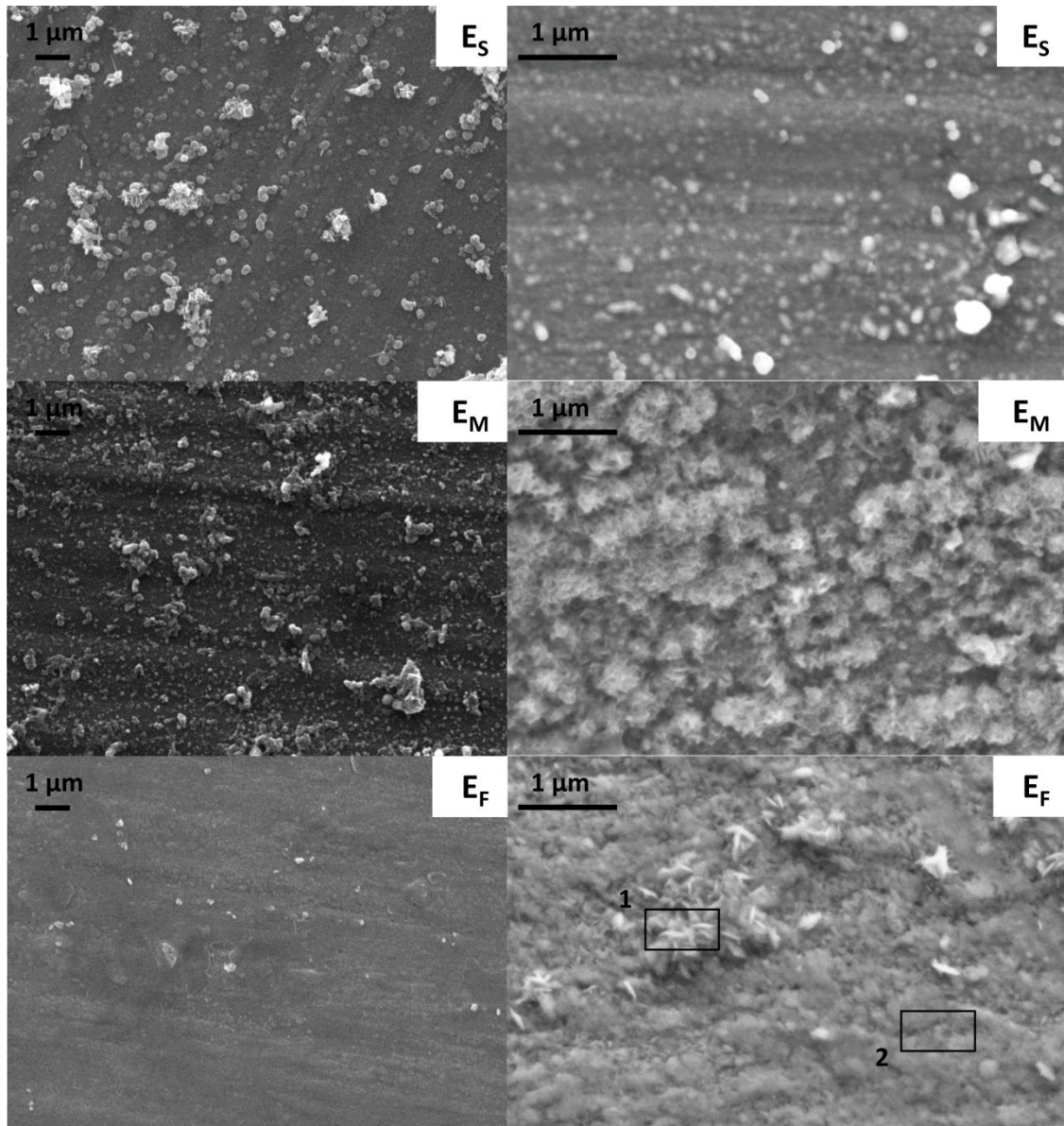


FIGURE 31. SEM IMAGES OF THE VARIOUS SAMPLES (LEFT: 20 KEV, RIGHT: 7 KEV; E_S: SQUALENE, 0 PHR CARBON BLACK; E_M: METATHESIS, 0 PHR CARBON BLACK; E_F: FILTER PAPER, 0 PHR CARBON BLACK) (SEM IMAGES ON THE RIGHT SIDE RECORDED BY PETER PÖLT)

To analyze the effects of the different methods on the elemental composition of the sulfide layers of the various samples, additional characterization was done by EDX analysis of the specimens. As mentioned before, any calculated elemental

concentrations are rather roughly approximated values than accurate results. But the obtained values can be evaluated in comparison to each other to analyze a general behavior.

TABLE 16. EDX RESULTS (20 KEV) OF THE VARIOUS SAMPLES

	Squalene		Metathesis			Filter paper		
	E _S	N _S	E _M	N _M	T _M	E _F	N _F	T _F
C	106 ± 4	148 ± 7	126 ± 24	251 ± 82	733 ± 215	91 ± 10	85 ± 19	97 ± 12
O	35 ± 2	28 ± 3	37 ± 3	37 ± 8	39 ± 1	36 ± 2	30 ± 0	39 ± 5
S	15 ± 1	11 ± 0	7 ± 2	7 ± 2	7 ± 1	8 ± 1	8 ± 1	9 ± 2
Fe	64 ± 8	62 ± 7	62 ± 20	56 ± 22	55 ± 8	60 ± 10	54 ± 6	74 ± 12
Cu	100 ± 0	100 ± 0	100 ± 0	100 ± 0	100 ± 0	100 ± 0	100 ± 0	100 ± 0
Zn	58 ± 1	63 ± 1	61 ± 1	62 ± 3	59 ± 3	60 ± 2	59 ± 1	57 ± 1

According to the EDX analysis of the specimens (see Table 16) the sulfidated wires consist mostly out of Cu, Zn, Fe, C, O and S. Most interesting for the comparison of the various preparation methods are the differences in the sulfur and the carbon levels. Again the squalene, the metathesis and the filter paper method cause, to some extent, very different results. Unlike the metathesis and the filter paper samples, in which the sulfur levels are mostly constant, the squalene samples show very different sulfur levels, depending on the compound formulation used. Mixtures without carbon black (E_S) result in higher sulfur levels than mixtures containing carbon black (N_S). This can be attributed to the higher viscosity of the squalene mixture caused by carbon black. As a consequence, diffusion might be hindered and therefore a lower sulfidation level can be achieved. These results show that for the squalene experiments, small changes in the compound may have great effects on the sulfidation, which cannot be observed in real rubber compounds. Further, not all aspects of a vulcanization reaction, such as the applied pressure, can be simulated in the squalene experiments. Therefore, results obtained should be considered with care and not be over-interpreted.

Sulfur levels for the metathesis samples are slightly lower than for the filter paper samples but carbon levels are higher. Carbon levels in the metathesis samples increase with increasing carbon black content and correlate very well with the increasing amount of dark areas found in the optical microscopy. Therefore, we can conclude that these dark areas are due to organic residues and/or immobilized carbon black. In the case of the filter paper samples, the filter paper effectively retains rubber molecules

and carbon black, so that the carbon levels are almost the same for all samples. On the other hand, retention of the rubber and carbon black leaves a greater percentage of the wire surface the possibility to react with the active sulfidating species, which in consequence leads to a higher sulfidation of the brass. Therefore, the detected amount of sulfur on the filter paper samples is higher than on comparable metathesis samples. However, these differences are very small and within measurement inaccuracy.

TABLE 17. EDX ANALYSIS (7 KEV) OF MARKED AREAS IN FIGURE 31, E_f

	1	2
C	77	71
O	41	45
S	50	29
Fe	5	6
Cu	100	100
Zn	52	68

Structures found on the filter paper sample were subjected to a closer examination by EDX (see Table 17). Here the electron energy was set to 7 keV to get an analysis of the surface structures only. C, O and Fe level are almost the same in both areas, but the sulfur level of the needle-shaped structures (area 1) is almost twice as high as the sulfur level of area 2 (no crystalline structures). Further, the ratio of copper to zinc is also higher in area 1. This confirms the theory that these needle-shaped structures mostly consist of Cu_xS.

Figure 32 shows the Raman spectra of the three specimens obtained from compound E. For the filter paper and the metathesis specimens the same peaks can be observed, whereas for the squalene sample the peak pattern is different. The Raman spectra of the filter paper sample and the metathesis sample show two major peaks: One around 573 cm⁻¹ and one at 474 cm⁻¹. The peak around 573 cm⁻¹ can be attributed to the ZnO layer on the wire surface.⁸⁴ The second peak around 474 cm⁻¹ is due to CuS on the surface.⁸⁵ Due to its metallic character and its thermal sensitivity, Cu₂S normally cannot be detected by Raman.⁸⁶ In the squalene spectra, the ZnO peak disappears and another peak around 286 cm⁻¹ turns up, which is very broad and therefore difficult to assign. The disappearance of the ZnO peak suggests a thicker sulfide layer. This theory

is supported by the higher S level detected in the EDX compared to the metathesis and the filter paper specimens.

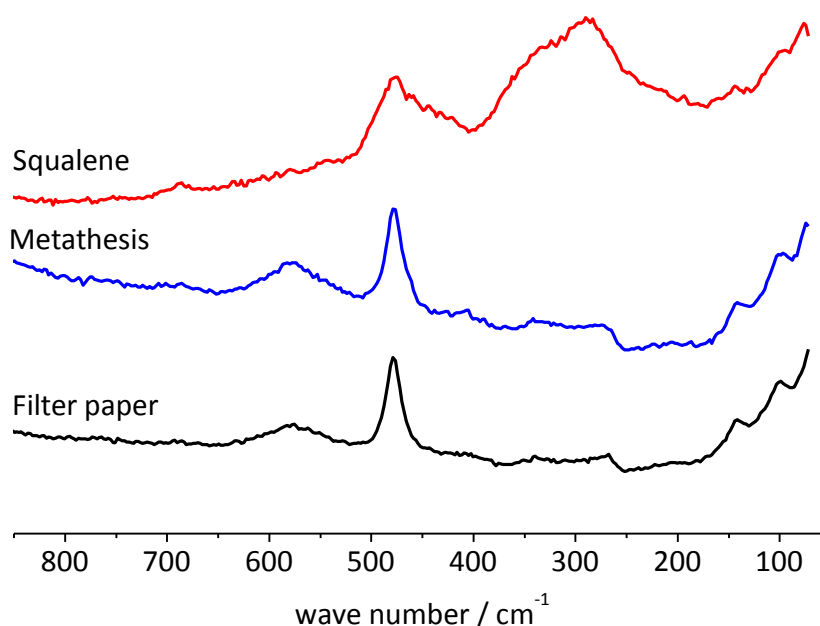


FIGURE 32. RAMAN SPECTRA OF SAMPLES OBTAINED FROM COMPOUND E

To analyze aging effects on the adhesion layer, the metathesis and the filter paper samples were subjected to a thermal aging treatment. For the squalene experiments no aged data could be obtained, because an aging treatment in squalene mixtures is not possible. Therefore, Figure 33 shows optical microscopy images and SEM images only of the thermally aged metathesis and filter paper samples. Furthermore, the images are reduced to the ones obtained from compound **E**, since the same effects can be observed on specimens obtained from compound **N** and compound **T** as well. Further, wires from compounds without carbon black are more suitable, because there are less carbon residues which might be interfering during the characterization. Comparison of the thermally aged specimens to the unaged specimens show, for both, the metathesis and the filter paper samples, changed optical appearance. This effect is especially visible in the case of the metathesis samples (**E_M**). Here, the unaged specimens have an orange color with bluish or greenish lamellar areas whereas the thermally aged specimens have a green surface. In the case of the filter paper samples

(E_F), the unaged specimens show a surface, which is partly orange and mostly blue. After the aging treatment the surface is almost completely covered in blue with a slightly green touch. The SEM analysis of the surface structures of the thermally aged metathesis samples shows similar structures than for the unaged specimens, but more widely spread. More interesting is the comparison of the unaged and the thermally aged filter paper samples. In the case of the unaged specimens only very few and small surface structures can be observed, whereas after the aging treatment the surface consists of finely distributed needle-shaped structures. Therefore, it might be concluded that in this case we have a mostly crystalline surface. These differences in the surface structures observed in the metathesis and the filter paper specimens can be explained by the influence of the filter paper. Due to the retention of most of the rubber compound components, there are less interfering substances on the surface and as a consequence, crystallization is much easier.

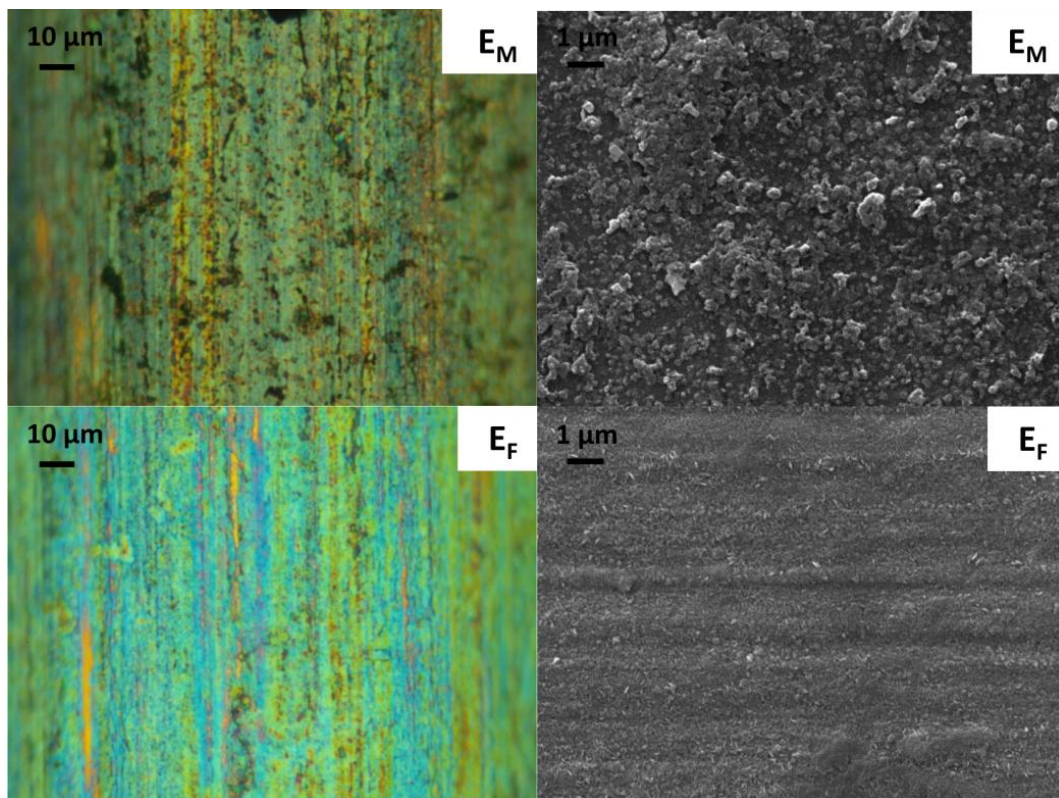


FIGURE 33. OPTICAL MICROSCOPY IMAGES (LEFT) AND SEM IMAGES (RIGHT) OF THE THERMALLY AGED WIRES (E_M : METATHESIS, 0 PHR CARBON BLACK; E_F : FILTER PAPER, 0 PHR CARBON BLACK)

EDX results of the thermally aged specimens are shown in Table 18. Sulfur levels are almost the same for the metathesis samples and the filter paper samples. However, carbon levels are higher for the metathesis samples than for the filter paper samples due to organic residues and immobilized carbon black. Further a slight increase in the sulfur levels with increasing amounts of carbon black can be observed in the case of the filter paper specimens. This might be an indication that carbon black increases the sulfidation, which is in accordance with results reported by Waddell et al.²⁹ The most interesting point is the increased sulfur content after the aging treatment, which can be seen by the comparison of the unaged values (Table 16) with the aged ones (Table 18). Therefore, it can be concluded, that the observed changes in color and structure are due to a further sulfidation of the brass layer.

TABLE 18. EDX RESULTS (20 KEV) OF THE THERMALLY AGED SAMPLES

	Metathesis			Filter paper		
	E _M	N _M	T _M	E _F	N _F	T _F
C	176 ± 12	230 ± 27	531 ± 150	88 ± 22	75 ± 20	72 ± 9
O	43 ± 3	38 ± 7	43 ± 9	37 ± 4	33 ± 3	40 ± 4
S	10 ± 1	8 ± 1	10 ± 4	9 ± 1	10 ± 1	11 ± 2
Fe	59 ± 5	73 ± 14	73 ± 31	59 ± 4	53 ± 4	69 ± 7
Cu	100 ± 0	100 ± 0	100 ± 0	100 ± 0	100 ± 0	100 ± 0
Zn	60 ± 1	60 ± 3	60 ± 3	58 ± 2	59 ± 1	56 ± 1

4.4.3 CONCLUSION

Three different options to investigate the sulfidation reaction of brass-plated steel wires were presented: two model systems (squalene experiments, filter paper experiments) and one which analyzes a real rubber-wire interface (olefin metathesis degradation).

In the case of the squalene experiments, a great influence of the compound composition on the obtained results can be observed. Small changes in the compounds (e.g. addition of carbon black) lead to different sulfur levels and as a result, to totally different appearances in the optical microscopy and in the SEM characterization and to different Raman spectra. Further, not all aspects of a vulcanization reaction, such as

the applied pressure, can be simulated in the squalene experiments, which is why the results obtained should be considered with care and not be over-interpreted.

Unlike the squalene experiments, small changes in the compounds in the filter paper experiments lead to almost no differences in the surface structures and compositions. In the unaged state only very few surface structures can be observed and after the aging treatment the surface is covered with finely distributed needle-shaped structures, which supports the theory of a crystalline Cu_xS interlayer. Such crystalline structures cannot be found on the squalene and, only to a very small extend, on the metathesis samples. Therefore, the crystallinity is most probably enhanced by the presence of the filter paper: due to the retention of most of the rubber compound components, there are less interfering substances on the surface and as a consequence, crystallization is much easier. Further, sulfur levels detected on the filter paper specimens are slightly higher than the sulfur levels on the metathesis samples. The filter paper has the function to retain components such as rubber molecules and carbon black. As a consequence, a greater percentage of the wire surface is free to react with the active sulfidating species, which in consequence leads to a higher sulfidation of the brass. Therefore, the detected amount of sulfur on the filter paper samples is higher than on comparable metathesis samples.

Similar to the filter paper samples, small changes in the compounds in the metathesis experiments lead to almost no differences in the surface structures and compositions. The only remarkable difference is an increased carbon level with increasing carbon black content in the compound mixture, due to organic residues and immobilized carbon black. However, it is not an exceedingly high amount and therefore, it should be no problem for most characterization techniques. Further, the metathesis method has a lot of advantages, such as the opportunity to use a real rubber system and no need of using an artificial interlayer. On the other hand, the degradation of actual rubber products with high carbon black loading might be problematic. Besides, it cannot be completely excluded that the high reactive metathesis initiator has an influence on the sulfide layer. However, no major influence was observed so far.

4.5 INFLUENCE OF DIFFERENT COMPOUND COMPONENTS ON RUBBER-BRASS ADHESION

4.5.1 COBALT STEARATE

Cobalt salts are supposed to be beneficial for the initial adhesion strength as well as for the durability of the adhesion between rubber and brass-plated steel cords and wires.¹ Therefore, this chapter analyzes the influence of cobalt stearate on rubber properties and rubber-brass adhesion. For this reason, brass-plated steel wires were treated for 20 minutes at 160 °C in a squalene mixture containing 0 or 1 phr cobalt stearate and 0 or 10 phr carbon black (Table 19, compounds **G**, **U**, **E** and **N**). Since experiments in squalene are only model systems, additional experiments in natural rubber were performed. Natural rubber compounds having the same composition as the squalene mixtures as well as a compound containing 50 phr carbon black (50 phr carbon black was used to get better comparability with rubber compounds utilized in technical products) and no or 1 phr cobalt stearate (Table 19) were used to prepare T-test specimens (**V**, **T**). Half of these T-test specimens were used to determine pull-out forces and rubber coverage, the other half was used to investigate the adhesion layer created in natural rubber compounds (by the filter paper method and the metathesis degradation method 1).

TABLE 19. COMPOUND FORMULATION TO STUDY THE INFLUENCE OF COBALT STEARATE ON RUBBER-BRASS ADHESION

	G^a	U^a	V	E^a	N^a	T
	phr					
Squalene / Natural rubber	100	100	100	100	100	100
Naphthenic oil	6	6	6	6	6	6
ZnO	7	7	7	7	7	7
Stearic acid	2	2	2	2	2	2
DCBS	0.7	0.7	0.7	0.7	0.7	0.7
Sulfur	6.25	6.25	6.25	6.25	6.25	6.25
N550 Carbon black	0	10	50	0	10	50
Cobalt stearate	0	0	0	1	1	1

^{a)} Labeled compounds were also used for squalene experiments

Vulcanization conditions were 20 minutes at 160 °C and 320 bar. Additionally the vulcanized rubber specimens were subjected to a thermally aging treatment (4 h at 150 °C). Physical properties of the unaged and the aged vulcanized compounds were tested, as well as the pull-out force and rubber coverage. The adhesion interface of the squalene treated wires (marked with a subscript S) as well as for sulfidated wires obtained by the filter paper method (marked with a subscript F) and the olefin metathesis method (marked with a subscript M) was studied using optical microscopy, focus variation microscopy and SEM-EDX.

TABLE 20. CURE CHARACTERISTICS (SCORCH TIME T₀₅, OPTIMUM CURING TIME T₉₀), PHYSICAL PROPERTIES, PULL-OUT FORCE AND RUBBER COVERAGE OF COMPOUNDS CONTAINING DIFFERENT AMOUNTS OF COBALT STEARATE AND CARBON BLACK

	G	U	V	E	N	T
t₀₅, min	1.5	1.4	1.2	2.4	1.8	1.5
t₉₀, min	17.4	15.7	12.7	12.2	11.6	9.4
Tear strength, N	22.3	19.6	92.1	15.7	20.8	67.9
Tensile strength, N/mm²	9.1	16.9	19.9	9.9	16.5	16.5
Elongation at break, %	617	628	415	593	606	370
Pull-out force, N	155 ± 46	205 ± 26	420 ± 39	260 ± 79	464 ± 38	505 ± 38
Coverage	1	2	3	3	3	3

Cure characteristics (scorch time t_{05} and optimum curing time t_{90}), physical properties, pull-out force and rubber coverage of the vulcanized compounds are listed in Table 20. It is evident that the addition of cobalt salt leads to an increase in scorch time and a decrease in cure time. The decrease of the cure time can be explained by the activating effect of cobalt on the DCBS decomposition rate²⁷, which results in a faster crosslinking. The optimal curing time is further decreased by an increasing content of carbon black. Tensile strength, tear strength and elongation at break for compounds without cobalt stearate (**G, U, V**) and compounds containing cobalt stearate (**E, N, T**) are almost the same. In literature, there are conflicting results reported for the tensile strength values. Jeon³³ noticed a slight increase of tensile strength values with increasing amount of cobalt boroacylate, whereas Chandra et al.²⁰ observed a reduction of the tensile strength levels with the addition of cobalt stearate as well as cobalt boroacylate. The effect of carbon black on the physical properties of the rubber compounds can be explained by its reinforcing nature. As a consequence, tear strength

and tensile strength increase with increasing carbon black content, while elongation at break decreases.

Pull-out force and rubber coverage of compounds containing different amounts of cobalt stearate and carbon black are shown in Table 20. Due to the reinforcing effect of carbon black, pull-out force values increase with increasing carbon black content. Furthermore, compounds containing cobalt stearate (**E, N, T**) showed higher pull-out forces and better rubber coverage than compounds without cobalt salt (**G, U, V**). These results are in accordance with literature, which report higher initial adhesion strength for cobalt containing compounds.²⁰

TABLE 21. PHYSICAL PROPERTIES, PULL-OUT FORCE AND RUBBER COVERAGE OF THERMALLY AGED COMPOUNDS CONTAINING DIFFERENT AMOUNTS OF COBALT STEARATE AND CARBON BLACK

	G	U	V	E	N	T
Tear strength, N	14.1	12.7	37.8	13.1	13.3	35.7
Tensile strength, N/mm²	1.4	1.9	4.9	-	1.6	4.7
Elongation at break, %	407	363	244	158	320	212
Pull-out force, N	208 ± 38	250 ± 48	464 ± 34	118 ± 35	242 ± 25	458 ± 41
Coverage	1	3	3	1	3	3

Physical properties, pull-out force and rubber coverage of thermally aged compounds are shown in Table 21. Tear strength, tensile strength and elongation at break all decrease during the aging treatment. With exception of compound **E** (1 phr cobalt stearate, 0 phr carbon black), values for compounds containing cobalt salt and compounds without cobalt salt are almost the same. For compound **E** no tensile strength values could be obtained since the specimen was not mechanically stable after the aging treatment.

After the aging treatment, adhesion values for the compound without cobalt stearate (**G, U, V**) increased, whereas compounds containing cobalt salt (**E, N, T**) showed inferior adhesion performance. All in all, the adhesion levels for compounds with and without cobalt salt are almost the same after the aging treatment. This is quite surprising, since cobalt salts are supposed to enhance the adhesion properties, especially after aging. However, there are several different aging treatments. Therefore, it might be possible that improvement of the aged adhesion values of cobalt containing compounds can be observed for alternative aging conditions.

Furthermore, according to the literature, cobalt stearate shows the least improvement compared to other cobalt salts, such as cobalt naphthenate and cobalt boroacrylate.³² On the other hand, improved adhesion values were observed for the unaged specimens (Table 20). One explanation might be that the initial binding layer for the cobalt free compound is not optimal for bonding (e.g. copper sulfide layer is not ideally textured) and improves a little during the aging (e.g. better surface texture), whereas the cobalt salt improves the performance of the initial binding layer of this compound. During the thermal aging treatment the adhesion layers of both, the cobalt containing and the cobalt free compound grow, which results in a change of the surface textures. For the cobalt free compound the aged binding layer gives better performance than the initial one, whereas for the cobalt containing one, the original binding layer was ideal and therefore, the result after the aging is inferior. As a consequence, almost the same adhesion performance is achieved for both compounds after the thermal aging treatment.

To prove these assumptions, the surfaces of wires treated in squalene mixtures and the ones of wires obtained by filter paper experiments and olefin metathesis reactions were investigated by optical microscopy, focus variation microscopy and SEM-EDX. Optical microscopy images of squalene treated wires are shown in Figure 34. The images show the wire surfaces after the reaction in squalene mixtures with different amount of cobalt stearate and carbon black. As can be seen in these images, the wire surfaces are different depending on the compound composition used. The wire from the mixture without cobalt stearate and carbon black (**G_S**) has a yellowish green color, the one from the mixture with 0 phr cobalt salt and 10 phr carbon black (**U_S**) is orange with blue lamellar areas. Specimen **E_S** (1 phr cobalt stearate, 0 phr carbon black) has a bluish green color with dark spots and **N_S** (1 phr cobalt stearate, 10 phr carbon black) is mostly bluish (containing some orange areas) with many dark spots. Based on the different colors, different sulfidation levels of the wires can be expected. According to the color, the sulfur level for sample **U_S** (10 phr carbon black, no cobalt stearate) is most probably the lowest, and for **E_S** (0 phr carbon black, 1 phr cobalt stearate) the highest.

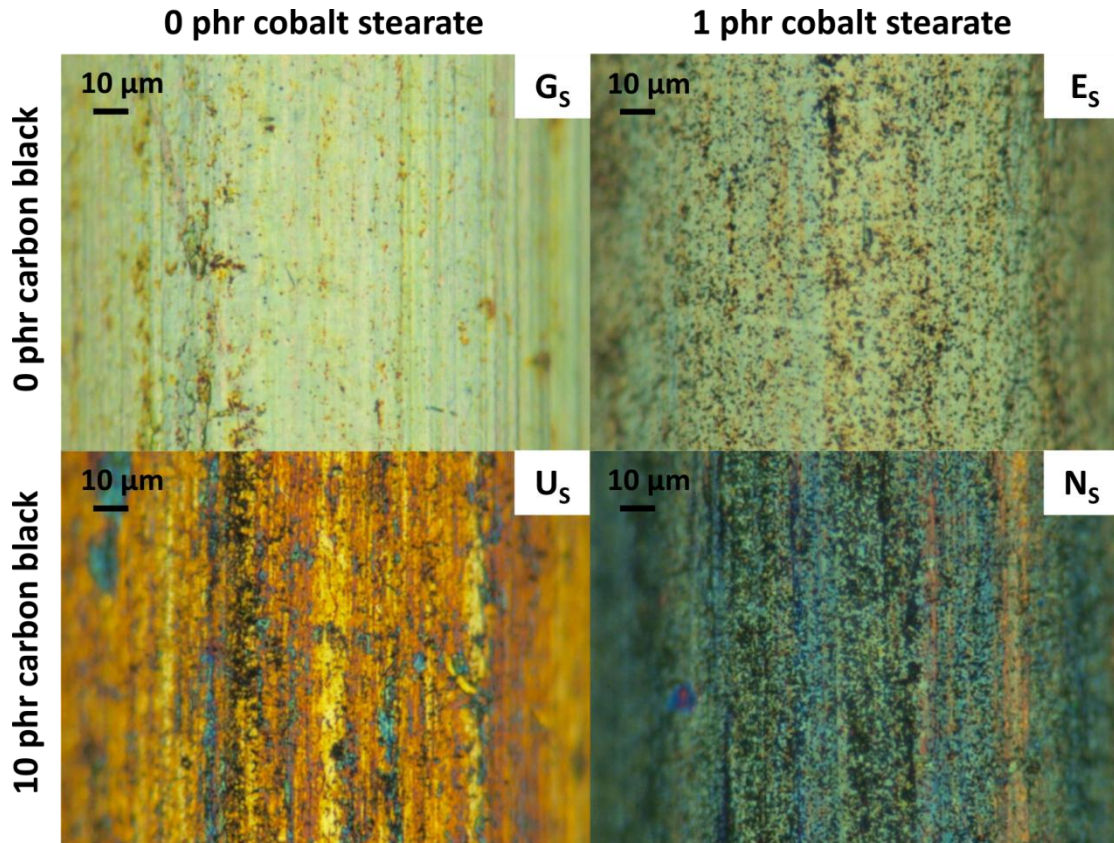


FIGURE 34. OPTICAL MICROSCOPY IMAGES OF SAMPLES OBTAINED BY SQUALENE EXPERIMENTS WITH DIFFERENT AMOUNTS OF COBALT STEARATE (G_S : 0 PHR COBALT STEARATE, 0 PHR CARBON BLACK; U_S : 0 PHR COBALT STEARATE, 10 PHR CARBON BLACK; E_S : 1 PHR COBALT STEARATE, 0 PHR CARBON BLACK; N_S : 1 PHR COBALT STEARATE, 10 PHR CARBON BLACK)

Focus variation microscopy images of squalene treated wires are shown in Figure 35. The images show a region of $145 \times 110 \mu\text{m}$ of the wire surface. For a better visualization of the surface structures the images were planarized (the cylindrical geometry of the wire was subtracted from the 3-dimensional image to reduce it to its surface structures) and stretched 10fold in z-direction. The color coded images help to estimate the surface roughness of the various specimens. The different colors observed in the optical microscopy images can be observed here as well. As far as the surface roughness is concerned, the specimens are almost the same with exception of sample N_S (1 phr cobalt stearate, 10 phr carbon black), which shows a high surface roughness.

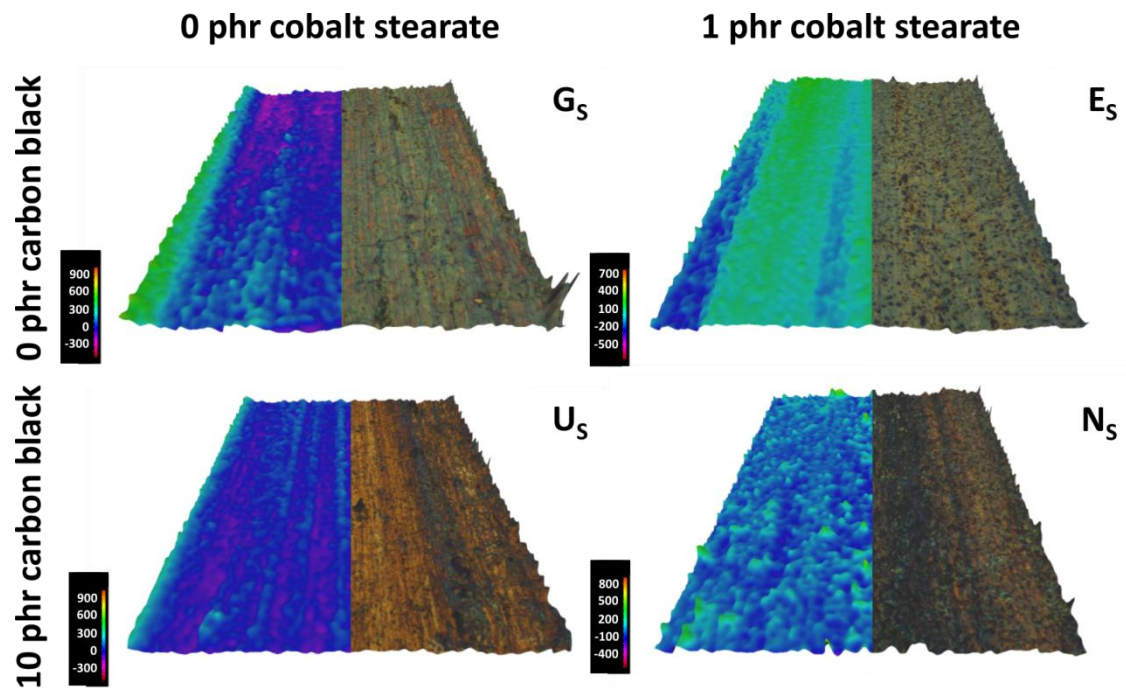


FIGURE 35. FOCUS VARIATION MICROSCOPY IMAGES OF SAMPLES OBTAINED BY SQUALENE EXPERIMENTS WITH DIFFERENT AMOUNTS OF COBALT STEARATE (G_S : 0 PHR COBALT STEARATE, 0 PHR CARBON BLACK; U_S : 0 PHR COBALT STEARATE, 10 PHR CARBON BLACK; E_S : 1 PHR COBALT STEARATE, 0 PHR CARBON BLACK; N_S : 1 PHR COBALT STEARATE, 10 PHR CARBON BLACK)

Optical microscopy images of the metathesis samples are shown in Figure 36. Unlike the squalene samples, there is almost no difference between the specimens of the different compounds. But, there is a small difference between the samples without (G_M , U_M , V_M) and the samples containing cobalt stearate (E_M , N_M , T_M). The specimens without cobalt stearate (G_M , U_M , V_M) are orange with blue lamellar areas, whereas the samples containing cobalt stearate (E_M , N_M , T_M) show a mostly greenish color with some orange lamellar areas. Further, an increasing amount of dark areas can be found on the surfaces with increasing carbon black content in the compound. This is most probably due to an increasing amount of carbonaceous residues, as was discussed before (chapter 4.4 - Comparison of different analytical methods). This is also confirmed by the focus variation microscopy images (Figure 37). For the specimens from compounds with 50 phr carbon black (V_M , T_M), organic residues can be clearly seen on the wire surfaces of the color coded images. Apart from that, the specimens look almost the same, which also suggests very similar sulfidation levels for all samples, irrespective of the carbon black or cobalt stearate concentration.

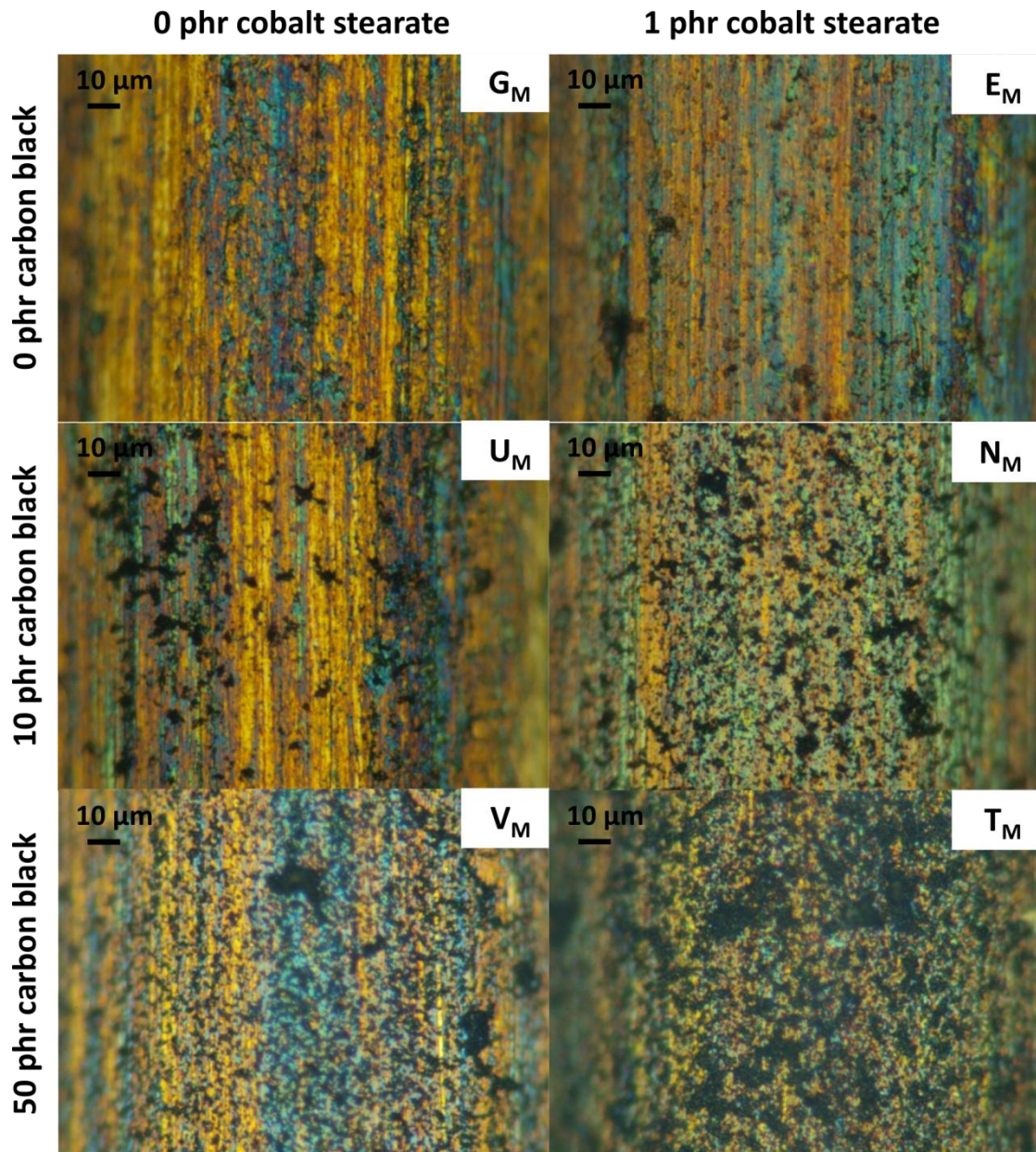


FIGURE 36. OPTICAL MICROSCOPY IMAGES OF SAMPLES OBTAINED BY THE OLEFIN METATHESIS METHOD (G_M: 0 PHR COBALT STEARATE, 0 PHR CARBON BLACK; U_M: 0 PHR COBALT STEARATE, 10 PHR CARBON BLACK; V_M: 0 PHR COBALT STEARATE, 50 PHR CARBON BLACK; E_M: 1 PHR COBALT STEARATE, 0 PHR CARBON BLACK; N_M: 1 PHR COBALT STEARATE, 10 PHR CARBON BLACK; T_M: 0 PHR COBALT STEARATE, 50 PHR CARBON BLACK)

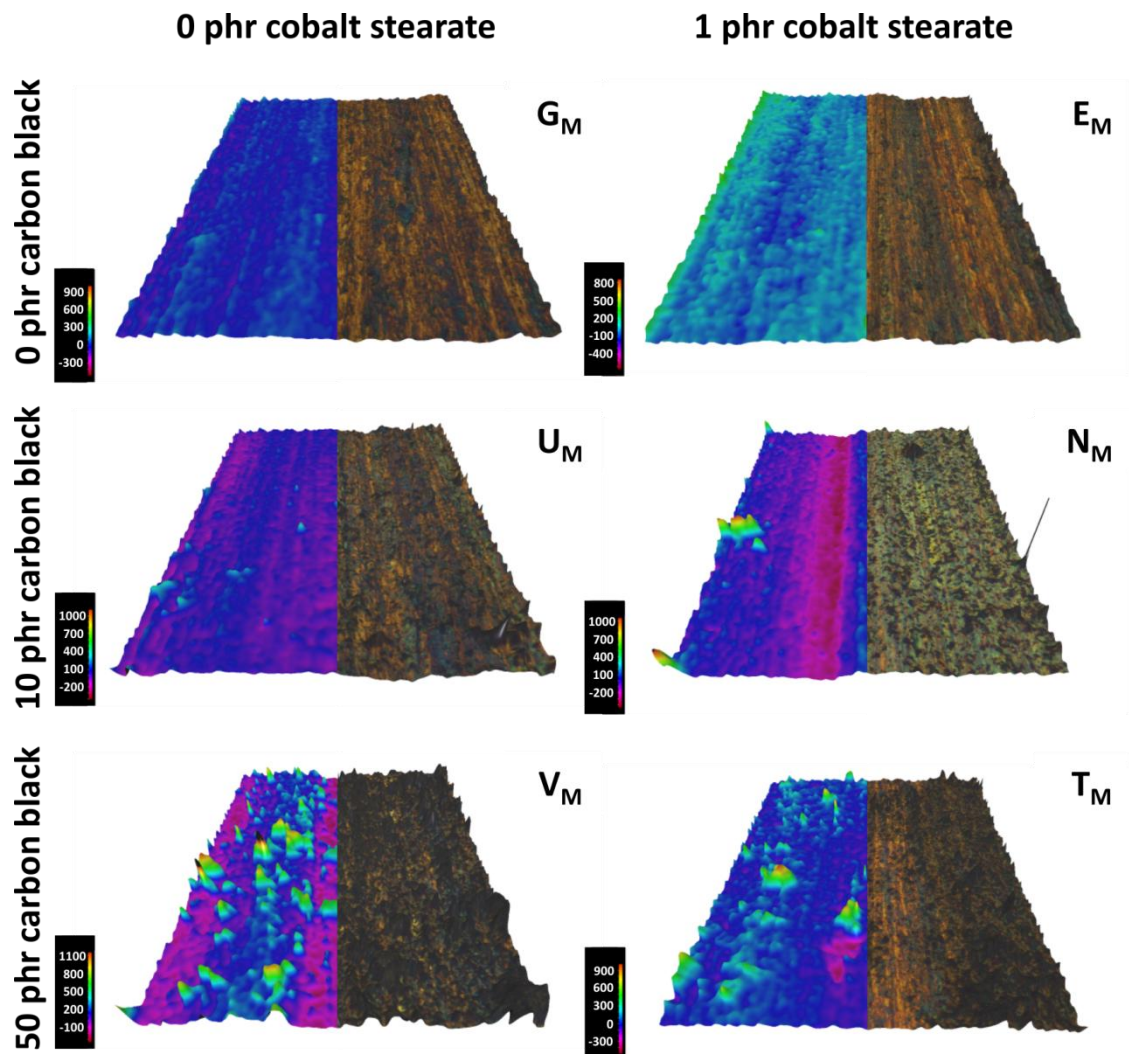


FIGURE 37. FOCUS VARIATION MICROSCOPY IMAGES OF SAMPLES OBTAINED BY THE OLEFIN METATHESIS METHOD (G_M : 0 PHR COBALT STEARATE, 0 PHR CARBON BLACK; U_M : 0 PHR COBALT STEARATE, 10 PHR CARBON BLACK; V_M : 0 PHR COBALT STEARATE, 50 PHR CARBON BLACK; E_M : 1 PHR COBALT STEARATE, 0 PHR CARBON BLACK; N_M : 1 PHR COBALT STEARATE, 10 PHR CARBON BLACK; T_M : 0 PHR COBALT STEARATE, 50 PHR CARBON BLACK)

Optical microscopy images of the filter paper samples can be seen in Figure 38. Similar to the metathesis samples, there are almost no differences between the specimens from the various mixtures visible. However, the optical appearances of the filter paper specimens are slightly different to the ones obtained by the metathesis experiments. The filter paper samples have a mostly bluish surface color for the specimens containing cobalt stearate (E_F , N_F , T_F), whereas the samples without cobalt stearate are also blue but with a higher percentage of orange areas in between (G_F , U_F , V_F). Unlike the metathesis samples, there is no effect of carbon black visible for the filter paper

samples. These findings are confirmed by the focus variation data (Figure 39). There, not many differences between samples from compounds without (G_F , U_F , V_F) and from compounds containing cobalt stearate (E_F , N_F , T_F) can be seen. The surfaces of all specimens seem to be very smooth without a lot of surface structures.

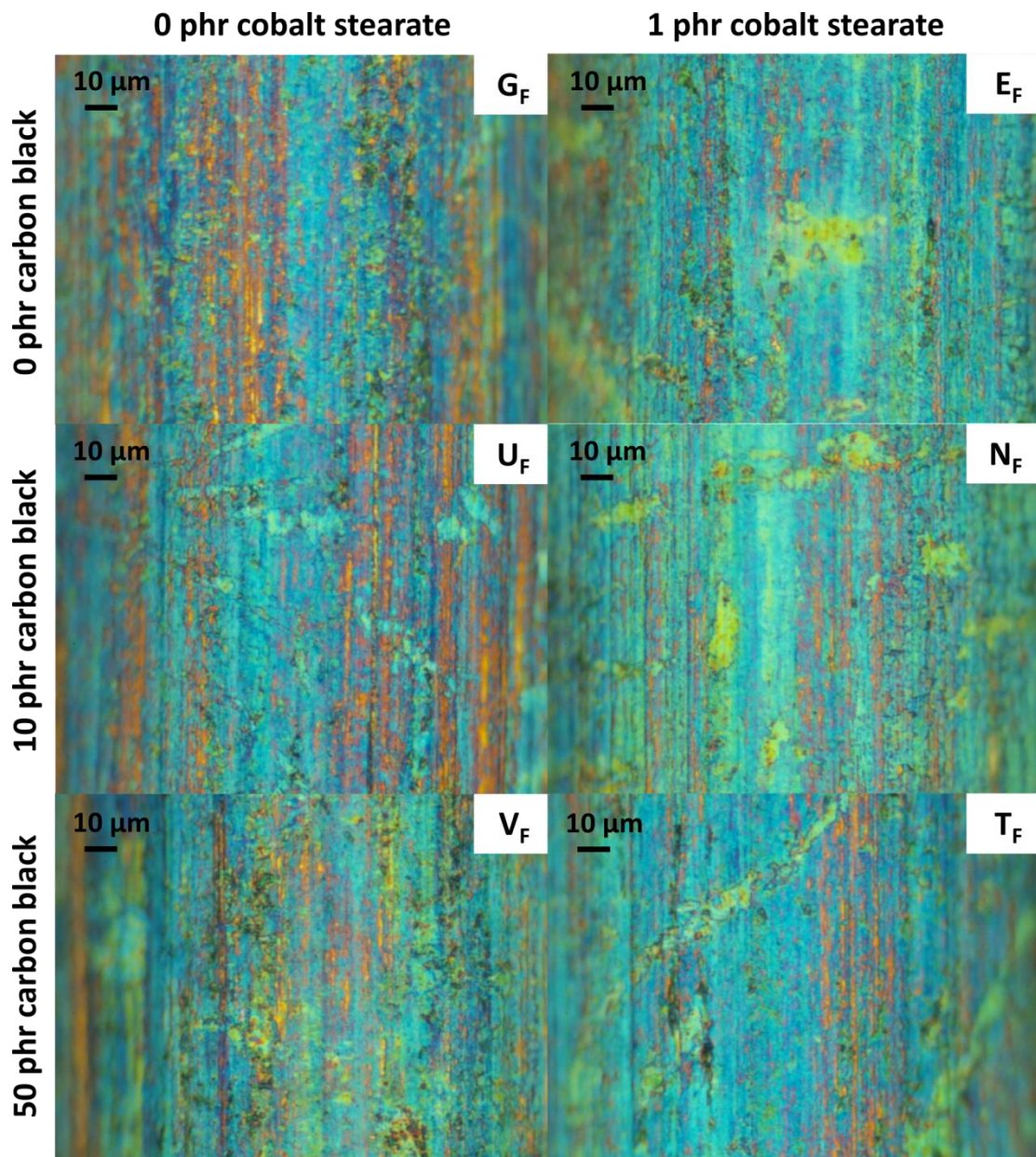


FIGURE 38. OPTICAL MICROSCOPY IMAGES OF FILTER PAPER SAMPLES (G_F : 0 PHR COBALT STEARATE, 0 PHR CARBON BLACK; U_F : 0 PHR COBALT STEARATE, 10 PHR CARBON BLACK; V_F : 0 PHR COBALT STEARATE, 50 PHR CARBON BLACK; E_F : 1 PHR COBALT STEARATE, 0 PHR CARBON BLACK; N_F : 1 PHR COBALT STEARATE, 10 PHR CARBON BLACK; T_F : 1 PHR COBALT STEARATE, 50 PHR CARBON BLACK)

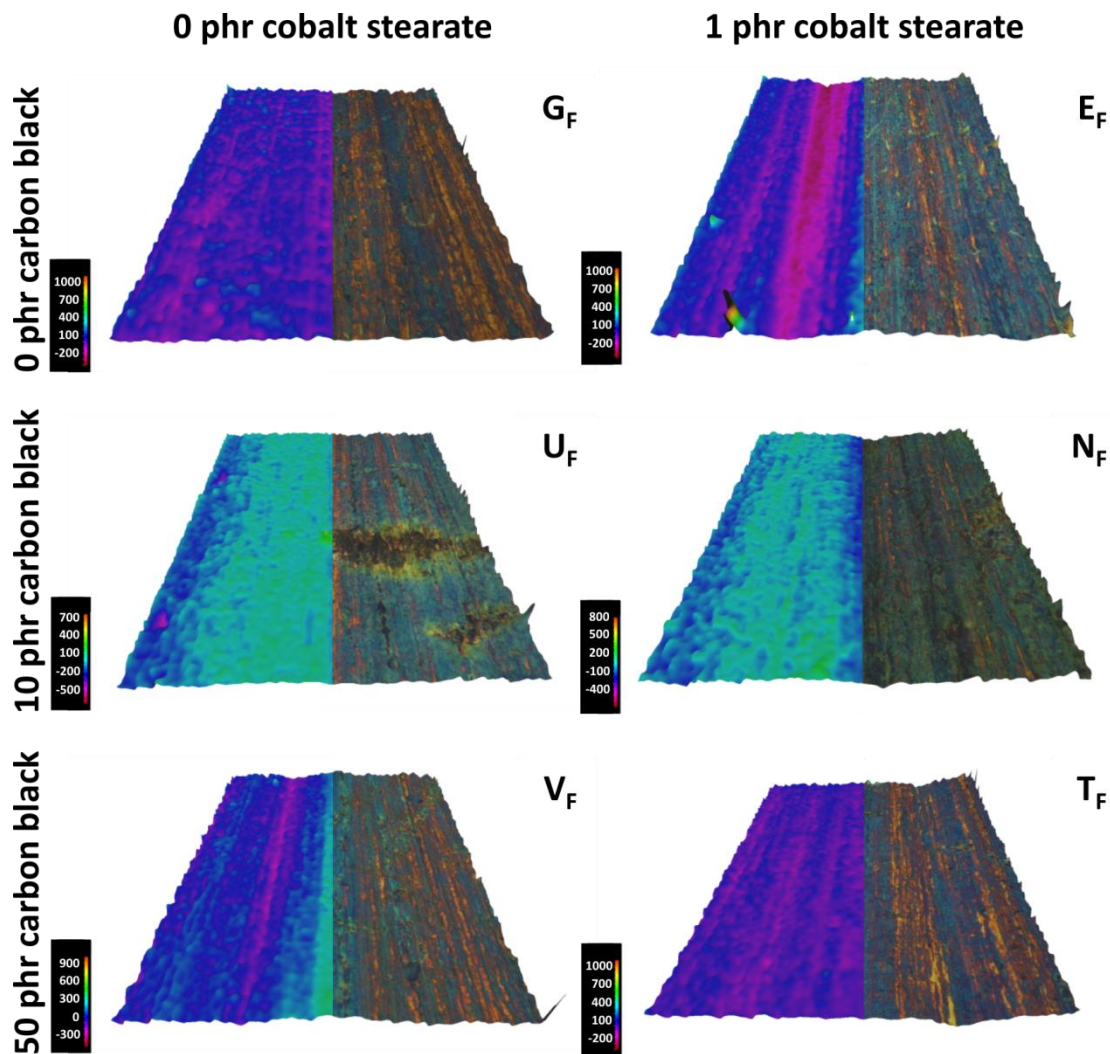


FIGURE 39. FOCUS VARIATION MICROSCOPY IMAGES OF FILTER PAPER SAMPLES (G_F : 0 PHR COBALT STEARATE, 0 PHR CARBON BLACK; U_F : 0 PHR COBALT STEARATE, 10 PHR CARBON BLACK; V_F : 0 PHR COBALT STEARATE, 50 PHR CARBON BLACK; E_F : 1 PHR COBALT STEARATE, 0 PHR CARBON BLACK; N_F : 1 PHR COBALT STEARATE, 10 PHR CARBON BLACK; T_F : 1 PHR COBALT STEARATE, 50 PHR CARBON BLACK)

Since the different sample preparation methods yielded totally different results in the optical characterization, additional characterization was done by scanning electron microscopy (SEM). SEM images of wires from compounds without carbon black are shown in Figure 40. Similar to the results obtained by optical microscopy, different surface structures can be observed in the SEM images depending on the sample preparation technique used. On the squalene samples nodule-shaped structures can be found. For the sample containing cobalt stearate (E_S) these structures are larger, whereas the structures on the specimen without cobalt stearate (G_S) are more finely

distributed and the whole surface seems to be rougher. On the metathesis samples, there is a contrary trend, as far as the surface roughness is concerned. Here, the surface of the wire from the cobalt salt containing compound (E_M) seems to be rougher. Furthermore, there are differences in the surface structures depending on whether there is cobalt in the compound or not. The structures on the wire from the compound without cobalt stearate (G_M) seem to be smaller compared to the ones of the wire from the compound containing cobalt salt (E_M). The extended surface, observed for the wire from compound E_M , is beneficial for the mechanically interlocking and as a result for the adhesion, explaining the higher pull-out forces for cobalt containing compounds. On the other hand, very small needle-shaped structures can be seen, which might get brittle when they grow further, e.g. during the aging treatment. For the specimen G_M , a further growth of the surface structures would lead to an increased surface, which would be beneficial for the adhesion. This would explain, why the adhesion levels for compound without cobalt stearate increase during the aging treatment, whereas the adhesion properties of cobalt salt containing compounds decrease. The same observations can be made for the filter paper specimens. Very small structures are found on the cobalt-free sample (G_F), whereas a very rough surface can be observed for the cobalt-containing specimen (E_F). The enhanced crystalline size, observed for wires from compounds containing cobalt stearate, indicates that the cobalt salt enhances the copper sulfide growth, which is in accordance with literature.^{20,38}

To analyze if the observed differences between the wire surfaces from compounds without and compounds containing cobalt stearate are due to different compositions of the adhesion layers, additional characterization was done by EDX analysis of the specimens. However, any calculated elemental concentrations are rather roughly approximated values than accurate results. But obtained values can be evaluated in comparison to each other to analyze a general behavior.

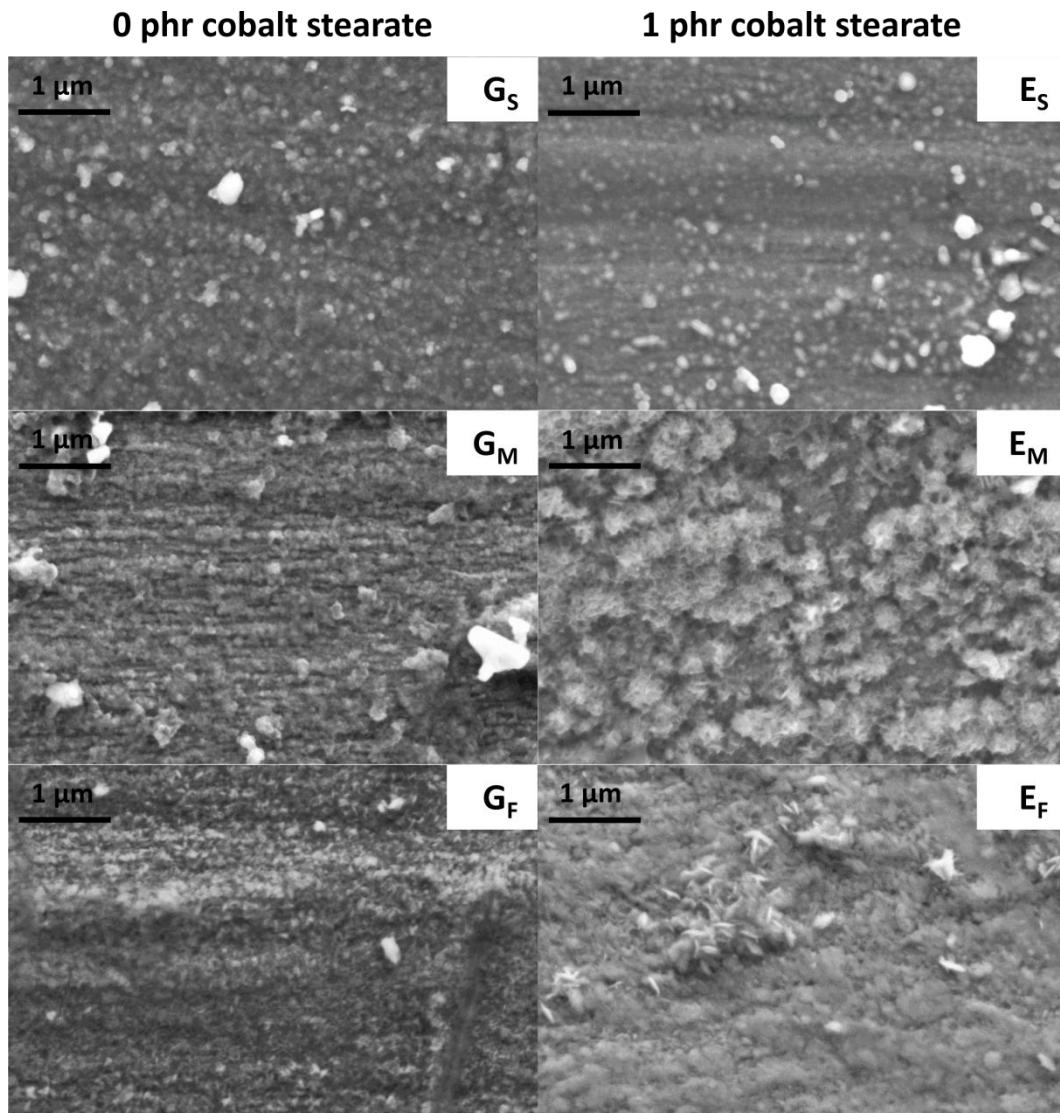


FIGURE 40. SEM IMAGES (7 KEV) OF WIRES FROM COMPOUNDS WITHOUT CARBON BLACK (G_S : SQUALENE, 0 PHR COBALT STEARATE; E_S : SQUALENE, 1 PHR COBALT STEARATE; G_M : METATHESIS, 0 PHR COBALT STEARATE; E_M : METATHESIS, 1 PHR COBALT STEARATE; G_F : FILTER PAPER, 0 PHR COBALT STEARATE; E_F : FILTER PAPER, 1 PHR COBALT STEARATE) (SEM IMAGES RECORDED BY PETER PÖLT)

According to the EDX analysis of the specimens (see Table 22) the sulfidated wires consist mostly out of Cu, Zn, Fe, C, O and S. Sometimes, cobalt was detected as well, but the amount was too small to be correctly analyzed. Copper was used as internal standard (the copper content should not change during the sulfidation reaction) and set to a value of 100. All other elements were normalized proportional to copper. Zinc, iron and oxygen levels are constant within the measuring inaccuracy; outliers in iron

level stem from irregular brass plating. Therefore, the most interesting elements are the sulfur and the carbon level, which vary quite a bit.

TABLE 22. EDX ANALYSIS (20 KEV) OF WIRE SURFACES FROM COMPOUNDS CONTAINING DIFFERENT AMOUNTS OF COBALT STEARATE AND CARBON BLACK

carbon black	0 phr cobalt stearate			1 phr cobalt stearate		
	0 phr	10 phr	50 phr	0 phr	10 phr	50 phr
	Squalene					
	G_S	U_S		E_S	N_S	
C	113 ± 3	111 ± 9		106 ± 4	148 ± 7	
O	28 ± 1	31 ± 2		35 ± 2	28 ± 3	
S	8 ± 1	4 ± 0		15 ± 1	11 ± 0	
Fe	64 ± 3	59 ± 5		64 ± 8	62 ± 7	
Cu	100 ± 0	100 ± 0		100 ± 0	100 ± 0	
Zn	60 ± 1	59 ± 0		58 ± 1	63 ± 1	
	Metathesis					
	G_M	U_M	V_M	E_M	N_M	T_M
C	86 ± 22	168 ± 49	379 ± 153	126 ± 24	251 ± 82	733 ± 215
O	37 ± 4	42 ± 6	39 ± 6	37 ± 3	37 ± 8	39 ± 1
S	6 ± 2	7 ± 3	7 ± 2	7 ± 2	7 ± 2	7 ± 1
Fe	69 ± 14	68 ± 12	64 ± 20	62 ± 20	56 ± 22	55 ± 8
Cu	100 ± 0	100 ± 0	100 ± 0	100 ± 0	100 ± 0	100 ± 0
Zn	58 ± 1	61 ± 2	59 ± 1	61 ± 1	62 ± 3	59 ± 3
	Filter paper					
	G_F	U_F	V_F	E_F	N_F	T_F
C	91 ± 28	71 ± 9	70 ± 15	91 ± 10	85 ± 19	97 ± 12
O	35 ± 1	32 ± 2	37 ± 6	36 ± 2	30 ± 0	39 ± 5
S	8 ± 2	6 ± 1	9 ± 2	8 ± 1	8 ± 1	9 ± 2
Fe	55 ± 5	59 ± 10	59 ± 10	60 ± 10	54 ± 6	74 ± 12
Cu	100 ± 0	100 ± 0	100 ± 0	100 ± 0	100 ± 0	100 ± 0
Zn	59 ± 1	60 ± 3	59 ± 2	60 ± 2	59 ± 1	57 ± 1

For the squalene samples, the detected amounts of carbon and sulfur are different depending on the cobalt and carbon black content of the mixture. Wires immersed into mixtures without carbon black (**G_S**, **E_S**) had higher sulfur content than wires from mixture containing carbon black (**U_S**, **N_S**). This can be attributed to the higher viscosity caused by carbon black. As a consequence, diffusion might be hindered and therefore, a lower sulfidation level can be achieved. Further, mixtures without cobalt stearate

(G_S , U_S) resulted in lower sulfur levels than mixtures containing cobalt stearate (E_S , N_S). A higher sulfidation level with the addition of cobalt salt could explain the better initial adhesion. Unfortunately, these results are not confirmed by the filter paper and the olefin metathesis experiments. For the wires obtained by the olefin metathesis method sulfur levels are the same, independent of the cobalt stearate and the carbon black level. The only differences are the increased carbon levels, which are, as mentioned before, due to immobilized organic residues. In the case of the filter paper samples, sulfur levels are slightly higher than for the metathesis samples but within measurement inaccuracy and again, mostly the same. Further, the filter paper effectively retains rubber molecules and carbon black, so that the carbon levels are very low and more or less the same for all samples.

Pull-out tests have shown clearly better initial adhesion for compounds containing cobalt salt. In the SEM images differences in the surface structures could be observed but in the elemental characterization the composition was more or less the same (with exception of the squalene samples). Therefore, the differences might be explained by different binding states of the elements. For example sulfur can be bound to both, copper and zinc. In the literature it is reported that cobalt addition diminishes the zinc sulfide formation and enhances the creation of copper sulfide.^{1,20} This assumption is further supported by the observation that the needle-shaped structures mainly consist of Cu_xS (see chapter 4.4 - Comparison of different analytical methods).

To investigate the influence of thermal aging on the adhesion interface, the T-test specimens for the filter paper and the metathesis experiments were subjected to a thermal aging treatment (4 h, 150 °C). For the squalene experiments no aged data could be obtained, because an aging treatment in squalene mixtures is not possible. Optical microscopy images of the wires from compounds without carbon black are shown in Figure 41. Specimens from compounds without carbon black were taken as an example, since the same effects can be seen in the other compounds as well. Further, wires from compounds without carbon black are more suitable, because there are less carbon residues which might be interfering during the characterization. Comparison of the thermally aged specimens to the unaged specimens show, for both, the metathesis and the filter paper samples, changed optical appearance. This effect is especially visible in the case of the metathesis samples (G_M , E_M). Here, the unaged specimens have an orange color with bluish or greenish lamellar areas whereas the thermally aged specimens have a green surface. This indicates a progressing sulfidation

during the aging treatment. A similar effect can be seen for the filter paper specimens (G_F , E_F): the unaged specimens show a surface, which is partly orange and mostly blue and after the aging treatment the surface is almost completely covered in blue with a slightly green touch. This change of surface color suggests an increased sulfidation level for the aged wires.

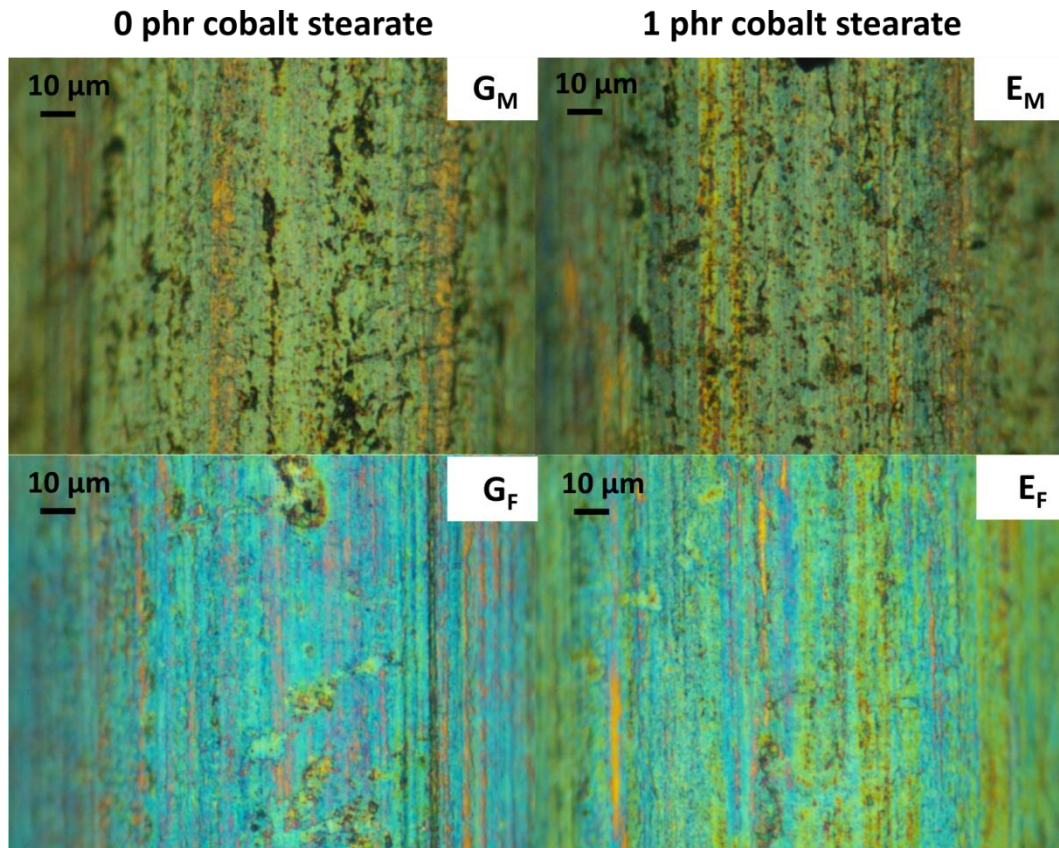


FIGURE 41. OPTICAL MICROSCOPY IMAGES OF WIRES FROM THERMALLY AGED COMPOUNDS WITHOUT CARBON BLACK (G_M : METATHESIS, 0 PHR COBALT STEARATE; E_M : METATHESIS, 1 PHR COBALT STEARATE; G_F : FILTER PAPER, 0 PHR COBALT STEARATE; E_F : FILTER PAPER, 1 PHR COBALT STEARATE)

The SEM images of the thermally aged metathesis and filter paper samples are shown in Figure 42. At the shown magnification, no obvious difference can be observed between the wire surfaces from compounds containing cobalt stearate and from compounds without cobalt salt for neither, the metathesis nor the filter paper specimens. The thermally aged metathesis samples show very large surface structures, which are most probably due to incompletely removed rubber. In the case of the filter

paper specimens, needle-shaped structures can be seen, even at this magnification. It looks like as if these structures extensively grow during the aging, which, as a consequence, get brittle and might easily break.

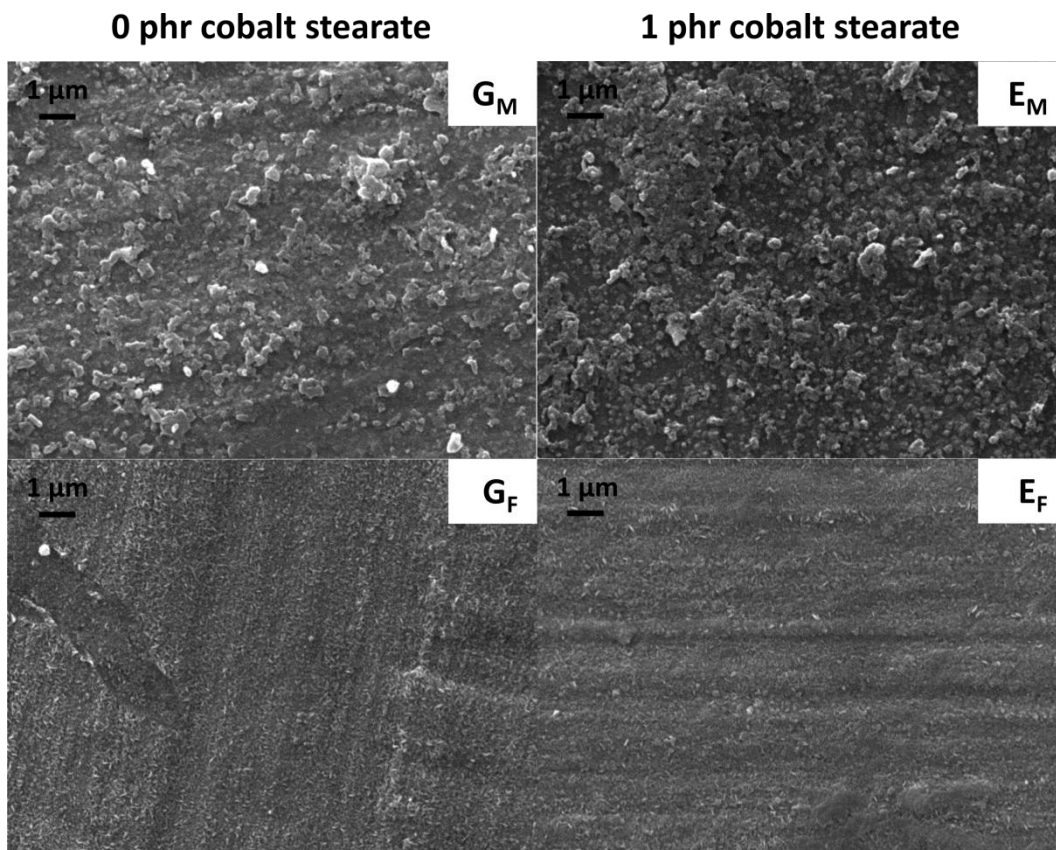


FIGURE 42. SEM IMAGES (20 KEV) OF WIRES FROM THERMALLY AGED COMPOUNDS WITHOUT CARBON BLACK (G_M: METATHESIS, 0 PHR COBALT STEARATE; E_M: METATHESIS, 1 PHR COBALT STEARATE; G_F: FILTER PAPER, 0 PHR COBALT STEARATE; E_F: FILTER PAPER, 1 PHR COBALT STEARATE)

EDX results of the thermally aged specimens are shown in Table 23. Sulfur levels are almost the same for the metathesis samples and the filter paper samples. However, due to organic residues and/or immobilized carbon black, carbon levels are higher for the metathesis samples than for the filter paper samples. Further a slight increase in the sulfur levels with increasing amounts of carbon black can be observed especially in the case of the filter paper specimens. As far as the influence of cobalt stearate on the sulfidation level is concerned, no differences can be observed; sulfur levels are more or less the same for specimens from cobalt containing compounds and for specimens

from compounds without cobalt salt. The more interesting point is the increased sulfur content after the aging treatment, which can be seen by the comparison of the unaged values (Table 22) with the aged ones (Table 23). For example, for the unaged metathesis specimens the sulfur levels are around 7, whereas they are between 8 and 11 after the thermal aging. The same applies to the filter paper samples. Therefore, it can be concluded, that the observed changes in color and structure are due to a further sulfidation of the brass layer.

TABLE 23. EDX ANALYSIS (20 KEV) OF WIRE SURFACES FROM THERMALLY AGED COMPOUNDS CONTAINING DIFFERENT AMOUNTS OF COBALT STEARATE AND CARBON BLACK

carbon black	0 phr cobalt stearate			1 phr cobalt stearate		
	0 phr	10 phr	50 phr	0 phr	10 phr	50 phr
	Metathesis					
	G_M	U_M	V_M	E_M	N_M	T_M
C	172 ± 13	273 ± 17	779 ± 144	176 ± 12	230 ± 27	531 ± 150
O	42 ± 4	43 ± 3	44 ± 4	43 ± 3	38 ± 7	43 ± 9
S	8 ± 2	10 ± 1	11 ± 2	10 ± 1	8 ± 1	10 ± 4
Fe	84 ± 25	57 ± 7	59 ± 8	59 ± 5	73 ± 14	73 ± 31
Cu	100 ± 0	100 ± 0	100 ± 0	100 ± 0	100 ± 0	100 ± 0
Zn	57 ± 3	61 ± 1	60 ± 1	60 ± 1	60 ± 3	60 ± 2
	Filter paper					
	G_F	U_F	V_F	E_F	N_F	T_F
C	67 ± 4	70 ± 14	69 ± 13	88 ± 22	75 ± 20	72 ± 9
O	36 ± 1	39 ± 5	37 ± 2	37 ± 4	33 ± 3	40 ± 4
S	9 ± 1	8 ± 1	11 ± 1	9 ± 1	10 ± 1	11 ± 2
Fe	64 ± 3	58 ± 10	59 ± 4	59 ± 4	53 ± 9	69 ± 7
Cu	100 ± 0	100 ± 0	100 ± 0	100 ± 0	100 ± 0	100 ± 0
Zn	59 ± 1	60 ± 1	59 ± 3	58 ± 2	59 ± 1	56 ± 1

4.5.1.1 CONCLUSION

Addition of cobalt stearate to the compound not only changed the cure characteristics (t_{05} increased, t_{90} decreased) but also the physical properties of the vulcanized rubber. After a thermal aging treatment, physical properties for both, cobalt-free and cobalt-containing compounds decrease. Adhesion properties for unaged compounds are better with the addition of cobalt stearate.

In the squalene experiments, there are major differences visible between the wires from the different compounds, but these differences were not observed on the filter paper and the olefin metathesis samples. On the surfaces of these samples the optical characterization showed only small differences between cobalt-containing and cobalt-free samples and in the elemental characterization the composition was more or less the same. But on the other hand, in the SEM characterization differently textured surfaces were observed. Therefore, the differences might be explained by different binding states of the elements. For example sulfur can be bound to both, copper and zinc. In the literature it is reported that cobalt addition diminishes the zinc sulfide formation and enhances the creation of copper sulfide.^{1,20}

After the aging treatment, adhesion values for the compound without cobalt stearate increased, whereas compounds containing cobalt salt showed inferior adhesion performance, compared to initial adhesion values. A possible explanation was that the initial binding layer for the cobalt free compound is not perfect for bonding (e.g. copper sulfide layer is not ideally textured) and improves a little during the aging (e.g. better surface texture), whereas the cobalt salt improves the performance of the initial binding layer of this compound. During the thermal aging treatment the adhesion layers of both, the cobalt containing and the cobalt free compound grow, which can be observed by the change of the surface color and an increased sulfur level. As a result, the surface textures change as well. For the cobalt free compound the aged binding layer gives better performance than the initial one, whereas for the cobalt containing one, the original binding layer was ideal and therefore, the result after the aging is inferior. As a consequence, in this case, almost the same adhesion performance is achieved for both compounds after the thermal aging treatment.

4.5.2 ANTIOXIDANT AGENT

The previous chapter dealt with the influence of cobalt stearate on rubber-to-brass adhesion. In that study, adhesion values for thermally aged compounds without cobalt salt were higher than for comparable compounds containing cobalt stearate. This is quite surprising, since cobalt salts are supposed to enhance the adhesion properties, especially after aging. However, cobalt in the rubber may have deteriorating effects on the thermal stability of the rubber network.¹⁶ To eliminate the possibility that the reduced adhesion values after the aging treatment are due to the negative influence of cobalt on the rubber stability, rubber compounds with additional antioxidant agents (N-isopropyl-N'-phenyl-*p*-phenylenediamine (IPPD) and N-(1,3-dimethylbutyl)-N'-phenyl-*p*-phenylenediamine (6PPD), see Figure 43) were prepared.

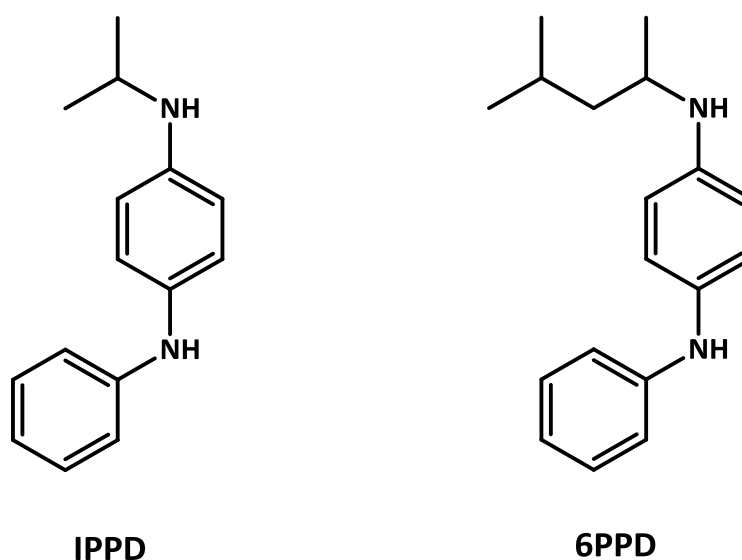


FIGURE 43. N-ISOPROPYL-N'-PHENYL-*P*-PHENYLENEDIAMINE (IPPD) AND N-(1,3-DIMETHYLBUTYL)-N'-PHENYL-*P*-PHENYLENEDIAMINE (6PPD)

Compound formulations are shown in Table 24. Compounds **G**, **U**, **V**, **E**, **N**, **T** are the mixtures without antioxidant agents, compounds **GA**, **UA**, **VA**, **EA**, **NA**, **TA** contain both IPPD and 6PPD. These compounds were vulcanized for 20 minutes at 160 °C and 320 bar. Additionally the vulcanized rubber specimens were subjected to a thermal aging treatment (4 h at 150 °C). Physical properties of the unaged and the aged vulcanized compounds were tested, as well as the pull-out force and rubber coverage.

Furthermore, the adhesion interface of the sulfidated wires obtained by the filter paper (marked with a subscript F) and the olefin metathesis method (marked with a subscript M) was studied using optical microscopy and SEM-EDX.

TABLE 24. COMPOUND FORMULATION TO STUDY THE INFLUENCE OF ANTIOXIDANT AGENT ON RUBBER-TO-BRASS ADHESION

	G/GA	U/UA	V/VA	E/EA	N/NA	T/TA
	phr					
Natural rubber	100	100	100	100	100	100
Naphthenic oil	6	6	6	6	6	6
ZnO	7	7	7	7	7	7
Stearic acid	2	2	2	2	2	2
DCBS	0.7	0.7	0.7	0.7	0.7	0.7
Sulfur	6.25	6.25	6.25	6.25	6.25	6.25
N550 Carbon black	0	10	50	0	10	50
Cobalt stearate	0	0	0	1	1	1
IPPD	0/0.75	0/0.75	0/0.75	0/0.75	0/0.75	0/0.75
6PPD	0/0.75	0/0.75	0/0.75	0/0.75	0/0.75	0/0.75

Compounds G, U, V, E, N, T contain no antioxidant agents, compounds GA, UA, VA, EA, NA, TA contain IPPD and 6PPD

Cure characteristics (scorch time t_{05} and optimum curing time t_{90}) and physical properties of the vulcanized compounds and the thermally aged compounds are listed in Table 25. It is evident that the addition of IPPD and 6PPD leads to a decrease in scorch time and to a partly decrease in cure time. Tear strength values decrease with addition of antioxidant agents, tensile strength and elongation at break values are almost the same as for compounds without antioxidant agent. During the aging treatment, tear strength, tensile strength and elongation at break all decrease. For compounds with high carbon black loading tear strength, tensile strength and elongation at break values are comparable for mixtures containing IPPD and 6PPD (**VA**, **TA**) and mixtures without antioxidant agents (**V**, **T**). In some cases values for antioxidant agent containing compounds are even better than for the compounds without. For the compounds with low or no carbon black loading, mixtures containing IPPD and 6PPD exhibit inferior behavior, especially as far as tensile strength and elongation at break are concerned. For compounds **GA**, **UA**, **E** and **EA** no tensile

strength data could be obtained, because the specimens were not mechanically stable after the aging treatment.

TABLE 25. CURE CHARACTERISTICS (SCORCH TIME T05, OPTIMUM CURING TIME T90) AND PHYSICAL PROPERTIES OF COMPOUNDS CONTAINING DIFFERENT AMOUNTS OF COBALT STEARATE AND ANTIOXIDANT AGENT

	G	GA	U	UA	V	VA	E	EA	N	NA	T	TA
Unaged												
t₀₅, min	1.5	1.1	1.4	1.2	1.2	1.0	2.4	1.8	1.8	1.5	1.5	1.3
t₉₀, min	17.4	17.4	15.7	15.3	12.7	11.5	12.2	10.8	11.6	10.6	9.4	8.3
Tear S.^{a)}, N	22	16	20	18	92	84	16	14	21	17	68	86
T.S.^{b)}, N/mm²	9.1	8.9	16.9	15.8	19.9	21.6	9.9	7.6	16.5	17.0	16.5	19.9
E.B.^{c)}, %	617	685	628	621	415	450	593	520	606	626	370	435
Thermally aged												
Tear S.^{a)}, N	14	11	13	13	38	39	13	10	13	13	36	42
T.S.^{b)}, N/mm²	1.4	-	1.9	-	4.9	5.3	-	-	1.6	1.2	4.7	5.1
E.B.^{c)}, %	407	207	363	162	244	237	158	97	320	117	212	216

^{a)} tear strength ^{b)} tensile strength ^{c)} elongation at break

Pull-out force and rubber coverage are shown in Table 26. Pull-out forces for compounds without and for compounds containing antioxidant agents are mostly the same within the tolerances. The rubber coverage of the pulled-out wires from compounds containing 6PPD and IPPD (**GA, UA, VA, EA, NA, TA**) is in most cases slightly lower than for compounds without antioxidant agents (**G, U, V, E, N, T**). After the aging treatment, for compounds with high carbon black loading, there are almost no differences in the adhesion levels between compounds with and compounds without antioxidant agents. For compounds with low or no carbon black content, adhesion properties for antioxidant agents containing compounds (**GA, UA, EA, NA**) are slightly lower than for compounds without (**G, U, E, N**). Furthermore, it is obvious that the addition of IPPD and 6PPD did not improve the physical properties or the adhesion values for cobalt containing compounds. Therefore, it might be concluded that it is not the negative influence of cobalt on the rubber stability, which reduces the adhesion values during the aging treatment.

TABLE 26. PULL-OUT FORCE AND RUBBER COVERAGE OF COMPOUNDS CONTAINING DIFFERENT AMOUNTS OF COBALT STEARATE AND ANTIOXIDANT AGENT

Unaged						
	G	U	V	E	N	T
Pull-out force, N	155 ± 46	205 ± 26	420 ± 39	260 ± 79	464 ± 38	505 ± 38
Coverage	1	2	3	3	3	3
	GA	UA	VA	EA	NA	TA
Pull-out force, N	156 ± 60	241 ± 41	482 ± 59	255 ± 78	428 ± 61	470 ± 61
Coverage	0	3	2	2	2	2
Thermally aged						
	G	U	V	E	N	T
Pull-out force, N	208 ± 38	250 ± 48	464 ± 34	118 ± 35	242 ± 25	458 ± 41
Coverage	1	3	3	1	3	3
	GA	UA	VA	EA	NA	TA
Pull-out force, N	167 ± 60	146 ± 13	447 ± 22	102 ± 28	134 ± 20	425 ± 42
Coverage	0	3	3	0	3	3

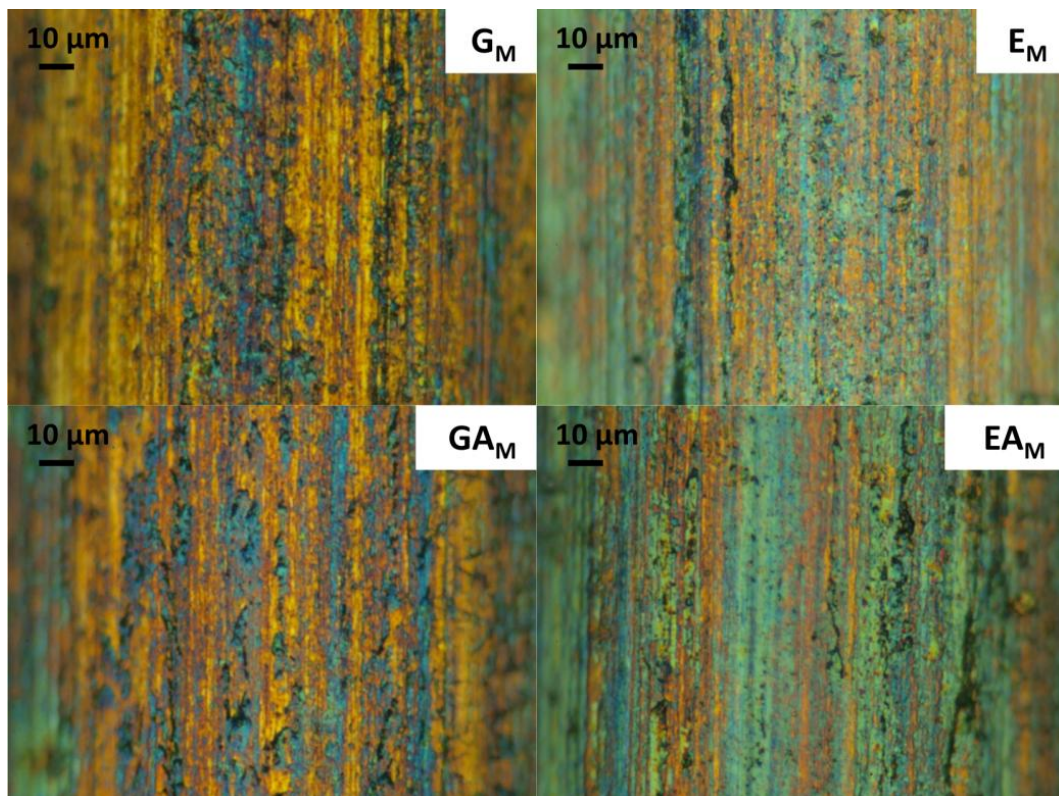


FIGURE 44. OPTICAL MICROSCOPY IMAGES OF SAMPLES OBTAINED BY THE OLEFIN METATHESIS METHOD (G_M : 0 PHR COBALT STEARATE, 0 PHR ANTIOXIDANT AGENTS; E_M : 1 PHR COBALT STEARATE, 0 PHR ANTIOXIDANT AGENTS; GA_M : 0 PHR COBALT STEARATE, 0.75 PHR IPPD, 0.75 PHR 6PPD; EA_M : 1 PHR COBALT STEARATE, 0.75 PHR IPPD, 0.75 PHR 6PPD)

To investigate the observed effects of the antioxidant agents on the adhesion layer, wires obtained by filter paper experiments and olefin metathesis reactions were investigated by optical microscopy and SEM-EDX. Only specimens from compound without carbon black were taken as an example, since the same effects can be seen in all compounds.

Optical microscopy images of the metathesis samples are shown in Figure 44. There is almost no difference between the specimens with and without antioxidant agents. But, as before, there is a small difference between the samples without and the sample containing cobalt stearate. The specimens without cobalt stearate (G_M , GA_M) are orange with blue lamellar areas, whereas the samples containing cobalt stearate (E_M , EA_M) show a more greenish color with some orange lamellar areas.

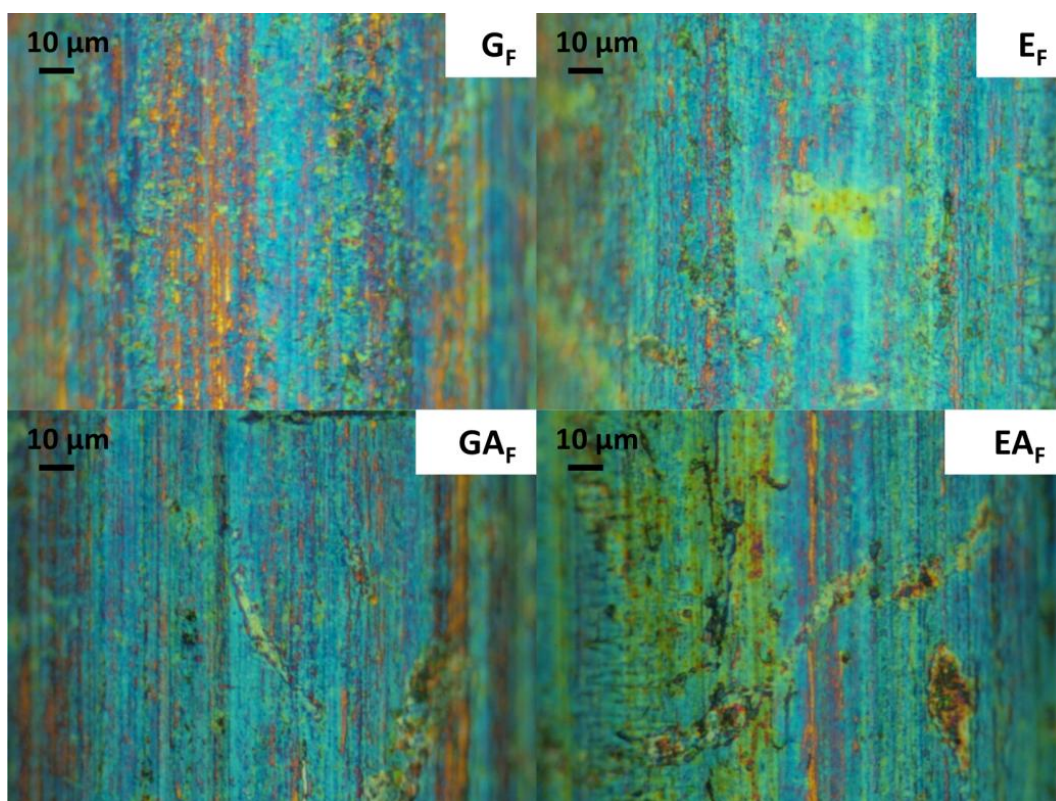


FIGURE 45. OPTICAL MICROSCOPY IMAGES OF SAMPLES OBTAINED BY FILTER PAPER EXPERIMENTS (G_F : 0 PHR COBALT STEARATE, 0 PHR ANTIOXIDANT AGENTS; E_F : 1 PHR COBALT STEARATE, 0 PHR ANTIOXIDANT AGENTS; GA_F : 0 PHR COBALT STEARATE, 0.75 PHR IPPD, 0.75 PHR 6PPD; EA_F : 1 PHR COBALT STEARATE, 0.75 PHR IPPD, 0.75 PHR 6PPD)

Optical microscopy images of the filter paper samples can be seen in Figure 45. Similar to the metathesis samples, there are almost no differences between the specimens from mixture containing IPPD and 6PPD and mixtures without. All samples have a mostly bluish surface color with some orange areas in between. However, it looks like as if samples from mixtures containing antioxidant agents (\mathbf{GA}_F , \mathbf{EA}_F) have slightly less orange areas than samples from compounds without.

SEM images of the metathesis samples are shown in Figure 46. There is almost no difference between the specimens with and without antioxidant agents. But, as before, there is a small difference between the samples without and the sample containing cobalt stearate. For the samples without cobalt salt (\mathbf{G}_M , \mathbf{GA}_M), there are only few surface structures whereas with the addition of cobalt stearate (\mathbf{E}_M , \mathbf{EA}_M) finely distributed structures can be found on the wire surfaces.

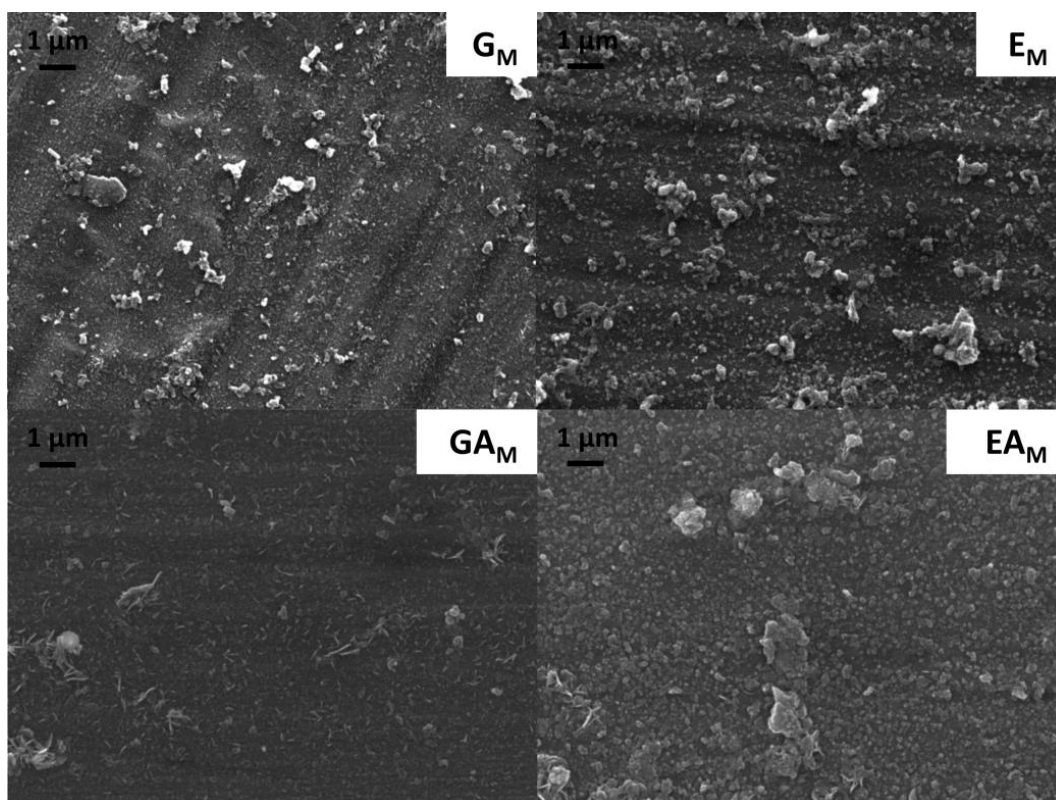


FIGURE 46. SEM IMAGES OF SAMPLES OBTAINED BY THE OLEFIN METATHESIS METHOD (\mathbf{G}_M : 0 PHR COBALT STEARATE, 0 PHR ANTIOXIDANT AGENTS; \mathbf{E}_M : 1 PHR COBALT STEARATE, 0 PHR ANTIOXIDANT AGENTS; \mathbf{GA}_M : 0 PHR COBALT STEARATE, 0.75 PHR IPPD, 0.75 PHR 6PPD; \mathbf{EA}_M : 1 PHR COBALT STEARATE, 0.75 PHR IPPD, 0.75 PHR 6PPD)

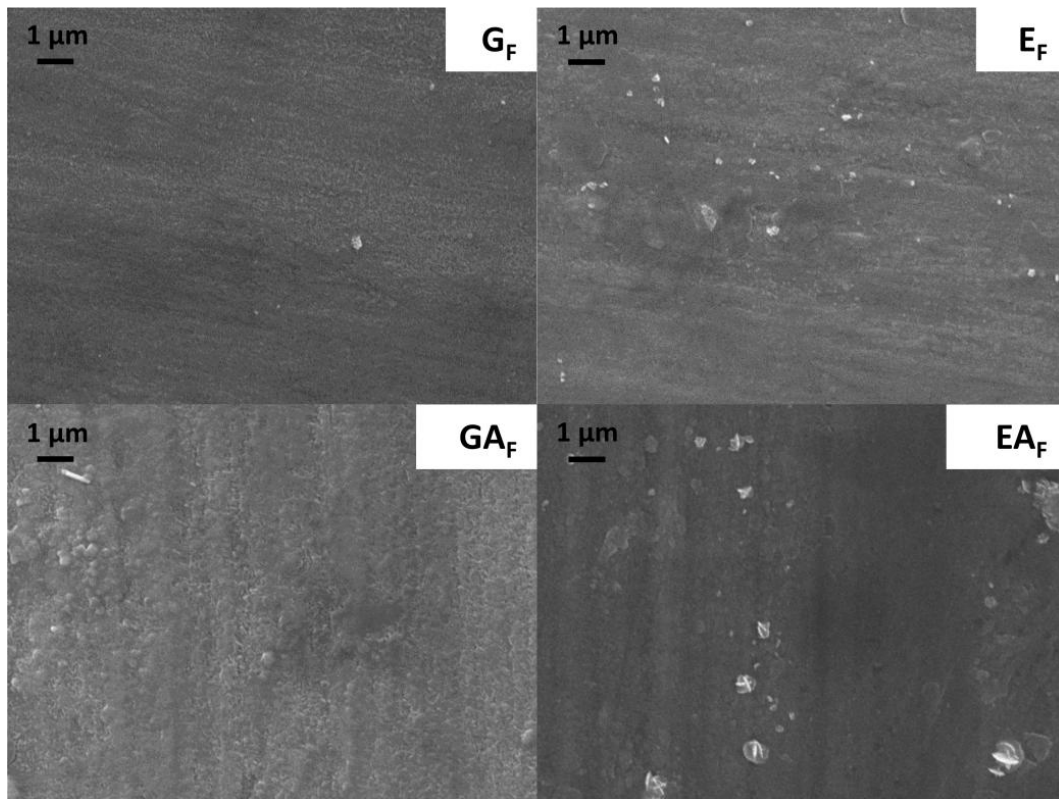


FIGURE 47. SEM IMAGES OF SAMPLES OBTAINED BY THE FILTER PAPER METHOD (G_F: 0 PHR COBALT STEARATE, 0 PHR ANTIOXIDANT AGENTS; E_F: 1 PHR COBALT STEARATE, 0 PHR ANTIOXIDANT AGENTS; GA_F: 0 PHR COBALT STEARATE, 0.75 PHR IPPD, 0.75 PHR 6PPD; EA_F: 1 PHR COBALT STEARATE, 0.75 PHR IPPD, 0.75 PHR 6PPD)

SEM images of the filter paper specimens can be seen in Figure 47. Similar to the metathesis samples, there are almost no differences between the specimens from mixture containing IPPD and 6PPD and mixtures without. Almost no surface structures can be found on any of the wire samples.

To analyze the composition of the sulfidated wires, the samples were further characterized using EDX (see Table 27). Zinc, iron and oxygen levels are constant within measuring inaccuracy; outliers in iron level stem from irregular brass plating. Therefore, the most interesting elements are the sulfur and the carbon level. For the metathesis samples, values for sulfidated wires from compounds without and compounds containing antioxidant agents are almost the same. Carbon levels vary a bit, but sulfur levels are constant. These results are in accordance with the results obtained by pull-out testing, that there is almost no difference in the adhesion levels of compounds containing antioxidant agents and compounds without.

TABLE 27. EDX ANALYSIS OF WIRE SURFACES FROM COMPOUNDS CONTAINING DIFFERENT AMOUNTS OF COBALT STEARATE AND ANTIOXIDANT AGENT

carbon black	0 phr cobalt stearate			1 phr cobalt stearate		
	0 phr	10 phr	50 phr	0 phr	10 phr	50 phr
	Metathesis					
	G_M	U_M	V_M	E_M	N_M	T_M
C	86 ± 22	168 ± 49	379 ± 153	126 ± 24	251 ± 82	733 ± 215
O	37 ± 4	42 ± 6	39 ± 6	37 ± 3	37 ± 8	39 ± 1
S	6 ± 2	7 ± 3	7 ± 2	7 ± 2	7 ± 2	7 ± 1
Fe	69 ± 14	68 ± 12	64 ± 20	62 ± 20	56 ± 22	55 ± 8
Cu	100 ± 0	100 ± 0	100 ± 0	100 ± 0	100 ± 0	100 ± 0
Zn	58 ± 1	61 ± 2	59 ± 1	61 ± 1	62 ± 3	59 ± 3
	GA_M	UA_M	VA_M	EA_M	NA_M	TA_M
C	70 ± 9	88 ± 4	427 ± 105	117 ± 21	122 ± 9	395 ± 142
O	38 ± 3	41 ± 3	44 ± 3	42 ± 7	40 ± 2	43 ± 6
S	5 ± 1	7 ± 1				
Fe	57 ± 6	63 ± 3	59 ± 13	58 ± 14	53 ± 7	63 ± 19
Cu	100 ± 0	100 ± 0	100 ± 0	100 ± 0	100 ± 0	100 ± 0
Zn	59 ± 1	59 ± 2	61 ± 1	61 ± 1	59 ± 1	59 ± 4
	Filter paper					
	G_F	U_F	V_F	E_F	N_F	T_F
C	91 ± 28	71 ± 9	70 ± 15	91 ± 10	85 ± 19	97 ± 12
O	35 ± 1	32 ± 2	37 ± 6	36 ± 2	30 ± 0	39 ± 5
S	8 ± 2	6 ± 1	9 ± 2	8 ± 1	8 ± 1	9 ± 2
Fe	55 ± 5	59 ± 10	59 ± 10	60 ± 10	54 ± 6	74 ± 12
Cu	100 ± 0	100 ± 0	100 ± 0	100 ± 0	100 ± 0	100 ± 0
Zn	59 ± 1	60 ± 3	59 ± 2	60 ± 2	59 ± 1	57 ± 1
	GA_F	UA_F	VA_F	EA_F	NA_F	TA_F
C	82 ± 23	98 ± 91	73 ± 19	105 ± 54	112 ± 28	63 ± 4
O	36 ± 3	42 ± 6	40 ± 6	40 ± 7	42 ± 6	38 ± 4
S	8 ± 1	10 ± 2	11 ± 3	9 ± 1	10 ± 1	10 ± 1
Fe	75 ± 4	77 ± 45	81 ± 59	69 ± 11	50 ± 13	72 ± 9
Cu	100 ± 0	100 ± 0	100 ± 0	100 ± 0	100 ± 0	100 ± 0
Zn	56 ± 2	56 ± 2	57 ± 2	58 ± 3	58 ± 1	60 ± 3

In the case of the filter paper specimens, wires from compounds containing IPPD and 6PPD had slightly higher sulfur levels than wires from comparable compounds without antioxidant agents, which is surprising since the adhesion levels are almost the same. Furthermore, on the metathesis samples no differences between the samples were observed, neither. On the other hand, in the optical microscopy slightly less orange

areas can be seen for samples from mixtures containing antioxidant agents (\mathbf{GA}_F , \mathbf{EA}_F), which might explain the higher sulfur levels.

Optical microscopy images of thermally aged samples are shown in Figure 48. The aged metathesis sample from the mixture without antioxidant agents (\mathbf{E}_M) has a green surface, the metathesis sample from the mixture containing IPPD and 6PPD (\mathbf{EA}_M) has a slightly yellow touch. The same applies to the filter paper specimens. Sample \mathbf{E}_F has a greenish-blue color, whereas sample \mathbf{EA}_F has a yellow touch. It seems as if the addition of antioxidant agents accelerates the aging reaction, which would explain the slightly lower pull-out force of sample \mathbf{EA} compared to sample \mathbf{E} .

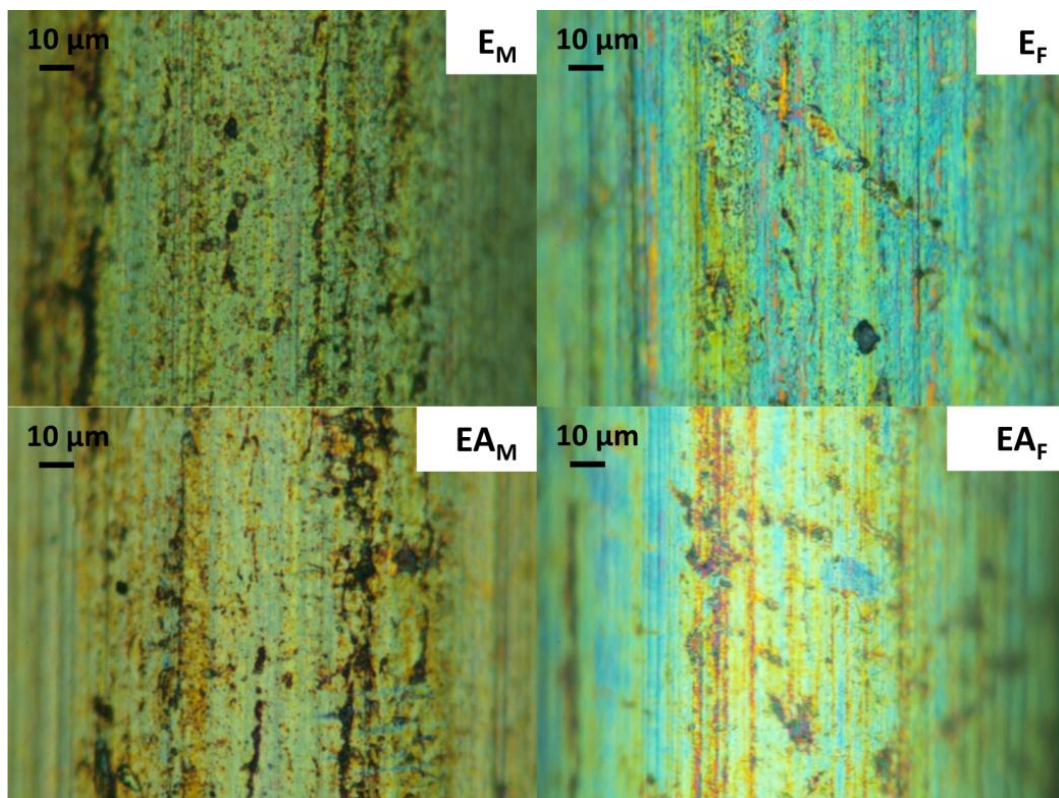


FIGURE 48. OPTICAL MICROSCOPY IMAGES OF THERMALLY AGED SAMPLES (\mathbf{E}_M : METATHESIS, 1 PHR COBALT STEARATE, 0 PHR ANTIOXIDANT AGENTS; \mathbf{EA}_M : METATHESIS, 1 PHR COBALT STEARATE, 0.75 PHR IPPD, 0.75 PHR 6PPD; \mathbf{E}_F : FILTER PAPER, 1 PHR COBALT STEARATE, 0 PHR ANTIOXIDANT AGENTS; \mathbf{EA}_F : FILTER PAPER, 1 PHR COBALT STEARATE, 0.75 PHR IPPD, 0.75 PHR 6PPD)

To clarify if the observed differences between the thermally aged specimens with and without antioxidant agents are only related to the color or if there are also structural

differences, the specimens were characterized using SEM (Figure 49). It is clearly visible that the structures found differ depending on the preparation method used (crystalline structures in the case of the filter paper specimens, mostly amorphous structures in the case of the metathesis samples). On the other hand, there are no major differences between the structures found on the sample without antioxidant agents (E) and samples containing IPPD and 6PPD (EA). Compared to the unaged specimens a change of the surface structures can be observed. For both, the metathesis as well as the filter paper specimens, it looks like the structures have grown in size (see Figure 46 and Figure 47).

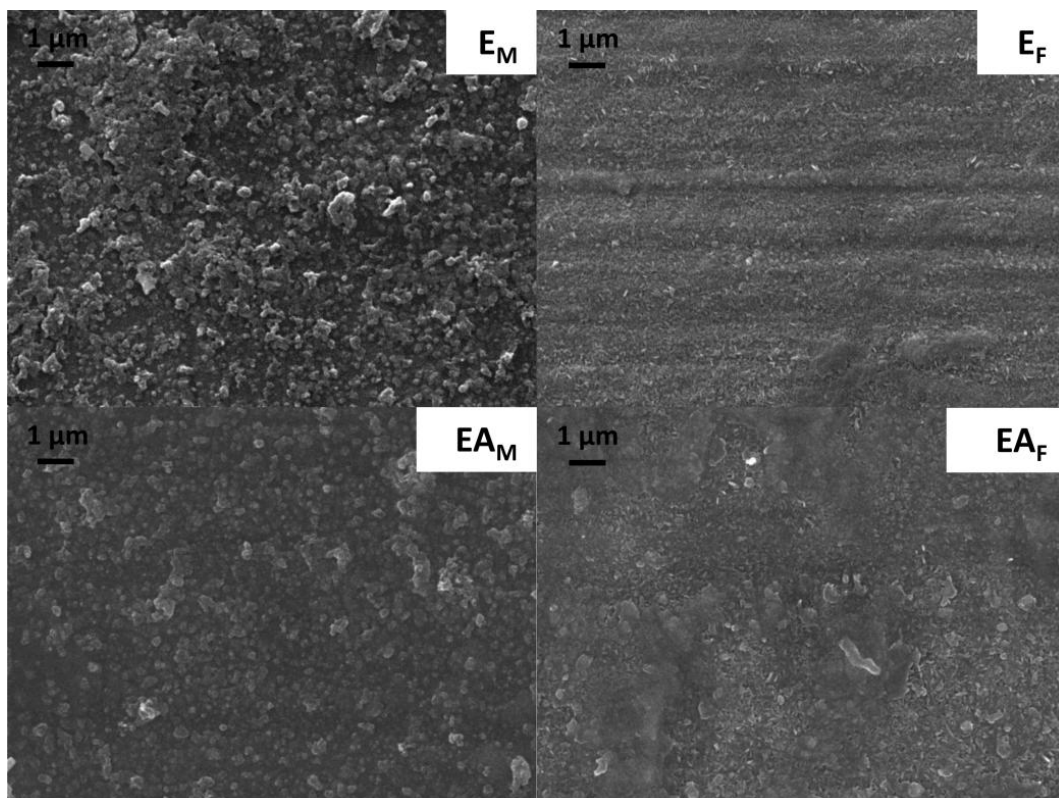


FIGURE 49. SEM IMAGES OF THERMALLY AGED SAMPLES (E_M : METATHESIS, 1 PHR COBALT STEARATE, 0 PHR ANTIOXIDANT AGENTS; EA_M : METATHESIS, 1 PHR COBALT STEARATE, 0.75 PHR IPPD, 0.75 PHR 6PPD; E_F : FILTER PAPER, 1 PHR COBALT STEARATE, 0 PHR ANTIOXIDANT AGENTS; EA_F : FILTER PAPER, 1 PHR COBALT STEARATE, 0.75 PHR IPPD, 0.75 PHR 6PPD)

EDX results for the thermally aged specimens are shown in Table 28. The sulfur levels for all samples are higher than for the unaged wires (Table 27), which corresponds well

with the observed changes in color and structure (Figure 48, Figure 49). For the metathesis samples, sulfur levels vary a little bit between wires from compounds containing antioxidant agents and wires from compounds without. However, no definite trend can be observed which testing series gives the higher sulfur levels.

TABLE 28. EDX ANALYSIS OF THE THERMALLY AGED WIRES FROM COMPOUNDS CONTAINING DIFFERENT AMOUNTS OF COBALT STEARATE AND ANTIOXIDANT AGENT

carbon black	0 phr cobalt stearate			1 phr cobalt stearate		
	0 phr	10 phr	50 phr	0 phr	10 phr	50 phr
	Metathesis					
	G_M	U_M	V_M	E_M	N_M	T_M
C	172 ± 13	273 ± 17	779 ± 144	176 ± 12	230 ± 27	531 ± 150
O	42 ± 4	43 ± 3	44 ± 4	43 ± 3	38 ± 7	43 ± 9
S	8 ± 2	10 ± 1	11 ± 2	10 ± 1	8 ± 1	10 ± 4
Fe	84 ± 25	57 ± 7	59 ± 8	59 ± 5	73 ± 14	73 ± 31
Cu	100 ± 0	100 ± 0	100 ± 0	100 ± 0	100 ± 0	100 ± 0
Zn	57 ± 3	61 ± 1	60 ± 1	60 ± 1	60 ± 3	60 ± 2
	GA_M	UA_M	VA_M	EA_M	NA_M	TA_M
C	183 ± 16	151 ± 21	454 ± 74	168 ± 23	225 ± 7	224 ± 66
O	46 ± 5	37 ± 4	45 ± 2	39 ± 2	43 ± 2	45 ± 3
S	8 ± 1	10 ± 0	10 ± 1	9 ± 1	13 ± 2	7 ± 1
Fe	68 ± 8	51 ± 5	44 ± 16	50 ± 3	56 ± 2	53 ± 15
Cu	100 ± 0	100 ± 0	100 ± 0	100 ± 0	100 ± 0	100 ± 0
Zn	58 ± 1	58 ± 1	62 ± 2	60 ± 0	61 ± 2	62 ± 1
	Filter paper					
	G_F	U_F	V_F	E_F	N_F	T_F
C	67 ± 4	70 ± 14	69 ± 13	88 ± 22	75 ± 20	72 ± 9
O	36 ± 1	39 ± 5	37 ± 2	37 ± 4	33 ± 3	40 ± 4
S	9 ± 1	8 ± 1	11 ± 1	9 ± 1	10 ± 1	11 ± 2
Fe	64 ± 3	58 ± 10	59 ± 4	59 ± 4	53 ± 9	69 ± 7
Cu	100 ± 0	100 ± 0	100 ± 0	100 ± 0	100 ± 0	100 ± 0
Zn	59 ± 1	60 ± 1	59 ± 3	58 ± 2	59 ± 1	56 ± 1
	GA_F	UA_F	VA_F	EA_F	NA_F	TA_F
C	111 ± 5	96 ± 12	187 ± 122	118 ± 5	97 ± 13	93 ± 16
O	41 ± 3	42 ± 2	53 ± 8	47 ± 1	43 ± 7	35 ± 3
S	10 ± 0	12 ± 1	15 ± 1	14 ± 1	10 ± 2	12 ± 4
Fe	52 ± 9	62 ± 7	87 ± 8	63 ± 4	47 ± 9	55 ± 12
Cu	100 ± 0	100 ± 0	100 ± 0	100 ± 0	100 ± 0	100 ± 0
Zn	58 ± 1	59 ± 3	51 ± 1	59 ± 1	59 ± 1	56 ± 1

For the filter paper samples, sulfur levels for the wires from compounds without IPPD and 6PPD are similar to the sulfur levels of the metathesis specimens. On the other hand, sulfur levels of wires from compounds containing antioxidant agents are slightly higher. However, the same trend was observed for the unaged filter paper samples. Then again, the higher sulfur levels for wires from compounds containing IPPD and 6PPD would explain the yellow touch observed in the optical microscopy.

4.5.2.1 CONCLUSION

The addition of antioxidant agents (IPPD, 6PPD) did not result in the expected improvement of the physical properties or the adhesion values for cobalt containing compounds. Therefore, it might be concluded that it is not the negative influence of the cobalt on the rubber stability, which reduces the adhesion values during the aging treatment. Furthermore, the addition of IPPD and 6PPD not only changed the cure characteristics (decrease in scorch time, partly decrease in cure time) but also the physical properties (e.g. decrease of tear strength). Pull-out forces were mostly the same for the unaged specimens and slightly lower for the thermally aged specimens.

The optical characterization showed almost no differences for unaged wires from compounds with and for unaged wires from compounds without IPPD and 6PPD. This is also confirmed by EDX analysis, where the sulfur levels are almost the same for the metathesis specimens. On the other hand, in the case of the filter paper specimens, wires from compounds containing IPPD and 6PPD had slightly higher sulfur content but within measurement inaccuracy.

During the aging treatment, the surface color and the surface structures change. This change is due to a further sulfidation of the wires, which is confirmed by a higher sulfur level detected in the EDX characterization.

All in all, it was observed that the addition of IPPD and 6PPD did not lead to any significant changes in the rubber compounds or in the rubber-brass adhesion.

5 SUMMARY AND OUTLOOK

The topic of this thesis was the investigation of the rubber-to-brass adhesion. The focus was set on the investigation of various factors (e.g. the compound composition) which might have an influence on the adhesion performance. In the future, this information may help to understand the adhesion mechanism of rubber to brass and as a result, may help to overcome some of the problems in reinforced rubber products.

Basically, this work can be divided into three major parts:

- The investigation of wires, which had a very similar composition, but showed very different adhesion behavior.
- The investigation and comparison of different analytical methods which allow the study of the sulfidation reaction or the adhesion interface.
- The investigation of the influence of various rubber compound ingredients such as stearic acid, cobalt stearate and antioxidant agents.

Three wires (**Sp2**, **Sp3**, **Sp6**), which had the same specifications, but behaved differently in terms of adhesion were analyzed to determine the reason for this effect. **Sp2** normally gives good adhesion, **Sp3** is rather poor and **Sp6** sometimes adheres very well and sometimes not at all. Analysis of the untreated wires showed differences regarding the surface texture, the brass composition (two brass phases, Cu content) and the brass layer thickness. Also during squalene experiments the three wires behaved differently. **Sp2** has a rough wire surface and the brass composition is very uniform with an optimal Cu content. In the squalene experiments, this wire had the highest sulfidation level. A possible explanation is that due to the rough wire surface, the sulfidation process starts more easily and further in a uniform way, which might be beneficial for a good adhesion. **Sp3** has a very smooth surface and the Cu content is lower than for **Sp2**. The sulfidation in the squalene experiments was lower than for **Sp2**. Most probably the smooth surface hinders the sulfidation and as a result the binding layer has no optimum thickness. **Sp6** has two distinct α -brass phases and an additional β -brass phase. This could be the explanation for the non-uniform distribution of the surface structures found in the squalene experiments. As a

consequence, some parts of the wire have a higher sulfidation level than others and therefore, adhesion is sometimes good and sometimes bad.

This indicates that both, the brass layer composition and the surface roughness, are important parameters for the adhesion of rubber to brass. The composition should be mostly uniform (and only α -brass) and further, a certain degree of surface roughness is necessary to ensure a good sulfidation.

During the squalene experiments, it was observed, that the surface color changes with the sulfidation level. For example, at a low sulfur level the wire surface is blue and then changes from green to yellow and finally to an orange color (see Figure 50). As a consequence, the surface color can help to estimate the sulfidation level. This was used to get a first impression of the surface composition of various samples.

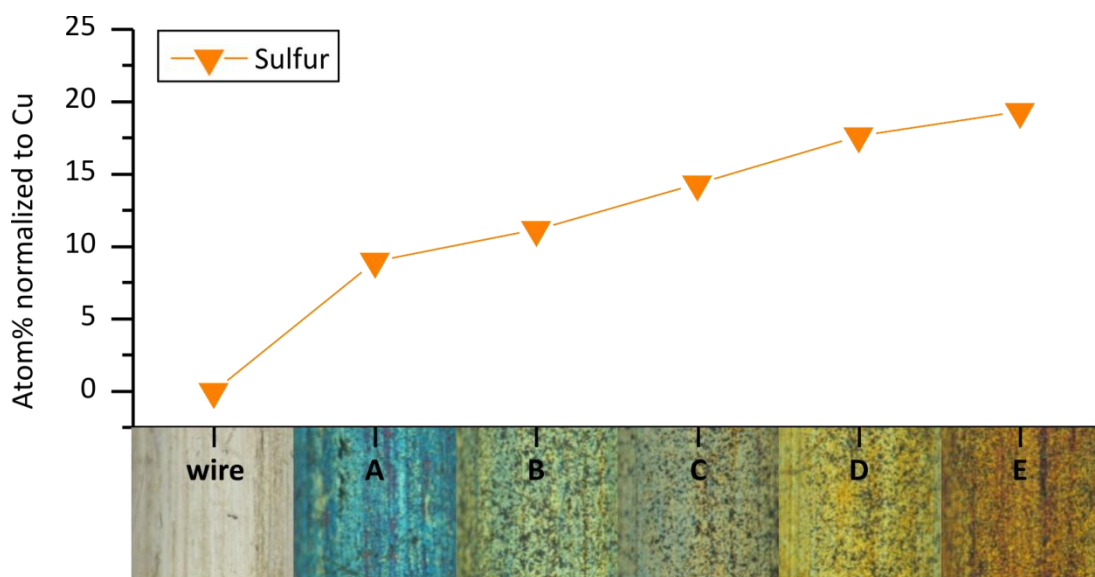


FIGURE 50. COMPARISON OF WIRE COLOR AND SULFUR LEVEL

In the next part, the influence of stearic acid loading on rubber-to-brass adhesion was studied with the help of squalene experiments, metathesis experiments, as well as by tests with natural rubber compounds (pull-out tests and determination of rubber properties). In the squalene experiments a great influence of stearic acid loading on the sulfidation reaction of brass-plated steel wires with rubber compounds could be

observed. Increasing amounts of stearic acid accelerate the reaction of the rubber compounds with the brass-plated steel wires. The enhanced sulfidation with increasing amount of stearic acid can be attributed to two different effects: first, a partly dissolution of the ZnO layer on top of the brass surface, which leads to a faster reaction of the brass, and second, an activation effect. The higher concentration of formed zinc stearate leads to a higher concentration of the active zinc-accelerator complex and thus the sulfidation reaction is enhanced. However, this was not confirmed by the metathesis experiments. Here, variation of the stearic acid loading amount showed no major differences of the adhesion layer.

Roughness parameter calculation of the focus variation data showed an optimal amount of stearic acid (1.0 phr stearic acid) to achieve maximum surface roughness. As far as the pull-out forces are concerned, best values were achieved for compounds with low stearic acid content. However, rubber coverage was 100 % and therefore the rubber properties have a strong impact on the measured adhesion values. Due to this fact it is not possible to directly correlate the results from the adhesion testing with the results obtained by the squalene experiments.

Because of the observed differences between the results obtained by the squalene and the metathesis experiments in the previous section, these methods were investigated more closely and the results compared to each other and a third method, the filter paper method, to analyze their advantages and limitations (see Figure 51).

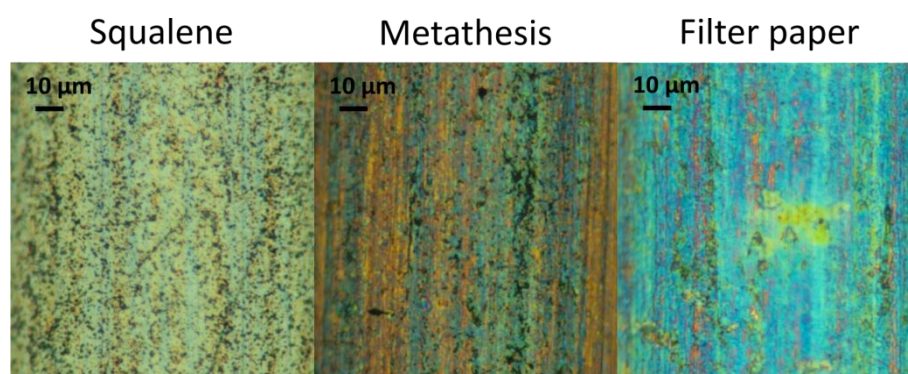


FIGURE 51. COMPARISON OF A SQUALENE, A METATHESIS AND A FILTER PAPER WIRE

In the case of the squalene experiments, a great influence of the compound composition on the obtained results could be observed. Small changes in the compounds led to different sulfur levels and as a result, to totally different optical appearances. Further, not all aspects of a vulcanization reaction, such as the applied pressure, can be simulated in the squalene experiments, which is why the results obtained should be considered with care and not be over-interpreted.

In the filter paper experiments small changes in the compounds led to almost no differences in the surface structures and compositions. In the unaged state only very few surface structures could be observed and after the aging treatment the surface was covered with finely distributed needle-shaped structures, which supports the theory of a crystalline Cu_xS interlayer. Such crystalline structures could not be found on the squalene and, only to a very small extend, on the metathesis samples. Therefore, the crystallinity is most probably enhanced by the presence of the filter paper: due to the retention of most of the rubber compound components, there are less interfering substances on the surface and as a consequence, crystallization is much easier. Further, sulfur levels detected on the filter paper specimens were a little bit higher than the sulfur levels on the metathesis samples. The filter paper has the function to retain components such as rubber molecules and carbon black. As a consequence, a greater percentage of the wire surface is free to react with the active sulfidating species, which in consequence leads to a higher sulfidation of the brass. Therefore, the detected amount of sulfur on the filter paper samples is higher than on comparable metathesis samples.

Similar to the filter paper samples, small changes in the compounds in the metathesis experiments led to almost no differences in the surface structures and compositions. The only remarkable difference was an increased carbon level with increasing carbon black content in the compound mixture, due to organic residues and immobilized carbon black. However, it was not an exceedingly high amount and therefore it should be no problem for most characterization techniques. Further, the metathesis method has a lot of advantages, such as the opportunity to use a real rubber system and no need of using an artificial interlayer. On the other hand, the degradation of actual rubber products with high carbon black loading might be problematic. Besides, it cannot be completely excluded that the high reactive metathesis initiator has an influence on the sulfide layer. However, no major influence was observed so far.

For future studies, a combined use of the presented methods might be advisable, however the squalene method is far off the real conditions and the results differ very much from the ones obtained by the other methods.

The last part of this thesis investigated the influence of different compound components such as cobalt stearate and antioxidant agents. Addition of cobalt stearate to the compound changed the cure characteristics and the physical properties of the vulcanized rubber. After a thermal aging treatment, physical properties for both cobalt-free and cobalt-containing compounds decrease. Adhesion properties for unaged compounds are better with the addition of cobalt stearate.

In the squalene experiments, there are major differences visible between the wires from the different compounds, but these differences were not observed on the filter paper and the olefin metathesis samples. On the surfaces of these samples the optical characterization showed only small differences between cobalt-containing and cobalt-free samples and in the elemental characterization the composition was more or less the same. But on the other hand, in the SEM characterization differently textured surfaces were observed. Therefore, the differences might be explained by different binding states of the elements. For example sulfur can be bound to both, copper and zinc. In the literature it is mentioned that cobalt addition diminishes the zinc sulfide formation and enhances the creation of copper sulfide.^{1,20}

After the aging treatment, adhesion values for the compound without cobalt stearate increased, whereas compounds containing cobalt salt showed inferior adhesion performance, compared to initial adhesion values. A possible explanation was that the initial binding layer for the cobalt free compound is not perfect for bonding (e.g. copper sulfide layer is not ideally textured) and improves a little during the aging (e.g. better surface texture), whereas the cobalt salt improves the performance of the initial binding layer of this compound. During the thermal aging treatment the adhesion layers of both, the cobalt containing and the cobalt free compound grow, which can be observed by the change of the surface color and an increased sulfur level. As a result, the surface textures change as well. For the cobalt free compound the aged binding layer gives better performance than the initial one, whereas for the cobalt containing one, the original binding layer was ideal and therefore, the result after the aging is

inferior. As a consequence, in this case, almost the same adhesion performance is achieved for both compounds after the thermal aging treatment.

The addition of antioxidant agents (IPPD, 6PPD) did not result in the expected improvement of the physical properties or the adhesion values for cobalt containing compounds. Therefore, it might be concluded that it is not the negative influence of the cobalt on the rubber stability, which reduces the adhesion values during the aging treatment. Furthermore, the addition of IPPD and 6PPD not only changed the cure characteristics but also the physical properties. Pull-out forces were mostly the same for the unaged specimens and slightly lower for the thermally aged specimens.

The optical characterization showed almost no differences for unaged wires from compounds with and for unaged wires from compounds without IPPD and 6PPD. This is also confirmed by EDX analysis, where the sulfur levels are almost the same for the metathesis specimens. On the other hand, in the case of the filter paper specimens, wires from compounds containing IPPD and 6PPD had slightly higher sulfur content but within measurement inaccuracy. During the aging treatment, the surface color and the surface structures change. This change is due to a further sulfidation of the wires, which is confirmed by a higher sulfur level detected in the EDX characterization. All in all, it was observed that the addition of IPPD and 6PPD did not lead to any significant changes in the rubber compounds or in the rubber-brass adhesion.

The studies on the influence of stearic acid and cobalt stearate on the adhesion between rubber and brass have shown that in most cases, changes of rubber compound formulations change the adhesion properties as well. However, sometimes, as in the case of the antioxidant agents, no major influence is observed. Therefore, in rubber compounding, the knowledge about the influence of the various compound ingredients can be useful to estimate their effect on the adhesion.

In this thesis, natural rubber was the only rubber type used. In the future, it might be interesting to investigate the application possibilities of the olefin metathesis degradation for several other rubber types, such as styrol-butadiene rubber (SBR),

nitrile-butadiene rubber (NBR), etc. This will allow expanding the studies on rubber-to-brass adhesion to a broader field of application.

6 EXPERIMENTAL

6.1 CHEMICALS

TABLE 29. LIST OF USED CHEMICALS INCLUDING PURITY AND SOURCE OF SUPPLY

Chemical	Source	Purity
Squalene	Sigma Aldrich	> 98 %
Toluene	VWR	rectapur
1-octene	Fluka	97 %
Grubbs catalyst, 2 nd generation	Sigma Aldrich	n.s.
Natural rubber	Semperit Technische Produkte GmbH	technical
Sulfur, oil content 5 %	Semperit Technische Produkte GmbH	technical
Zinc oxide	Semperit Technische Produkte GmbH	technical
Stearic acid	Semperit Technische Produkte GmbH	technical
N-dicyclohexylbenzothiazole 2-sulfenamide (DCBS)	Semperit Technische Produkte GmbH	technical
Cobalt stearate (Manobond CS95), 9.3-9.8 % Co	Semperit Technische Produkte GmbH	technical
Naphthenic oil (Gravex)	Semperit Technische Produkte GmbH	technical
Carbon black N550	Semperit Technische Produkte GmbH	technical
N-isopropyl-N'-phenyl- <i>p</i> -phenylenediamine (IPPD)	Semperit Technische Produkte GmbH	technical
N-(1,3-dimethylbutyl)-N'-phenyl- <i>p</i> -phenylenediamine (6PPD)	Semperit Technische Produkte GmbH	technical

6.2 EQUIPMENT AND METHODS

6.2.1 OPTICAL MICROSCOPY

Optical microscopy was performed using an Olympus BX60 microscope and an Olympus E-520 camera (setting P, no flash). Images were recorded at maximum light intensity. It was paid attention to always align the wires horizontally with the end pointing towards the operator.

6.2.2 FOCUS VARIATION MICROSCOPY

The morphology of the wire surface was studied with focus variation microscopy. The data was obtained with the infinite focus microscope from Alicona Imaging GmbH. It was paid attention to align the wires horizontally and parallel to the operator. A region of 145x110 μm was measured and, for a better visibility of the surface structures, the images were stretched 4fold in z-direction. In some cases the images were planarized (the cylindrical geometry of the wire was subtracted from the 3-dimensional image to reduce it to its surface structures) and for better visualization the images were stretched 10fold in z-direction.

6.2.3 ROUGHNESS CALCULATION

Calculations were done by Johannes Macher and Dieter Gruber. The focus variation data was used to calculate two different surface texture parameters, the mean surface roughness (Sa) and the skewness (Ssk). Sa is defined by the average roughness of a surface topography data array and it is calculated from:

$$Sa = \frac{1}{A} \iint |Z(x, y)| dx dy$$

Ssk , also known as ‘third moment’, represents the skewness of a surface topography data array. Based on a histogram of the heights of all topography array points the deviation from a normal distribution is represented by Ssk . It is calculated as follows:

$$Ssk = \frac{1}{S_q^3} \left[\frac{1}{A} \iint (Z(x, y))^3 dx dy \right]$$

6.2.4 SCANNING ELECTRON MICROSCOPY COUPLED WITH ENERGY DISPERSIVE X-RAY SPECTROSCOPY (SEM-EDX)

Microanalysis was performed by using a Tescan Vega3 scanning electron microscope with an energy dispersive X-ray spectrometer (Oxford Instruments, INCAx-act) attached to it. The electron energy used for the analysis was set to 20 keV. All elements starting from boron can be detected. Atom-percent of the elements were normalized proportional to Cu which was used as an internal standard. Fe cannot be used as internal standard since it varies depending on the brass layer thickness and Zn cannot be used neither because it may change during the sulfidation reaction. On the one hand, parts of the ZnO layer of the wire surface might get dissolved by the stearic acid from the compound and on the other hand, some ZnO from the compound can be deposited on the wire surface. During the sulfidation reaction, some of the Cu is converted into Cu_xS , but this reaction has no impact on the total Cu amount. Therefore, it is best to use Cu as internal standard.

Further microanalysis was performed by Peter Pölt, using a Zeiss Ultra 55 scanning electron microscope (Carl Zeiss NTS, Oberkochen, Germany) with an energy dispersive X-ray spectrometer (Genesis, EDAX Inc., Mahwah, NJ, USA) attached to it. The detection sensitivity of EDX is around 0.1 wt%. The electron energy used for the analysis was set to 7 or 15 keV. All elements starting from boron can be detected. Atom-percent of the elements were normalized proportional to Cu which was used as an internal standard.

6.2.5 RAMAN

Raman spectra were recorded by Boril Chernev. Raman data were acquired by using a LabRAM HR (Horiba Jobin Yvon), equipped with a HeNe laser (633 nm). By using a 40x objective, the laser was focused with the microscope on a field of $30 \times 30 \mu\text{m}$, and spectra were taken 3×10 seconds.

6.2.6 X-RAY DIFFRACTION (XRD)

X-Ray characterization was done by Franz-Andreas Mautner. The X-ray diffractograms were recorded with a Bruker D8 Advance Pert, planar sample, Bragg-Brentano

geometry, Cu-K α radiation. The samples were recorded from 20 to 90 °2 θ , step size 0.02 °2 θ , measuring time 20 s/step.

The Rietveld calculation was done by Brigitte Bitschnau with the program FULLPROF⁸⁷ and X'PertHighScorePlus by Panalytical. The starting geometries were obtained from the ICSD, Inorganic Crystal Structure Database, FIZ Karlsruhe.⁸⁸

6.2.7 VULCANIZATION

Vulcanization was done on a vulcanization press of Bucks Maschinenbau GmbH, type KV141.1. Vulcanization pressure was set to 320 bar. Cure rate data (scorch time t_{05} , optimum curing time t_{90} , minimum torque ML, maximum torque MH) of the rubber compounds were obtained according to DIN 53529/3. A typical rheometer curve can be seen in Figure 52.

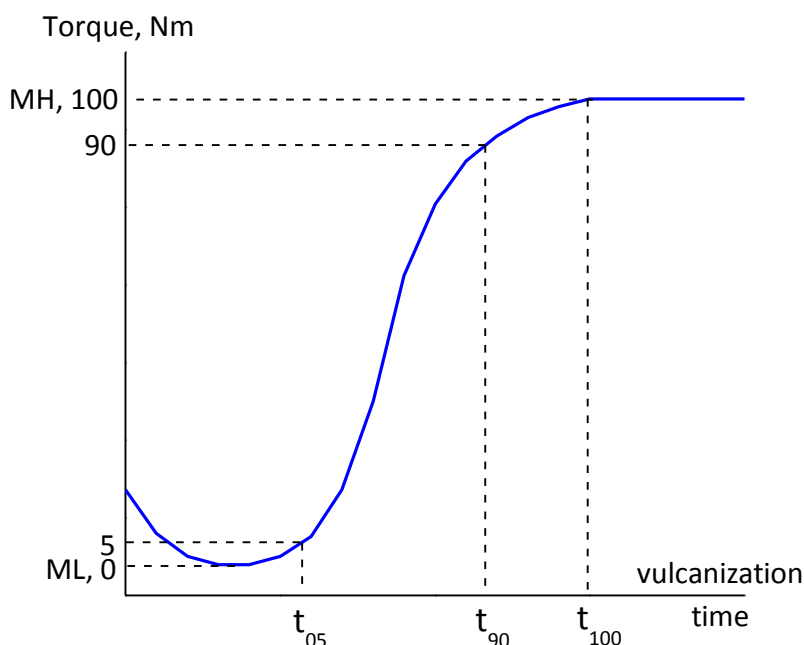


FIGURE 52. RHEOMETER CURVE OF A RUBBER COMPOUND DURING VULCANIZATION (ML: MINIMUM TORQUE, MH: MAXIMUM TORQUE, T_{05} : SCORCH TIME, T_{90} : OPTIMUM CURING TIME)

6.2.8 PULL-OUT TESTING

Pull-out testing was performed on a Zwick/Roell Z2.5 universal testing machine. T-test specimens were used to evaluate the adhesion performance by pulling out the wires at constant rate (=100 mm/min) applying a preload of 50 N. Rubber coverage was rated from 0 to 3 (0 = 0 %, 1 = 1-49 %, 2 = 50-99 %, 3 = 100 % rubber coverage). The adhesion was also measured after a thermal aging treatment (4 hours at 150 °C or 15 days at 90 °C).

6.2.9 RUBBER PROPERTIES TESTING

Elongation at break and tensile strength were measured according to DIN 53504 and tear strength was determined following the procedure described in ISO 34-2.

6.3 SQUALENE EXPERIMENTS

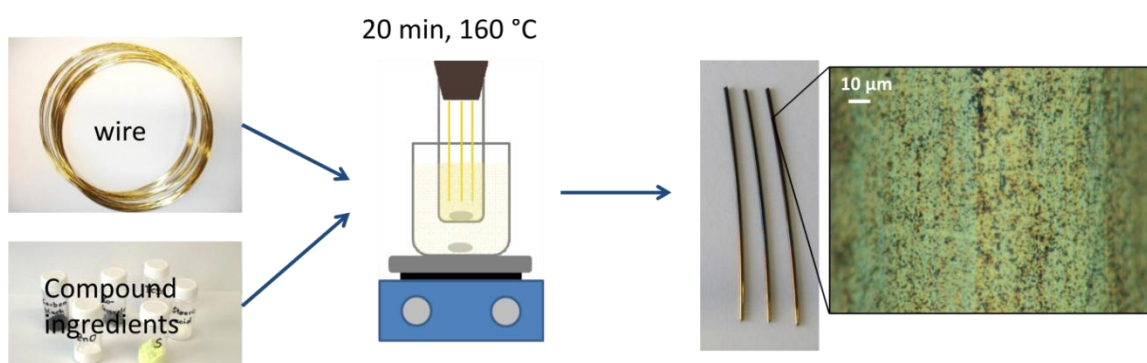


FIGURE 53. SCHEMATIC ILLUSTRATION OF THE SQUALENE EXPERIMENTS

Squalene experiments (see Figure 53) were performed according to Hamed et al.⁴⁵ A representative squalene mixture composition is shown in Table 30. The exact composition of the various samples used in this thesis can be found in the respective chapters in the results and discussion section.

TABLE 30. REPRESENTATIVE COMPOSITION OF A SQUALENE MIXTURE

	phr
Squalene	100
Naphthenic oil	6
ZnO	7
Stearic acid	2
Cobalt stearate	1
Sulfur	6.25
DCBS	0.7
N550 Carbon black	0/10

This mixture contained squalene, naphthenic oil, zinc oxide, stearic acid, cobalt stearate, sulfur, DCBS and 0 or 10 phr of carbon black. Based on this mixture, the amounts of individual components were varied to study the influence of the various vulcanization components on the adhesion between rubber and brass. Before the reaction, brass-coated wires were cut to the required length and washed with toluene. Squalene was heated with naphthenic oil to 160 °C. Then zinc oxide and stearic acid

were added and stirred for 1 minute. Subsequently, cobalt stearate and carbon black were added and stirred for another minute followed by DCBS and sulfur. After another minute of stirring the wires were immersed into the squalene mixture for 20 minutes. It was carefully paid attention to retain a turbulent stirring during the reaction to get a uniform reaction on the wire surface. Then the sulfidated wires were removed, washed with toluene and stored in vials under a nitrogen atmosphere until characterization.

6.4 FILTER PAPER EXPERIMENTS

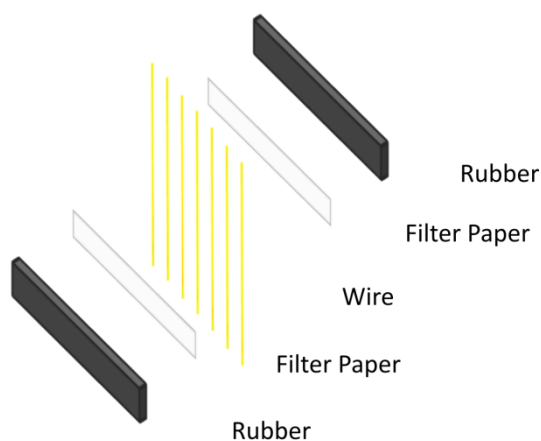


FIGURE 54. SCHEMATIC ILLUSTRATION OF THE FILTER PAPER EXPERIMENTS

For the filter paper experiments T-test specimens were prepared similar to ASTM D 1871 with an inserted filter paper (Whatman type 40 or 540, with particle retention in liquid of 8 μm) in between the wires and the uncured rubber pad (see Figure 54). A representative natural rubber compound composition is shown in Table 31. The exact composition of the various samples used in this thesis can be found in the respective chapters in the results and discussion section.

TABLE 31. REPRESENTATIVE COMPOSITION OF A NATURAL RUBBER COMPOUND USED FOR THE FILTER PAPER EXPERIMENTS

	phr
Natural rubber	100
Naphthenic oil	6
ZnO	7
Stearic acid	2
Cobalt stearate	1
Sulfur	6.25
DCBS	0.7
N550 Carbon black	0/10/50

This compound contained natural rubber, naphthenic oil, zinc oxide, stearic acid, cobalt stearate, sulfur, DCBS and 0, 10 or 50 phr of carbon black. Based on this

compound, the amounts of individual components were varied to study the influence of the various vulcanization components on the rubber-to-brass adhesion. The compounds were vulcanized for 20 minutes at 160 °C and 320 bar with embedment lengths of 10 mm. For thermal aging the T-test samples were stored 4 hours at 150 °C or 15 days at 90 °C. After the vulcanization and in some cases additional aging, treatment clean adhesion interfaces were obtained by peeling of the filter paper placed in between the wires and the rubber (see Figure 55). The filter paper allows the active sulfidating species (sulfur, accelerator, etc.) to get through and react with the brass layer, whereas it retains interfering components, such as rubber molecules and carbon black.³⁷

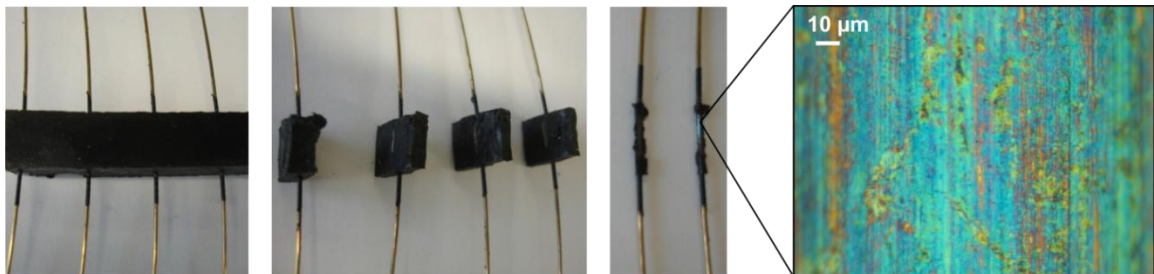


FIGURE 55. EXPOSURE OF THE ADHESION INTERFACE AFTER THE FILTER PAPER EXPERIMENTS

6.5 OLEFIN METATHESIS EXPERIMENTS

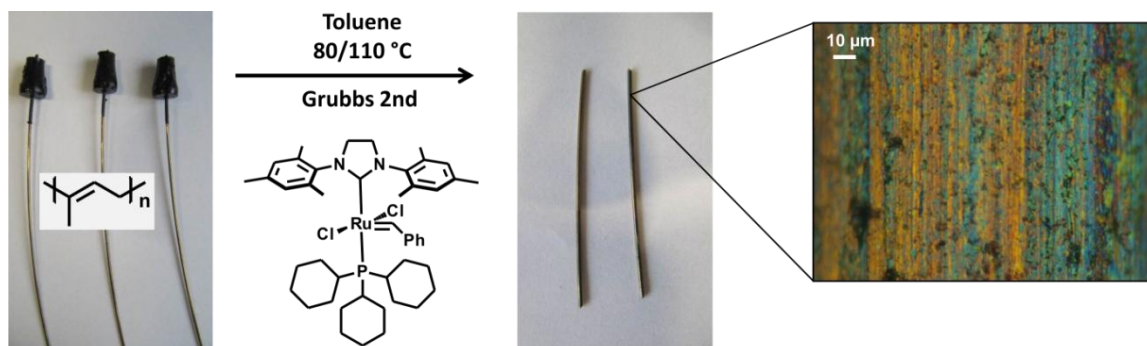


FIGURE 56. SCHEMATIC ILLUSTRATION OF THE OLEFIN METATHESIS EXPERIMENTS

For the metathesis experiments T-test specimens were prepared similar to ASTM D 1871. A representative natural rubber compound composition is shown in Table 31. The exact composition of the various samples used in this thesis can be found in the respective chapters in the results and discussion section. This compound contained natural rubber, naphthenic oil, zinc oxide, stearic acid, cobalt stearate, sulfur, DCBS and 0, 10 or 50 phr of carbon black. Based on this compound, the amounts of individual components were varied to study the influence of the various vulcanization components on the rubber-to-brass adhesion. The compounds were vulcanized for 20 minutes at 160 °C and 320 bar with embedment lengths of 10 mm. For thermal aging the T-test samples were stored 4 hours at 150 °C or 15 days at 90 °C.

6.5.1 OLEFIN METATHESIS DEGRADATION METHOD 1

To remove the rubber from the wire surface an olefin metathesis reaction was used, which was carried out under inert atmosphere using Schlenk techniques. First, specimens for the reaction were soaked in toluene. Then, 2.5 mL of toluene were placed in a Schlenk flask and heated up to 80/110 °C (80 °C for samples without carbon black, 110 °C for carbon black containing specimens). Grubbs 2nd initiator (3 mg) was added together with 1 mL of toluene followed by the immersion of the rubber-wire specimens. After one hour of reaction time the specimens were removed, washed with toluene and if there was some rubber left on the wire the procedure was repeated

until a clean surface was obtained. These wires were stored in vials under nitrogen atmosphere until characterization.

6.5.2 OLEFIN METATHESIS DEGRADATION METHOD 2

To remove the rubber from the wire surface an olefin metathesis reaction was used, which was carried out under inert atmosphere using Schlenk techniques. First, specimens for the reaction were soaked in toluene. Then, 2.5 mL of toluene were placed in a Schlenk flask and heated up to 80/110 °C (80 °C for samples without carbon black, 110 °C for carbon black containing specimens). Grubbs 2nd initiator (3 mg) was added together with 1 mL of toluene followed by the immersion of the rubber-wire specimens. 50 µL of 1-octene was added and after one hour of reaction time the specimens were removed, washed with toluene and if there was some rubber left on the wire the procedure was repeated until a clean surface was obtained. These wires were stored in vials under nitrogen atmosphere until characterization.

7 APPENDIX

7.1 LIST OF ABBREVIATIONS

6PPD	N-(1,3-dimethylbutyl)-N'-phenyl- <i>p</i> -phenylenediamine
AES	Auger electron microscopy
CBS	cyclohexylbenzothiazole sulfenamide
DCBS	N-dicyclohexylbenzothiazole 2-sulfenamide
EDX	energy dispersive X-ray spectroscopy
FIB	focused ion beam
GIXRD	grazing-incident X-ray diffraction
HMMM	hexamethoxymethylmelamine
IPPD	N-isopropyl-N'-phenyl- <i>p</i> -phenylenediamine
keV	kilo electron volt
MBS	2-morpholinothiobenzothiazole
MBT	2-mercaptobenzothiazole
MBTS	2,2'-dithiobenzothiazole
MH	maximum torque
ML	minimum torque
NR	natural rubber
n.s.	not specified
phr	per hundred rubber
Ra	averaged roughness of a one-dimensional profile scan
RF	resorcinol/formaldehyde

Sa	mean surface roughness
SEM	scanning electron microscopy
SIMS	secondary ion mass spectrometry
Ssk	skewness
t ₀₅	scorch time
t ₉₀	optimum curing time
TCAT	tire cord adhesion test
TEM	transmission electron microscopy
TMTD	tetramethylthiuram disulfide
TOF	time-of-flight
wt	weight
XPS	X-ray photoelectron spectroscopy
XRD	X-ray diffraction

7.2 LIST OF TABLES

Table 1. EDX results for Sp2, Sp3 and Sp6	28
Table 2. X-ray diffraction results for Sp2, Sp3 and Sp6	30
Table 3. Compound formulation E.....	31
Table 4. EDX results for Sp2, Sp3 and Sp6 after the squalene experiment.....	33
Table 5. Compound formulation to study the relationship of optical appearance and composition	35
Table 6. Compound formulation to compare optical microscopy images and SEM-EDX results.....	39
Table 7. Compound formulations to study the effect of stearic acid on rubber-brass adhesion.....	47
Table 8. Natural rubber compound formulations to study the effect of stearic acid on rubber-brass adhesion.....	48
Table 9. Cure characteristics (scorch time t05, optimum curing time t90, minimum torque ML, maximum torque MH) of rubber compounds with different amounts of stearic acid determined from the rheometer curves	48
Table 10. EDX analysis of the SEM images in Figure 25.....	51
Table 11. Tensile strength, elongation at break, and tear strength of rubber compounds with different amounts of stearic acid	55
Table 12. Pull-out force and rubber coverage of rubber compounds with different amounts of stearic acid.....	57
Table 13. Squalene mixture formulations containing 10 phr carbon black	59
Table 14. EDX analysis of the SEM images in Figure 29.....	62
Table 15. Compound formulation to study the influence of the sample preparation method.....	64
Table 16. EDX results (20 keV) of the various samples.....	67
Table 17. EDX analysis (7 keV) of marked areas in Figure 31, E _F	69
Table 18. EDX results (20 keV) of the thermally aged samples	72
Table 19. Compound formulation to study the influence of cobalt stearate on rubber-brass adhesion	74
Table 20. Cure characteristics (scorch time t05, optimum curing time t90), physical properties, Pull-out force and rubber coverage of compounds containing different amounts of cobalt stearate and carbon black	75
Table 21. Physical properties, pull-out force and rubber coverage of thermally aged compounds containing different amounts of cobalt stearate and carbon black.....	76

Table 22. EDX analysis (20 keV) of wire surfaces from compounds containing different amounts of cobalt stearate and carbon black	86
Table 23. EDX analysis (20 keV) of wire surfaces from thermally aged compounds containing different amounts of cobalt stearate and carbon black.....	90
Table 24. Compound formulation to study the influence of antioxidant agent on rubber-to-brass adhesion	93
Table 25. Cure characteristics (scorch time t05, optimum curing time t90) and physical properties of compounds containing different amounts of cobalt stearate and antioxidant agent.....	94
Table 26. Pull-out force and rubber coverage of compounds containing different amounts of cobalt stearate and antioxidant agent	95
Table 27. EDX analysis of wire surfaces from compounds containing different amounts of cobalt stearate and antioxidant agent	99
Table 28. EDX analysis of the thermally aged wires from compounds containing different amounts of cobalt stearate and antioxidant agent.....	102
Table 29. List of used chemicals including purity and source of supply.....	111
Table 30. Representative composition of a squalene mixture	116
Table 31. Representative composition of a natural rubber compound used for the filter paper experiments.....	118

7.3 LIST OF FIGURES

Figure 1. Car tire sales in Europe between 2003 and 2010.....	1
Figure 2. Schematic image of brass-coated steel wire surface	3
Figure 3. Schematic image of the brass-rubber interface after vulcanization	4
Figure 4. Stage 1, formation of active intermediate from the accelerator	6
Figure 5. Stage 2, absorption of the accelerator fragments on the brass surface.....	7
Figure 6. Stage 3, sulfur insertion	8
Figure 7. Stage 4, Complex decomposition and sulfide layer growth	8
Figure 8. Stage 5, rubber cross-linking	9
Figure 9. Structures of cobalt adhesion promoters A: cobalt disoap, B: cobalt boroacylate	12
Figure 10. Cross-linking of RF resin and HMMM	15
Figure 11. One-component melamine resin.....	15
Figure 12. Scheme of silane-rubber cross-linking.....	18
Figure 13. TCAT pull-out testing and different failure modes of the pulled wires (a: adhesive failure, b: partly adhesive, partly cohesive failure, c: cohesive failure of the rubber)	20
Figure 14. T-test sample for pull-out testing	21
Figure 15. Optical microscopy images (top), focus variation microscopy images (middle) and scanning electron microscopy images (bottom) of the different wire samples (SEM images recorded by Peter Pölt)	28
Figure 16. X-ray diffraction pattern of Sp2, Sp3 and Sp6	30
Figure 17. optical microscopy images (top), focus variation microscopy images (middle, 145x110 μm) and SEM images (bottom) of Sp2, Sp3 and Sp6 after the squalene experiment.....	32
Figure 18. Wires obtained after different reaction times in a squalene mixture (compound E).....	36
Figure 19. Planarized focus variation microscopy images in real color (left) and color coded (right) of the untreated wire (top) and the wire after 20 minutes in the squalene mixture of compound E (bottom).....	37
Figure 20. EDX analysis of squalene specimens from different compounds (A-E).....	38
Figure 21. Optical microscopy image (left), SEM image (right, top) and EDX results (right, bottom) of the wire obtained in a squalene experiment without ZnO (compound F) (SEM image recorded by Peter Pölt).....	40

Figure 22. Optical microscopy image (left), SEM image (right, top) and EDX results (right, bottom) of the wire obtained in a squalene experiment without cobalt stearate (compound G) (SEM image recorded by Peter Pölt)	41
Figure 23. Optical microscopy image (left), SEM image (right, top) and EDX results (right, bottom) of a wire obtained in a squalene experiment containing both, ZnO and cobalt stearate (compound E) (SEM image recorded by Peter Pölt)	42
Figure 24. Elemental maps of a sulfidated wire from compound E (images recorded by Peter Pölt)	43
Figure 25. Optical microscopy images (left) and SEM images (middle and right) of untreated wire and samples H _S , A _S -E _S	49
Figure 26. Planarized focus variation microscopy image in real color (left) and color coded (right) of a wire after the squalene experiment in compound B _S	52
Figure 27. Mean surface roughness (S _a) and skewness (S _{sk}) of the untreated sample and the samples after the squalene experiments in compounds A _S -E _S	53
Figure 28. Pull-out force of rubber compounds with different stearic acid concentrations	56
Figure 29. Optical microscopy images and SEM images of samples from squalene mixtures containing 10 phr carbon black (left) and of metathesis samples (right) to study the influence of stearic acid on rubber-brass adhesion	61
Figure 30. Optical microscopy images of the various samples (E _S : squalene, 0 phr carbon black; N _S : squalene, 10 phr carbon black; E _M : metathesis, 0 phr carbon black; N _M : metathesis, 10 phr carbon black; T _M : metathesis, 50 phr carbon black; E _F : filter paper, 0 phr carbon black; N _F : filter paper, 10 phr carbon black; T _F : filter paper, 50 phr carbon black).....	65
Figure 31. SEM images of the various samples (left: 20 keV, right: 7 keV; E _S : squalene, 0 phr carbon black; E _M : metathesis, 0 phr carbon black; E _F : filter paper, 0 phr carbon black) (SEM images on the right side recorded by Peter Pölt)	67
Figure 32. Raman spectra of samples obtained from compound E	70
Figure 33. Optical microscopy images (left) and SEM images (right) of the thermally aged wires (E _M : metathesis, 0 phr carbon black; E _F : filter paper, 0 phr carbon black) ..	71
Figure 34. Optical microscopy images of samples obtained by squalene experiments with different amounts of cobalt stearate (G _S : 0 phr cobalt stearate, 0 phr carbon black; U _S : 0 phr cobalt stearate, 10 phr carbon black; E _S : 1 phr cobalt stearate, 0 phr carbon black; N _S : 1 phr cobalt stearate, 10 phr carbon black).....	78

Figure 35. Focus variation microscopy images of samples obtained by squalene experiments with different amounts of cobalt stearate (G _S : 0 phr cobalt stearate, 0 phr carbon black; U _S : 0 phr cobalt stearate, 10 phr carbon black; E _S : 1 phr cobalt stearate, 0 phr carbon black; N _S : 1 phr cobalt stearate, 10 phr carbon black)	79
Figure 36. Optical microscopy images of samples obtained by the olefin metathesis method (G _M : 0 phr cobalt stearate, 0 phr carbon black; U _M : 0 phr cobalt stearate, 10 phr carbon black; V _M : 0 phr cobalt stearate, 50 phr carbon black; E _M : 1 phr cobalt stearate, 0 phr carbon black; N _M : 1 phr cobalt stearate, 10 phr carbon black; T _M : 0 phr cobalt stearate, 50 phr carbon black)	80
Figure 37. Focus variation microscopy images of samples obtained by the olefin metathesis method (G _M : 0 phr cobalt stearate, 0 phr carbon black; U _M : 0 phr cobalt stearate, 10 phr carbon black; V _M : 0 phr cobalt stearate, 50 phr carbon black; E _M : 1 phr cobalt stearate, 0 phr carbon black; N _M : 1 phr cobalt stearate, 10 phr carbon black; T _M : 0 phr cobalt stearate, 50 phr carbon black)	81
Figure 38. Optical microscopy images of filter paper samples (G _F : 0 phr cobalt stearate, 0 phr carbon black; U _F : 0 phr cobalt stearate, 10 phr carbon black; V _F : 0 phr cobalt stearate, 50 phr carbon black; E _F : 1 phr cobalt stearate, 0 phr carbon black; N _F : 1 phr cobalt stearate, 10 phr carbon black; T _F : 1 phr cobalt stearate, 50 phr carbon black)..	82
Figure 39. Focus variation microscopy images of filter paper samples (G _F : 0 phr cobalt stearate, 0 phr carbon black; U _F : 0 phr cobalt stearate, 10 phr carbon black; V _F : 0 phr cobalt stearate, 50 phr carbon black; E _F : 1 phr cobalt stearate, 0 phr carbon black; N _F : 1 phr cobalt stearate, 10 phr carbon black; T _F : 1 phr cobalt stearate, 50 phr carbon black)	83
Figure 40. SEM images (7 keV) of wires from compounds without carbon black (G _S : squalene, 0 phr Cobalt stearate; E _S : squalene, 1 phr cobalt stearate; G _M : metathesis, 0 phr Cobalt stearate; E _M : metathesis, 1 phr cobalt stearate; G _F : filter paper, 0 phr Cobalt stearate; E _F : filter paper, 1 phr cobalt stearate) (SEM images recorded by Peter Pölt)	85
Figure 41. Optical microscopy images of wires from thermally aged compounds without carbon black (G _M : metathesis, 0 phr Cobalt stearate; E _M : metathesis, 1 phr cobalt stearate; G _F : filter paper, 0 phr Cobalt stearate; E _F : filter paper, 1 phr cobalt stearate).....	88
Figure 42. SEM Images (20 keV) of wires from thermally aged compounds without carbon black (G _M : metathesis, 0 phr Cobalt stearate; E _M : metathesis, 1 phr cobalt stearate; G _F : filter paper, 0 phr Cobalt stearate; E _F : filter paper, 1 phr cobalt stearate)	89

Figure 43. N-isopropyl-N'-phenyl- <i>p</i> -phenylenediamine (IPPD) and N-(1,3-dimethylbutyl)-N'-phenyl- <i>p</i> -phenylenediamine (6PPD).....	92
Figure 44. Optical microscopy images of samples obtained by the olefin metathesis method (G_M : 0 phr cobalt stearate, 0 phr antioxidant agents; E_M : 1 phr cobalt stearate, 0 phr antioxidant agents; GA_M : 0 phr cobalt stearate, 0.75 phr IPPD, 0.75 phr 6PPD; EA_M : 1 phr cobalt stearate, 0.75 phr IPPD, 0.75 phr 6PPD).....	95
Figure 45. Optical microscopy images of samples obtained by filter paper experiments (G_F : 0 phr cobalt stearate, 0 phr antioxidant agents; E_F : 1 phr cobalt stearate, 0 phr antioxidant agents; GA_F : 0 phr cobalt stearate, 0.75 phr IPPD, 0.75 phr 6PPD; EA_F : 1 phr cobalt stearate, 0.75 phr IPPD, 0.75 phr 6PPD).....	96
Figure 46. SEM images of samples obtained by the olefin metathesis method (G_M : 0 phr cobalt stearate, 0 phr antioxidant agents; E_M : 1 phr cobalt stearate, 0 phr antioxidant agents; GA_M : 0 phr cobalt stearate, 0.75 phr IPPD, 0.75 phr 6PPD; EA_M : 1 phr cobalt stearate, 0.75 phr IPPD, 0.75 phr 6PPD)	97
Figure 47. SEM images of samples obtained by the filter paper method (G_F : 0 phr cobalt stearate, 0 phr antioxidant agents; E_F : 1 phr cobalt stearate, 0 phr antioxidant agents; GA_F : 0 phr cobalt stearate, 0.75 phr IPPD, 0.75 phr 6PPD; EA_F : 1 phr cobalt stearate, 0.75 phr IPPD, 0.75 phr 6PPD).....	98
Figure 48. Optical microscopy images of thermally aged samples (E_M : metathesis, 1 phr cobalt stearate, 0 phr antioxidant agents; EA_M : metathesis, 1 phr cobalt stearate, 0.75 phr IPPD, 0.75 phr 6PPD; E_F : filter paper, 1 phr cobalt stearate, 0 phr antioxidant agents; EA_F : filter paper, 1 phr cobalt stearate, 0.75 phr IPPD, 0.75 phr 6PPD)	100
Figure 49. SEM images of thermally aged samples (E_M : metathesis, 1 phr cobalt stearate, 0 phr antioxidant agents; EA_M : metathesis, 1 phr cobalt stearate, 0.75 phr IPPD, 0.75 phr 6PPD; E_F : filter paper, 1 phr cobalt stearate, 0 phr antioxidant agents; EA_F : filter paper, 1 phr cobalt stearate, 0.75 phr IPPD, 0.75 phr 6PPD).....	101
Figure 50. Comparison of wire color and sulfur level.....	105
Figure 51. Comparison of a squalene, a metathesis and a filter paper wire.....	106
Figure 52. Rheometer curve of a rubber compound during vulcanization (ML: minimum torque, MH: maximum torque, T_{05} : scorch time, t_{90} : optimum curing time).....	114
Figure 53. Schematic illustration of the squalene experiments.....	116
Figure 54. Schematic illustration of the filter paper experiments	118
Figure 55. Exposure of the adhesion interface after the filter paper experiments	119
Figure 56. Schematic illustration of the olefin metathesis experiments.....	120

7.4 LITERATURE

- (1) Fulton, W. S. *Rubber Chemistry and Technology* **2005**, 78, 426-457.
- (2) Statista, I. 223868 Absatz von PKW Reifen in Europa.
<http://de.statista.com/statistik/daten/studie/223868/umfrage/absatz-von-pkw-reifen-in-europa/> accessed 2012-11-15.
- (3) Statista, I. 223869 Absatz von Reifen für LKW und Busse in Europa.
<http://de.statista.com/statistik/daten/studie/223869/umfrage/absatz-von-reifen-fuer-lkw-und-busse-in-europa/> accessed 2012-11-15.
- (4) Statista, I. 223875 Umsatzstärkste Reifenhersteller weltweit.
<http://de.statista.com/statistik/daten/studie/223875/umfrage/umsatzstaerkste-reifenhersteller-weltweit/> accessed 2012-11-15.
- (5) Kretschmar, T.; Hofer, F.; Hummel, K. *Kautschuk, Gummi, Kunststoffe* **1992**, 45, 1038-1043.
- (6) Kretschmar, T.; Hofer, F.; Hummel, K. *Kautschuk, Gummi, Kunststoffe* **1993**, 46, 710-717.
- (7) Kim, J. M.; van Ooij, W. J. *Rubber Chemistry and Technology* **2002**, 75, 199-214.
- (8) van Ooij, W. J. *Kautschuk, Gummi, Kunststoffe* **1977**, 30, 739-45, 833-8.
- (9) Davies, J. R. *Kautschuk, Gummi, Kunststoffe* **1984**, 37, 493-496.
- (10) Jeon, G. S.; Kang, U. I.; Jeong, S. W.; Choi, S. J.; Kim, S. H. *Journal of Adhesion* **2005**, 19, 1325-1348.
- (11) van Ooij, W. J.; Kleinhesselink, A. *Applications of Surface Science* **1980**, 4, 324-339.
- (12) Giridhar, J.; van Ooij, W. *Surface and Coatings Technology* **1992**, 53, 243-255.
- (13) Giridhar, J.; van Ooij, W. J. *Surface and Coatings Technology* **1992**, 52, 17-30.
- (14) van Ooij, W. J.; Giridhar, J.; Ahn, J. H. *Kautschuk, Gummi, Kunststoffe* **1991**, 44, 348359.
- (15) Shemenski, R. M.; Su, Y.-Y. *Gummi Fasern Kunststoffe* **2003**, 56, 777-785.
- (16) van Ooij, W. J. *Rubber Chemistry and Technology* **1984**, 57, 421-456.

-
- (17) Röthemeyer, F.; Sommer, F. *Kautschuk Technologie*; Carl Hanser Verlag: München, Wien, 2006.
- (18) Fulton, W. S.; Wilson, J. C. In *Handbook of Rubber Bonding*; Rapra Technology Limited, 2003; pp. 197-212.
- (19) Hotaka, T.; Ishikawa, Y.; Mori, K. *Rubber Chemistry and Technology* **2007**, *80*, 61-82.
- (20) Chandra, A. K.; Mukhopadhyay, R.; Konar, J.; Ghosh, T. B.; Bhowmick, A. K. *Journal of Materials Science* **1996**, *31*, 2667-2676.
- (21) Haemers, G.; Mollet, J. *Journal of Elastomers and Plastics* **1978**, *10*, 241-261.
- (22) Maesele, A.; Debruyne, E. *Rubber Chemistry and Technology* **1969**, *42*, 613-24.
- (23) van Ooij, W. J. In *Handbook of Rubber Bonding*; Rapra Technology Limited, 2003; pp. 163-195.
- (24) Hamed, G. R.; Donatelli, T. *Rubber Chemistry and Technology* **1983**, *56*, 450-464.
- (25) Orband, A.; Anthoine, G.; Roebuck, H. *Kautschuk, Gummi, Kunststoffe* **1986**, *39*, 37-42.
- (26) van Ooij, W. J.; Weening, W. E.; Murray, P. F. *Rubber Chemistry and Technology* **1981**, *54*, 227-254.
- (27) Kim, J. M.; van Ooij, W. J. *Journal of Adhesion Science and Technology* **2003**, *17*, 165-178.
- (28) Fulton, W. S. *Rubber Chemistry and Technology* **2006**, *79*, 790-805.
- (29) Waddell, W. H.; Evans, L. R.; Goralski, E. G.; Snodgrass, L. J. *Rubber Chemistry and Technology* **1996**, *69*, 48-58.
- (30) Evans, L. R.; Hope, J. C.; Okel, T. A.; Waddell, W. H. *Gummi Fasern Kunststoffe* **1996**, *49*, 128-133.
- (31) Jeon, G. S.; Han, M. H. *Journal of Adhesion Science and Technology* **1999**, *13*, 153-168.
- (32) Chandra, A. K.; Biswas, A.; Murkhopadhyay, R.; Bhowmick, A. K. *Journal of Adhesion* **1994**, *44*, 177-196.
- (33) Jeon, G. S. *Journal of Adhesion Science and Technology* **2009**, *23*, 913-930.

-
- (34) van Ooij, W. J.; Harakuni, P. B.; Buytaert, G. *Rubber Chemistry and Technology* **2009**, *82*, 315-339.
- (35) Hamed, G. R.; Huang, J. *Rubber Chemistry and Technology* **1991**, *64*, 285-295.
- (36) van Ooij, W. J.; Biemond, M. E. F. *Rubber Chemistry and Technology* **1984**, *57*, 686-702.
- (37) Hotaka, T.; Ishikawa, Y.; Mori, K. *Rubber Chemistry and Technology* **2007**, *80*, 61-82.
- (38) Fulton, W. S.; Smith, G. C.; Titchener, K. J. *Applied Surface Science* **2004**, *221*, 69-86.
- (39) Patil, P. Y.; Ooij, W. J. *Rubber Chemistry and Technology* **2005**, *78*, 155-173.
- (40) Magg, H. *Kautschuk, Gummi, Kunststoffe* **1993**, *46*, 139-145.
- (41) Patil, P. Y.; van Ooij, W. J. *Rubber Chemistry and Technology* **2006**, *79*, 82-93.
- (42) Patil, P. Y.; van Ooij, W. J. *Journal of Adhesion Science and Technology* **2004**, *18*, 1367-1394.
- (43) Hotaka, T.; Ishikawa, Y.; Mori, K. *Rubber Chemistry and Technology* **2005**, *78*, 175-187.
- (44) Jeon, G. S. *Journal of Adhesion Science and Technology* **2010**, *24*, 709-729.
- (45) Hamed, G. R.; Paul, R. *Rubber Chemistry and Technology* **1997**, *70*, 541-548.
- (46) Jayaseelan, S. K.; van Ooij, W. J. *Gummi Fasern Kunststoffe* **2003**, *56*, 497-509.
- (47) Ziegler, E.; Macher, J.; Gruber, D.; Pölt, P.; Kern, W.; Lummerstorfer, T.; Feldgitscher, C.; Holzner, A.; Trimmel, G. *Rubber Chemistry and Technology* **2012**, *85*, 264-276.
- (48) Kim, J. M. *Rubber Chemistry and Technology* **2005**, *78*, 844-854.
- (49) Hammer, G. E. *Journal of Vacuum Science & Technology A: Vacuum, Surfaces, and Films* **2001**, *19*, 2846-2850.
- (50) Jeon, G. S.; Han, M. H.; Seo, G. *Korean Journal of Chemical Engineering* **1999**, *16*, 248-252.
- (51) Krone, R. *Kautschuk, Gummi, Kunststoffe* **1993**, *46*, 233-235.

-
- (52) Lehrle, R. S.; Niderost, K. J. *Progress in Rubber and Plastics Technology* **1992**, *8*, 221-239.
- (53) Weening, W. E. *Kautschuk, Gummi, Kunststoffe* **1978**, 227-232.
- (54) Ball, J. J.; Gibbs, H. W.; Tate, P. E. R. *The Journal of Adhesion* **1990**, *32*, 29-44.
- (55) van Ooij, W. J.; Kleinhesselink, A.; Leyenaar, S. R. *Surface Science* **1979**, *89*, 165-173.
- (56) Kretzschmar, T.; Hummel, K.; Hofer, F.; Grogger, W.; Grubbauer, G. *Fresenius' Journal of Analytical Chemistry* **1994**, *349*, 235-236.
- (57) Pieroth, M.; Elschner, A. *Kautschuk, Gummi, Kunststoffe* **1993**, *46*, 112-115.
- (58) Yamauchi, M. T.; Shimizu, T.; Doi, M.; Yasunaga, D.; Nakayama, T.; Okumura, K. *Rubber Chemistry and Technology* **2003**, *76*, 1045-1054.
- (59) Holtkamp, D.; Elschner, A.; Mueller, G.; Pieroth, M. *Surface and Interface Analysis* **1995**, *23*, 155-162.
- (60) Jeon, G. S.; Han, M. H.; Seo, G. *Korean Journal of Chemical Engineering* **1999**, *16*, 434-440.
- (61) Ishikawa, Y.; Hotaka, T. *Gummi Fasern Kunststoffe* **2004**, *57*, 642-652.
- (62) van Ooij, W. J. *Surface Science* **1977**, *68*, 1-9.
- (63) Jeon, G. S.; Kang, U. I.; Jeong, S. W.; Choi, S. J.; Kim, S. H. *Journal of Adhesion Science and Technology* **2005**, *19*, 1325-1348.
- (64) Jeon, G. S. *Journal of Adhesion Science and Technology* **2008**, *22*, 1223-1253.
- (65) Buytaert, G.; Coornaert, F.; Dekeyser, W. *Rubber Chemistry and Technology* **2009**, *82*, 430-441.
- (66) Buytaert, G.; Liang, H.; Pax, G.; Reis, P. *Rubber & Plastics News* **2010**, 14-15.
- (67) Dogakin, B.; Beniska, J. *Rubber Chemistry and Technology* **1958**, *31*, 329-342.
- (68) Beniska, J.; Dogakin, B. *Rubber Chemistry and Technology* **1959**, *32*, 780-784.
- (69) Akiba, M.; Hashim, A. S. *Progress in Polymer Science* **1997**, *22*, 475-521.
- (70) Whitehouse, D. *Surface and their measurement*; Kogan Page Science: Warwick, U.K., 2002.

-
- (71) Michigan Metrology, LLC. <http://www.michimet.com> accessed 2010-10-19.
- (72) Hummel, K.; Kiattanavith, N.; Bernard, E. *Die angewandte Makromolekulare Chemie* **1993**, *207*, 137-143.
- (73) Hummel, K.; Stelzer, F.; Hobisch, G.; Hartmann, B. *Die angewandte Makromolekulare Chemie* **1987**, *155*, 143-149.
- (74) Stelzer, F.; Hobisch, G.; Pongratz, T.; Hummel, K. *Journal of Molecular Catalysis* **1988**, *46*, 433-444.
- (75) Hummel, K. *Pure and Applied Chemistry* **1982**, *54*, 351-364.
- (76) Korshak, Y. V.; Tlenkopatchev, M. A.; Dolgoplosk, B. A.; Aveikina, E. G.; Kutepov, D. F. *Journal of Molecular Catalysis* **1982**, *15*, 207-218.
- (77) Zümreoglu-Karan, B.; Bozkurt, C.; Imamoglu, Y. *Polymer Journal* **1992**, *24*, 25-29.
- (78) Reyx, D.; Campistrion, I. *Die Angewandte Makromolekulare Chemie* **1997**, *247*, 197-211.
- (79) Craig, S. W.; Manzer, J. A.; Coughlin, E. B. *Macromolecules* **2001**, *34*, 7929-7931.
- (80) Wolf, S.; Plenio, H. *Green Chemistry* **2011**, *13*, 2008.
- (81) Solanky, S. S.; Campistrion, I.; Laguerre, A.; Pilard, J.-F. *Macromolecular Chemistry and Physics* **2005**, *206*, 1057-1063.
- (82) Saetung, N.; Campistrion, I.; Pascual, S.; Pilard, J.-F.; Fontaine, L. *Macromolecules* **2011**, *44*, 784-794.
- (83) Gutiérrez, S.; Tlenkopatchev, M. a. *Polymer Bulletin* **2010**, *66*, 1029-1038.
- (84) Zhaochun, Z.; Baibiao, H.; Yongqin, Y.; Deliang, C. *Materials Science and Engineering B* **2001**, *86*, 109-112.
- (85) Ishii, M.; Shibata, K.; Nozaki, H. *Journal of solid state chemistry* **1993**, *105*, 504-511.
- (86) Mernagh, T. P.; Trudu, A. G. *Chemical Geology* **1993**, *103*, 113-127.
- (87) Rodriguez-Carvajal, J. *Physica B* **1992**, *192*, 55.
- (88) FIZ Karlsruhe Inorganic Crystal Structure Database. <http://www.fiz-karlsruhe.de/icsd.html?&L=\%22%20onfocus%3D\%22blurLink%28this%29%3B> accessed: 2012-11-06.

7.5 PUBLICATIONS

PAPERS

2012

Investigation of the influence of stearic acid on rubber-brass adhesion - Ziegler, E.; Macher, J.; Gruber, D.; Pölt, P.; Kern, W.; Lummerstorfer, T.; Feldgitscher, C.; Holzner, A.; Trimmel, G.; *Rubber Chemistry and Technology* **2012**, 85 (2), 264 – 276.

PROCEEDINGS

2011

Investigation of the influence of stearic acid on rubber-brass adhesion - Ziegler, E.; Macher, J.; Gruber, D.; Pölt, P.; Kern, W.; Lummerstorfer, T.; Feldgitscher, C.; Holzner, A.; Trimmel, G.; *Proceedings of the ACS Rubber Division Technical Meeting & Educational Symposium*, Cleveland (Ohio) **2011**, 21 – 46.

ORAL PRESENTATIONS

2012

Wie untersuche ich die Gummi-Metall Adhäsionsschicht?: Vergleich unterschiedlicher analytischer Methoden - Ziegler, E.; Kern, W.; Hochenauer, R.; Holzner, A.; Trimmel, G.; *PCCL Symposium*, Leoben (Austria), 2012-10-04.

Untersuchungen zur Gummi-Messing Adhäsionsschicht: Vergleich unterschiedlicher analytischer Methoden - Ziegler, E.; Kern, W.; Hochenauer, R.; Holzner, A.; Trimmel, G.; *Deutsche Kautschuk Tagung*, Nürnberg (Germany), 2012-07-02.

How to investigate the rubber-brass adhesive interface: Comparison of different analytical methods - Ziegler, E.; Kern, W.; Hochenauer, R.; Holzner, A.; Trimmel, G.; *International Rubber Conference*, Jeju-si (South Korea), 2012-05-21.

Study of the rubber-brass adhesion interface: Comparison of different sample preparation methods - Ziegler, E.; Kern, W.; Hochenauer, R.; Holzner, A.; Trimmel, G.; *Chemie und Technologie von Materialien*, Graz (Austria), 2012-05-09.

2011

Investigation of the influence of stearic acid on rubber-brass adhesion - Ziegler, E.; *Chemie und Technologie von Materialien*, Graz (Austria), 2011-11-09

Investigation of the influence of stearic acid on rubber-brass adhesion - Ziegler, E.; Macher, J.; Gruber, D.; Pölt, P.; Kern, W.; Lummerstorfer, T.; Feldgitscher, C.; Holzner, A.; Trimmel, G.; *ACS Rubber Division, 180th Technical Meeting*, Cleveland (Ohio), 2011-10-11.

Polymer-Metal-Composites: Investigation of the rubber-brass adhesion mechanism by utilizing squalene as low molecular-weight model compound for NR - Ziegler, E.; Feldgitscher, C.; Holzner, A.; Trimmel, G.; *DocDays 2011*, Graz (Austria), 2011-06-07.

Polymer-Metall-Verbunde: Untersuchungen zur Haftschicht zwischen Gummi und Messing - Ziegler, E. E.; Haberfellner, E.; Trimmel, G.; *Chemie und Technologie von Materialien*, Graz (Austria), 2011-06-01.

Polymer-Metall-Verbunde: Untersuchungen zur Haftschicht zwischen Gummi und Messing - Ziegler, E.; Haberfellner, E.; Macher, J.; Gruber, D.; Kern, W.; Feldgitscher, C.; Holzner, A.; Trimmel, G.; *PCCL-Symposium 2011*, Leoben (Austria), 2011-05-19.

POSTERS**2010**

Investigation of the binding-sulfide layer formation on brass-coated steel wires using squalene as low-molecular model compound for NR - Ziegler, E.; Gruber, D.; Macher, J.; Kern, W.; Feldgitscher, C.; Holzner, A.; Trimmel, G.; *Austrian-Slovenian Polymer Meeting*, Leoben (Austria), 201-09-08.

7.6 CURRICULUM VITAE

PERSONAL DETAILS

Name	Ziegler Elisabeth Eva
Address	Morellenfeldgasse 41/5/23 8010 Graz
Mail	elisabeth.ziegler@tugraz.at
Date of birth	08.07.1986
Citizenship	Austria

EDUCATION AND QUALIFICATIONS

1992 – 1996	Elementary school in Graz
1996 – 2004	Secondary school in Graz June 2004: school leaving examination (equivalent to A-levels) with excellent success
2004 – 2008	Graz University of Technology – Diploma study Technical Chemistry Closed with bachelor degree
2008 – 2009	Graz University of Technology – Master study Technical Chemistry Master thesis: “Synthesis and Characterization of Poly(thiophenes) and Fluorene-thiophene-copolymers”
2010 – 2013	PhD thesis at Graz University of Technology under supervision of Assoc.Prof. DI Dr. Gregor Trimmel
Jun. – Aug. 2008	Practical internship at Syracuse University (New York, USA)